# CHARACTERIZATION OF TSPO 18 KDA

# IN NEUROSTEROID SYNTHESIS AND MITOCHONDRIAL METABOLISM

## CHARAKTERISIERUNG VON TSPO 18 KDA

## IN DER NEUROSTEROIDSYNTHESE UND DEM MITOCHONDRIALEN STOFFWECHSEL


**DISSERTATION**

ZUR ERLANGUNG DES DOKTORGRADES

DER NATURWISSENSCHAFTEN (DR. RER. NAT.)

DER NATURWISSENSCHAFTLICHEN FAKULTÄT IV

CHEMIE UND PHARMAZIE

DER UNIVERSITÄT REGENSBURG

vorgelegt von

**Luisa Scheck, geb. Wolf**

aus

**Schmalkalden**

im

**Februar 2017**

Promotionsgesuch eingereicht am: 24. Februar 2017

Die Arbeit wurde angeleitet von: Prof. Dr. med. Dr. rer. nat. Ekkehard Haen

## Table of contents

## Acknowledgements

Schreiben musste ich diese Arbeit zwar allein – doch an ihrem guten Gelingen waren einige mir nahestehender Menschen beteiligt, denen ich dafür Dank schulde.
An erster Stelle muss mein Doktorvater Prof. Dr. Ekkehard Haen genannt werden. Herzlichen Dank für die Unterstützung. Ein besonderer Dank geht an Prof. Dr. Christian Wetzel und Dr. Vladimir Milenkovic, die mir die technischen Möglichkeiten und das technische Know-how gegeben und vermittelt haben, die Arbeit in dieser methodischen Vielfalt durchzuführen. Darüber hinaus möchte ich Prof. Rupprecht und Dr. Nothdurfter für die Zusammenarbeit danken.
Auch Dr. Markus Reichold, Dr. Michael Gruber und Prof. Dr. Marina Kreutz als meine Kooperationspartner sind hier besonders zu benennen. Für mich war es äußerst wertvoll, dass es ehrliche und offene Kritik gab und eine sehr gute Kooperationsarbeit. Für diese Ehrlichkeit, die Kollegialität und die tolle Zusammenarbeit der Institute bin ich sehr dankbar.
Ein persönlicher Dank gilt meinen Mann Johannes Scheck. Wenn ich mit dem Kopf mal wieder nicht zuhause, sondern bei der Arbeit war, ist er es gewesen, der mich dabei immer unterstützt und motiviert hat. Dieser Beistand ist für mich nicht selbstverständlich, sondern ein sehr besonderes Gut.
Darüber hinaus möchte ich meinen Laborassistentinnen Heike Haloff-Buestrich, Tatjana Jahner, Doris Melchner, Petra Störtebecker, Martina Domani und Regina Lindner sowie meiner Kollegin Angelika Bauer danken, die mich jahrelang motiviert haben und mir Rückhalt boten.

## Abstract

The translocator protein (18 kDa) (TSPO) is a highly conserved, ubiquitous protein with a high affinity in binding cholesterol. Located in the outer mitochondrial membrane (OMM), TSPO has been discussed as the key protein for the cholesterol transport and therefore as a critical factor in steroidogenesis for a long time. Since recent *in vivo* and *in vitro* studies using TSPO knock-out models have been refuting its role in steroidogenesis, it is still an open question if TSPO is involved in neurosteroidogenesis. Furthermore, studies of the last two years started to characterize TSPO as a key protein in mitochondrial metabolism, assuming that TSPO has a regulatory function in calcium ($Ca^{2+}$) homoeostasis, glucose homoeostasis, mitochondrial respiration and ROS (reactive oxygen species) production. In this thesis the link between TSPO and the regulation of mitochondrial metabolism and neurosteroid synthesis was analyzed to characterize a possible role of TSPO.

In order to ascertain a possible involvement of TSPO in neurosteroidogenesis, a TSPO knock-down in mouse brain cells was performed to measure pregnenolone concentration as a precursor of neurosteroid synthesis by means of ELISA technique (enzyme-linked immunosorbent assay) and GC/MS (gaschromatography/mass spectroscopy). I was able to show that TSPO regulates neurosteroid synthesis of brain microglia cells.

The regulatory function of TSPO in mitochondrial $Ca^{2+}$ homoeostasis was analyzed by means of $Ca^{2+}$ imaging via FURA-2 dye. The results showed no significant differences in $Ca^{2+}$ homoeostasis of TSPO knock-down and scramble cells. Using drug treatment, both TSPO agonists XBD173 and PK11195 showed TSPO unrelated effects. Only LPS and Ro5-4864 treatment lead to the assumption that the presence of TSPO might be necessary to protect the cell from cell death under special conditions.

Considering TSPO as a regulatory protein of the mitochondrial energy metabolism, the mitochondrial membrane potential was analyzed under different conditions using the ratiometric JC-1 dye. My results show a direct link between the TSPO knock-down and the significantly reduced energy state of the cell.

To further characterize TSPO as a regulator of the mitochondrial energy metabolism, the respiration was analyzed by means of High Resolution Respirometry via

Oxygraph O2k. As a result I found a direct link between TSPO knock-down and an increased maximal respiration indicating the high energy demand of the cell.
This thesis describes the controversial role of TSPO in steroidogenesis according to new findings and characterizes the function of TSPO as a regulatory protein in neurosteroidogenesis. Moreover, this thesis presents new insights for TSPO as a regulatory protein in the mitochondrial metabolism.

## Translation of the Abstract (German)

Das Translokatorprotein (18 kDa) (TSPO) ist ein hochkonserviertes, ubiquitäres Protein mit einer hohen Bindungsaffinität gegenüber Cholesterol. TSPO, was in der äußeren Mitochondrienmembran lokalisiert ist, wurde lange Zeit als Schlüsselprotein für den Cholesterintransport und somit als kritischer Faktor für die Steroidsynthese diskutiert. Doch die jüngsten *in vivo*- und *in vitro*-Studien, die vor allem auf genetischen TSPO Knock-out Modellen basieren, widerlegen sehr eindeutig diese Rolle von TSPO als Schlüsselprotein in der Steroidsynthese. Dennoch ist es gegenwärtig nicht geklärt, ob TSPO an der Neurosteroidsynthese beteiligt sein könnte. Darüber hinaus begannen Forscher in den letzten zwei Jahren, TSPO als ein Schlüsselprotein auf einem neuen Gebiet, dem mitochondrialen Stoffwechsel, zu charakterisieren. Dabei wurde untersucht, ob TSPO eine regulatorische Funktion im mitochondrialen Stoffwechsel übernimmt. Darunter zählen unter anderem die Kalzium-Homöostase, der Blutzuckerstoffwechsel, die mitochondriale Atmung und die Entstehung reaktiver Sauerstoffspezies.

In dieser Arbeit wurde die Verbindung zwischen TSPO und der Regulation des mitochondrialen Metabolismus sowie der Neurosteroidsynthese analysiert, um die Rolle von TSPO in diesem Gebiet zu charakterisieren.

Um eine mögliche Beteiligung von TSPO an der Neurosteroidsynthese zu ermitteln, wurde ein TSPO-Knock-down in BV-2 Mikrogliazellen durchgeführt, um die Konzentration von Pregnenolon (Ausgangsstoff für die Neurosteroidsynthese) mittels ELISA-Technik (enzymgebundenes, antikörperbasierte Nachweisverfahren) und GC / MS (Gaschromatographie / Massenspektroskopie) zu bestimmen. Ich konnte zeigen, dass TSPO die Neurosteroidsynthese von BV-2 Mikrogliazellen reguliert.

Um die regulatorische Funktion von TSPO in der mitochondrialen Kalzium-Homöostase zu untersuchen, wurde der Kalzium Haushalt von BV-2 Scramble Zellen und BV-2-TSPO-Knock-down Zellen mittels eines Bildgebungs-Experimentes (Calcium Imaging via FURA-2-Farbstoff) analysiert. Die Ergebnisse zeigten keine signifikanten Unterschiede im Kalzium-Stoffwechsel von BV-2-TSPO-Knock-Down und BV-2 Scramble Zellen. Nach einer medikamentösen Behandlung mit ausgewählten Substanzen zeigten XBD173 und PK11195 (TSPO-Agonisten) lediglich TSPO-unabhängige Effekte. Nur die Ergebnisse der LPS- und Ro5-4864-

Behandlung führen zu der Annahme, dass die Anwesenheit von TSPO erforderlich ist, um die Zelle unter besonderen Bedingungen vor dem Zelltod zu schützen.
Weiterhin wurde TSPO als regulatorisches Protein des mitochondrialen Energiestoffwechsels betrachtet. Dafür wurde das mitochondriale Membranpotential unter verschiedenen Bedingungen unter Verwendung des ratiometrischen JC-1-Farbstoffs untersucht. Die Ergebnisse zeigen, dass ein TSPO-Knock-down mit einem reduzierten Energiezustand der Zelle (somit erhöhter Energiebedarf) einhergeht.
Zur weiteren Charakterisierung des regulatorischen Einflusses von TSPO auf den mitochondrialen Energiestoffwechsel, wurde die mitochondriale Atmung mittels zwei verschiedenen Methoden, des hochauflösenden Respirometers Oxygraph O2k und des Seahorse Flux Analyzers analysiert. Als Ergebnis war eine direkte Verbindung zwischen dem TSPO-Knock-down und einer erhöhten maximalen Respiration zu erkennen, die wiederum mit dem hohen Energiebedarf der Zelle einhergeht.
Diese Dissertationsarbeit untersucht und charakterisiert die Funktion von TSPO als regulatorisches Protein in der Neurosteroidsynthese und die darüber hinaus erlangten, neuen Erkenntnisse über TSPO als regulatorisches Protein im mitochondrialen Stoffwechsel.

# 1 TSPO 18kDa - a controversial protein of the OMM

The discovery of TSPO as an alternative binding site for the benzodiazepines in 1977 resulted in being named the peripheral benzodiazepine receptor (PBR) (Braestrup & Squires, 1977). The versatile TSPO expression throughout the entire body (Li et al., 2015) and the early discovery as a high-affinity cholesterol binding protein in the OMM (Li & Papadopoulos, 1998) established a link between TSPO, cholesterol transport and biosynthesis of steroids (Papadopoulos et al., 1997); (Rupprecht et al., 2010). Papadopoulos et al. described TSPO as an essential component of the cholesterol transport across the mitochondrial membrane, thereby providing the rate-limiting step of steroid production. Thus, almost 30 years after its discovery the PBR was renamed into Translocator protein 18 kDa (TSPO 18kDa) due to the new findings about its molecular function in cholesterol translocation (Papadopoulos et al., 2006). For a long period of time TSPO was discussed as the critical factor in steroidogenesis and TSPO knock-out in mice were reported as being early embryonically lethal (Papadopoulos et al., 1997). This believe based on a single study from 1997, using TSPO whole-body knock-out mice, unfortunately this study did neither provide any details about the used methods nor about the design of the knock-out mice (Papadopoulos et al., 1997). Recently, TSPO as the key player in steroid synthesis has been called into doubt. Kelly-Hershkovitz et al. indicated in 1998 the very first assumptions of steroid synthesis underlying TSPO function may be incorrect, requiring further examination (Kelly-Hershkovitz et al., 1998). More recent studies using global KO mice or steroidogenic-tissue-specific KO mice revealed unexpected results: a genetic TSPO deficiency or loss has no effects on steroid biosynthesis (Morohaku et al., 2014) or embryonic growth nor does it lead to phenotypic abnormalities (Tu et al., 2014); (Banati et al. 2014). Most surprisingly was the examination of a human adrenal cell line which did not express endogenous TSPO, but was still competent in producing steroids (Tu et al, 2014). This led to a reappraisal of TSPO's biological role in steroid synthesis and its importance throughout the body (Selvaraj & Tu, 2016).

## 1.1 Expression of TSPO

TSPO 18 kDa is a highly conserved protein found in every organ of mammals (Anholt et al., 1985) and also in bacteria (Yeliseev & Kaplan, 1995). However, the particularly

highest expression levels have been found in steroid-synthesizing cells and tissues of adrenal glands, gonads, placenta, testis (De Souza et al., 1985) (Papadopoulos et al., 2006). This was basically the link of numerous studies attempting TSPOs function to steroidogenesis (Papadopoulos et al., 1997), undermining that TSPO is not solely expressed in steroid-synthesizing cells or tissues. An abundant TSPO expression was found in cells and tissues which do not produce steroids such as heart, kidney (Gehlert et al., 1985), lung, liver, spleen and bone marrow (Anholt et al., 1985) suggesting a broader function for this protein.

TSPO expression in the CNS is extremely weak (Daugherty et al., 2013) and focused on microglia (Casellas et al., 2002) and reactive astrocytes (Maeda, et al., 2007). The expression levels in the CNS, primarily in brain microglia cells (Banati et al., 1997) readily increase when exposed to pathological stressors or physicochemical abnormalities (Rupprecht et al., 2010). For over 20 years, TSPO has been used as an imaging biomarker of active disease or disease-related tissue (Liu et al., 2014a). Therefore, radiolabeled TSPO ligands are used in positron emission tomography (PET) to image the increased TSPO expression in areas of neuroinflammation in vivo in patients with brain diseases (Vivash & O'Brien, 2016).

More precisely, TSPO is an integral membrane protein of 169 amino acids located at the contact sites between the outer (OMM) and inner mitochondrial membrane (IMM) (Anholt et al., 1986). However, its expression has also been reported in the nucleus (Hardwick et al., 1999) and on the erythrocyte membrane (Olson et al., 1988) whereby none of these two alternative localizations have been verified. Due to its localization in the mitochondrial membrane TSPO is now thought to partake in the regulation of mitochondrial functioning (Gatliff & Campanella, 2012); (Selvaraj & Tu, 2016).

## 1.2 TSPO structure and resulting functions

In 1993 a TSPO 3D structure was modeled, deriving from a seven-transmembrane rhodopsin structure, which was almost the only membrane protein structure available at this time. This 3D structure spanned only one mitochondrial phospholipid layer (Bernassau et al., 1993). Later, a murine TSPO protein structure replaced the early model and described the presence of at least five-alpha-helical transmembrane segments (Murail et al., 2008). Two years later, an electron cryo-microscopy study revealed a five-transmembrane structure of Rhodobacter sphaeroides TSPO

(RsTSPO) (Korkov et al, 2010) which is assumed to build TSPO homo dimers. This model favored speculations about TSPO acting as a channel with a hydrophobic interior core, lined by the cholesterol-binding CRAC (cholesterol-recognition amino acid consensus) motif. This aspect underlined the assumption of TSPO playing a role in translocation of lipophilic substrates – especially cholesterol – across the OMM thereby representing the rate-limiting step in steroidogenesis (Rupprecht et al., 2010).

The most recent 3D high-resolution structure of mammalian TSPO was obtained by means of nuclear magnetic resonance (NMR) technique whereupon TSPO was reconstituted into dodecylphosphocholine (DPC) micelles and complexed with its high-affinity ligand PK11195 (Jaremko et al., 2014). This study of Jaremko et al. opened new perspectives in TSPO structure (Jaremko et al., 2014).

### 1.3 Recent TSPO structure

The TSPO structure comprises 169 amino acids which are organized in five transmembrane helices (TM1 to TM5) tightly packed in a clockwise order TM1-TM2-TM5-TM4-TM3 when viewed from the cytosol (Jaremko et al., 2014). The loops between the transmembrane helices are short, with the exception of the TM1-TM2 loop (Jaremko et al., 2014). Because of the high sequence conservation of TSPO, the topology of the structure is likely to be retained in other mammalian species as well as bacterial homologs (Jaremko et al, 2014).

The TSPO structure also owns an N- and a C-terminal tail, whereby the C-terminus in TM5 is equipped with the cholesterol-recognition amino acid consensus (CRAC) motif binding cholesterol in nanomolar concentration (Jamin et al., 2005). The 3D structure of Jaremko et al. revealed that the side chain including CRAC motif do not form a channel-like core for cholesterol binding and translocation as previously assumed (Rupprecht et al., 2010), rather they are located on the outside of the TSPO structure pointing towards the membrane area.

Furthermore, they investigated a highly positive charge of the CRAC motif side chain and positively and negatively charged patches on the IMS side of the receptor. These different charged areas on the extra- and intra-mitochondrial side might be important for recognition of endogenous ligands and proteins interacting with TSPO (Jaremko et al, 2014).

All these findings indicate a fundamental doubt in the ability of TSPO to form a cholesterol translocating channel. Jaremko et al. attempted to explain this phenomenon by the (already known) ability of cholesterol to dimerize (Harris, 2010) which further may modulate the oligomerization of TSPO thereby forming a channel. This assumption was based on a study of several transporters which function as dimers (Morrison & Henzler-Wildman, 2012). Furthermore, a TSPO oligomerization was demonstrated through covalent tyrosine cross-links under unique circumstances, rather than based on cholesterol dimerization (Delavoie et al., 2003).
The most recent study about TSPO structure demonstrates that the amino acids N158–S159, which are part of the cholesterol binding CRAC motif are disordered in the absence of PK11195, but show a stable helical conformation upon PK11195 binding. Further, it is assumed that a conformational stabilization of the CRAC motif might influence the interaction of mammalian TSPO with cholesterol. However, a 3D structure of TSPO in complex with cholesterol is not available to date and it is unknown if cholesterol binding might vice versa modulate binding of ligands to a binding site (Jaremko et al., 2015b).

### 1.4 TSPO ligands

TSPO ligands have a potential for diagnostic and therapeutic applications which makes TSPO a topic of natural interest for pharmacologists (Arbo et al., 2015). The best-characterized synthetic ligand of TSPO is the isoquinoline carboxamide PK11195 (N-butan-2-yl-1-(2-chlorophenyl)-N-methylisoquinoline-3-carboxamide), which binds to TSPO with nanomolar affinity in many species (Fur et al., 1983); (Owen & Matthews, 2011). PK11195 is used as a TSPO ligand in positron emission tomography to visualize brain inflammation in patients with neuronal damage (Owen & Matthews, 2011). The binding was found to be in a 1:1 stoichiometry between TSPO and PK11195 and is described as a binding pocket formed by TSPOs five transmembrane helices in the upper cytosolic part of the helical bundle (Jaremko et al., 2014). Additionally, it is already known, that the PK11195 ligand-binding site is flexible and instable in the absence of PK11195 binding, but stabilized in a rigid and stable conformation when PK11195 is bound (Jaremko et al., 2015b). Interestingly, PK11195 is able to inhibit the neurosteroid-inducing effects of other TSPO binding drugs like FGIN-1-27 (Korneyev et al., 1993), indoleacetamides (Kozikowski et al.,

1993), YL-IPA08 (Zhang et al., 2014), CB-34 (Serra et al., 1999), and TTN (Do-Rego et al., 1998).

Another predominantly investigated synthetic TSPO ligand is the diazepam derivate Ro5-4864 (7-Chloro-5-(4-chlorophenyl)-1-methyl-3H-1,4-benzodiazepin-2-one) which also binds TSPO with nanomolar affinity, whereby the binding affinity is higher for PK11195 ($K_d < 20$ nM) (Fur et al., 1983). It was former known as a convulsant (Weissmann et al., 1983) and anxiogenic substance (File & Lister, 1983) and was discussed as a TSPO agonist (Fur et al., 1983), (Selvaraj & Tu, 2016). Now it is used as a potent imaging ligand (Weissmann & Raveh, 2003) and recently assumed to be a neuroprotective agent (Palzur et al., 2016).

In the last 25 years, additional TSPO ligands, such as alpidem, have been developed. They also bind to both TSPO and the $GABA_A$ receptor. Alpidem was already officially admitted for anxiety treatment from 1991-1994, but was finally withdrawn due to leading to liver dysfunction with severe or even lethal consequences (Baty, et al., 1994). There might be a significant correlation between these side effects and the $GABA_A$ receptor binding in liver tissue (Langer et al., 1990). DAA1106 is another selective TSPO ligand binding with sub-nanomolar affinity (Venneti et al., 2007). There are many more synthetic ligands (Rupprecht et al., 2010), most of which have been developed as neuroimaging agents and diagnostic tools, used to detect regions of neuroinflammation, correlating with various neuronal pathologies (Chauveau et al., 2008). XBD173, also termed as AC-5216 or emapunil, is a selective TSPO phenylpurine ligand. XBD173 is known to bind with high affinity to TSPO, thereby exerting anxiolytic, antidepressive, and neuroprotective effects (Kita et al., 2009), (Kita et al., 2004), (Qui et al., 2013). Another established TSPO ligand is the benzoxazine etifoxine, which also binds with a high affinity to TSPO, thereby stimulating neurosteroid synthesis (Verleye et al., 2005), (Wolf et al., 2015). Etifoxine is not only selective for TSPO, but also binds to $GABA_A$ receptors (Hamon et al., 2003). The anxiolytic etifoxine effect may result from direct targeting $GABA_A$ receptors (Nguyen et al., 2006).

Furthermore, several endogenous ligands for TSPO exist, such as diazepam-binding inhibitors (DBIs), porphyrins and cholesterol. The TSPO amino acid sequence consists of the cholesterol-binding amino acid consensus (CRAC) motif suggesting a molecular mechanism for cholesterol binding and/or transport (Li et al., 2001). This

led to a model of TSPO as a cholesterol transport channel in the OMM playing an indispensable role in steroidogenesis (Papadopoulos et al., 1997).

In 1991, TSPO was reported to interact with the diazepam-binding inhibitor (also known as the Acyl-CoA binding protein/ACBP), which was assumed to stimulate steroid production at very modest levels (Papadopoulos et al., 1991). DBIs bind with micromolar affinity to both TSPO and the $GABA_A$ receptor.

Porphyrins, which are tetrapyrrolic pigments and important in heme biosynthesis pathways, are considered endogenous ligands binding TSPO (Verma et al.1987). The highly conserved porphyrin binding property of TSPO (Zhao et al., 2016) was initially assumed to partially rescue cells from porphyrin induced phototoxicity (Ratcliffe & Matthews, 1995). Although the ability of PPIX binding to TSPO remains unchanged, recent studies using TSPO knockout mice/cell lines have established that TSPO plays no critical physiological role related to PPIX and heme biosynthesis (Banati et al. 2014; Zhao et al. 2016).

## 2 New perspectives for TSPO

In regard to the above-mentioned experimental observations of the last three years the role TSPO in steroidogenesis is questionable. As various TSPO knock-out studies allowed deeper insight in TSPO function, a genetic TSPO deletion does not affect steroidogenesis (Morohaku et al., 2014), (Tu et al., 2014), (Banati et al., 2014), (Šileikytė et al., 2014). Moreover, these observations led in the assumption that previous pharmacological effects on steroidogenesis, mostly obtained by the use of TSPO ligands, could be unspecific or unrelated to TSPO (Tu et al., 2015), (Šileikytė et al., 2014). Although these early ligand studies helped to figure out structural, biochemical and pharmacological information, the precise physiological and pathological function is still unknown (Selvaraj & Stocco, 2015), (Gatliff & Campanella, 2016), (Selvaraj & Tu, 2016).

Since these TSPO knock-out models refuted the role of TSPO in steroidogenesis, there is still an open question of TSPO involvement in neurosteroidogenesis (Selvaraj & Tu, 2016). Additionally, there is some indication for a role of TSPO in calcium homoeostasis (Gatliff & Campanella, 2012), mitochondrial respiration (Banati et al., 2014), stress response in relation to ROS (Gatliff et al., 2014) and other bioenergetic

parameters reflecting mitochondrial health (Gatliff & Campanella, 2016), (Tu et al., 2016).

## 2.1 TSPO in neurosteroid synthesis of brain mitochondria

Steroid biosynthesis is mainly performed by adrenal, gonads, placenta, thymus, skin and brain. In these tissues mitochondria are able to produce steroids *de novo* from a precursor molecule. While it is known that e.g. both, adrenal and gonadal steroid production is regulated by hormones, there is still no evidence for hormone regulation in neurosteroid synthesis (Papadopoulos, 2014).

The precursor molecule of the neurosteroid synthesis is cholesterol (figure 1). As a free molecule, it is located in various intracellular stores e.g. the endoplasmatic reticulum (ER). However, it can also be found in cellular membranes as structural cholesterol. The slightly water-soluble molecule needs special mechanisms to get from intracellular stores to the OMM, where it stays segregated from structural cholesterol. Cholesterol is then being transported from the OMM to cytochrome P450 CYP11A1 in the inner mitochondrial membrane (IMM) (Papadopoulos, 2014) which mediates a conversion from cholesterol to pregnenolone (figure 1).

In a further step, pregnenolone, the precursor of all neurosteroids, is enzymatically metabolized into progesterone. Progesterone, on the one hand is metabolized by 5α-reductase into 5α-dihydroprogesterone (5α-DHP) and afterwards converted into allopregnanolone (3α,5α-THP) by 3α-hydroxysteroiddehydrogenase (3α-HSD). On the other hand, progesterone is also metabolized into deoxycorticosterone (DOC) by 21-hydroxylase followed by a 5α-reductase oxidation into 5α-dihydrodeoxycorticosterone (5α-DHDOC). Then, a 3α-hydroxysteroiddehydrogenase (3α-HSD) converts 5α-DHDOC into tetrahydrodeoxycorticosterone (THDOC) (figure 1). Both, allopregnanolone and THDOC are neurosteroids acting on the $GABA_A$ receptor, thereby causing in vivo anxiolytic effects (Stoffel-Wagner, 2003), (Pinna et al., 2006).

Since more than half a decade, researchers have been trying to figure out the exact mechanism transferring cholesterol from intracellular stores to OMM, moving cholesterol from OMM to IMM, and finally connecting cholesterol with CYP11A1.However, today still no specific mechanism is known to carry out all these steps. Only a few proteins have been discovered, which may work together in a large protein complex and may perform these functional steps.

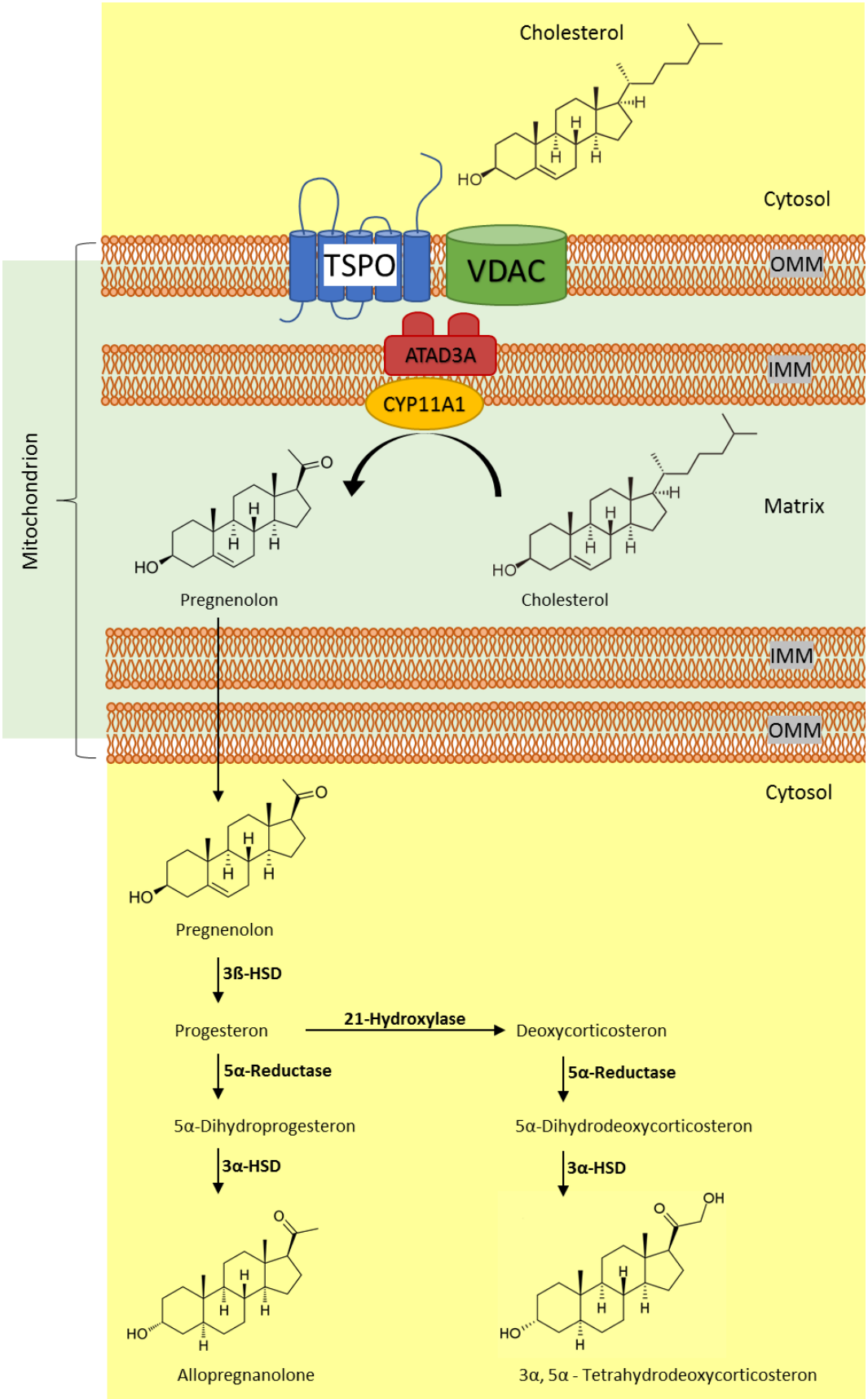


**Figure 1 The role of TSPO in neurosteroid synthesis. TSPO is hypothetically associated with other proteins such as VDAC (voltage dependent anion channel) and ATAD3A (AAA domain containing 3A) in the IMM (inner mitochondrial membrane). Cholesterol binds to the CRAC Domain of TSPO and is then translocated to the IMM. This translocation only works through a multi protein complex (transducteosome) with VDAC and the mitochondrial matrix protein ATAD3A. The mechanism in detail is still under investigation. Cholesterol is then metabolized to pregnenolone by CYP11A, which is the neurosteroid precursor molecule.**

This hypothetical protein complex includes the steroidogenic acute regulatory protein (StAR), the translocator protein 18kDa (TSPO), and the voltage-dependent anion channel (VDAC) (Papadopoulos, 2014). For a long time, TSPO was considered to form a channel (Rupprecht et al., 2010) promoting the transport of cholesterol into the mitochondrial matrix, the rate-limiting step in neurosteroid synthesis. The early crystal structure of TSPO, which explains the role of TSPO in cholesterol transport as a kind of sliding mechanism, was discovered by new investigations. This sliding mechanism through the external protein surface requires the association of TSPO with other proteins (Li et al., 2015).

Rone et al. hypothesized the cholesterol transfer through a complex named the “transduceosome”. In this transduceosome, cytosolic StAR pushes the cholesterol transport to OMM by interacting with OMM proteins such as TSPO and VDAC (Bose et al., 2002). Afterwards, the cholesterol transfer from OMM to IMM is supposed to be accomplished via a bridging complex between the VDAC in the OMM and adenine nucleotide translocase (ANT) in the IMM (Thomson, 2003). In a later study, blue native page analysis on steroidogenic tissue mitochondria identified two protein complexes, namely a 66 kDa and an 800 kDa protein complex, both binding cholesterol. A breakdown of these complexes provided the evidence that the 800 kDa protein complex contains the OMM components of the transduceosome: TSPO, VDAC, the matrix protein ATAD3A and the IMM protein CYP11A; but not ANT, as supposed before (Papadopoulos et al., 2015). The experimental addition of StAR protein to this 800 kDa complex resulted in an increase of cholesterol binding and an increase in steroid formation. Consequently, StAR was required to initiate the transport of cholesterol to the IMM and VDAC might act as an anchor for TSPO and StAR. The matrix protein ATAD3A is assumed to form the bridge between OMM and IMM, which allows cholesterol to access to CYP11A1 in the IMM (figure 1) (Rone et al., 2012). The 66 kDa protein complex consists of TSPO and other proteins. In case of being stimulated, TSPO assembles to trimers and associates with the 800 kDa complex, where it is then co-located with VDAC. The StAR protein gathers cholesterol and induces the binding to TSPO. From there, cholesterol is translocated to the IMM through the formation of a contact site by VDAC and the mitochondrial matrix protein ATAD3A present in the 800 kDa complex. Cholesterol is then metabolized to pregnenolone by CYP11A1 (also present in the IMM part of the 800

kDa complex), supported by the electron transfer proteins ferredoxin and ferredoxin reductase. This forms the mitochondrial metabolon (Rone et al., 2012).

Some studies found ANT to be the bridging protein which forms a contact site between OMM and IMM proteins to transport cholesterol (Thomson, 2003). However, it was shown in MS (mass spectroscopy) and FRET studies (fluorescence resonance energy transfer studies, which are used to determine if two fluorophores are within a certain distance to each other) (Rone et al., 2012) that ANT is not part of the protein complex, which promotes cholesterol transport and steroid formation. ATAD3A, which is located in the OMM, bridges the OMM and IMM and forms a contact site (Gilquin et al., 2010). A knockdown of this protein decreases steroid production assuming that cholesterol can neither pass the intermembrane space nor reach the IMM (Rone et al., 2012). The long isoform of ATAD3A, which may connect with other organelles such as the endoplasmic reticulum (ER) may form mitochondria-ER contact sites (Hubstenberger, 2008). These contact sites, termed “mitochondria associated membranes” (MAMs), play an important role in the transfer of lipids such as cholesterol. MAMs may establish a link between CYP11A1 and the site of cholesterol biosynthesis in the ER. VDAC also plays a role in MAM formation as it interacts with the inositol-1,4,5-triphosphate receptor in the ER, which is responsible for $Ca^{2+}$ transfer. Studies showed that increased $Ca^{2+}$ concentration in the matrix regulates the enzymes of the Krebs cycle. Especially isocitrate dehydrogenase is found in both, the 66 kDa and 800 kDa mitochondrial complexes, further providing nicotinamide adenine dinucleotide phosphate (NADPH). NADPH is used by ferredoxin reductase for the electron transport chain for CYP11A1 activity (Bernadi P., 1999). Further, this increased activity augments ATP production which is necessary for ATAD3A and mitochondrial function (Rone et al., 2012).

## 2.2 TSPO in mitochondrial $Ca^{2+}$ homoeostasis

It was already shown in 1960 that isolated mitochondria are able to accumulate $Ca^{2+}$ (Vashington & Murphy, 1962). Since it is known that mitochondria act at some neuronal synapses to store $Ca^{2+}$ or release $Ca^{2+}$ persistently from the mitochondrial matrix, brain mitochondrial $Ca^{2+}$ signaling receives more attention. Thereby mitochondria contribute to neurotransmitter release from the presynaptic site (Jonas, 2006). Moreover, $Ca^{2+}$ excess in cellular or mitochondrial space triggers apoptosis. $Ca^{2+}$ operates as an important second messenger regulating a variety of cellular

functions such as contraction, secretion, metabolism, gene expression, cell survival and cell death (Berridge M. J., 2012).

During mitochondrial $Ca^{2+}$ accumulation under physiological conditions, mitochondria have just a 10 – 30 nanometer distance to the ER resulting in close proximity to the $IP_3R$ receptors of the ER (Rizzuto et al., 1998).

High levels of $IP_3R$ and SERCA have been found in the ER at these special contact sites to mitochondria creating $Ca^{2+}$ micro domains. On the mitochondrial side, VDAC may perform the $Ca^{2+}$ uptake in mitochondria (Gincel et al., 2001). The proven correlation between VDAC expression level and the transfer efficiency of $Ca^{2+}$ micro domains from the ER to mitochondria relies on studies showing that VDAC overexpression increases $Ca^{2+}$ permeability at ER-mitochondria contact sites, mitochondrial $Ca^{2+}$ accumulation, and $Ca^{2+}$ transfer between the two organelles (Rapizzi et al., 2002). VDAC is also co-located with $IP_3R$'s and the glucose-regulated protein 75 (Grp-75) as a complex at the ER-mitochondria contact sites. This is possibly the link between VDAC and $IP_3R$ (Szabadkai et al., 2006).

With regard to these findings, the mitochondrial $Ca^{2+}$ accumulation and release under conditions of a direct ER-mitochondria link is possible, but there are still unknown participants. TSPO could have an outstanding role as a linking position, closely located to VDAC at the ER-mitochondria contact sites (Gatliff & Campanella, 2012). Recently, there is only little evidence that TSPO plays an important role in the $Ca^{2+}$ homoeostasis:

It has been shown that TSPO is also expressed in mitochondria of human colon cancer cells (HT-29). The high-affinity TSPO ligand PK11195 promotes a rapid intracellular $Ca^{2+}$ increase in a dose-dependent manner. This increase is unaffected by extracellular $Ca^{2+}$ and flunitrazepam (a partial TSPO agonist and inhibitor of TSPO's cholesterol transport function). Ostuni et al. assumed this PK11195-induced $Ca^{2+}$ increase as an indicator for the involvement of TSPO in the process of elevating the $Ca^{2+}$ concentration (Ostuni et al., 2007). However, flunitrazepam is only a partial agonist for TSPO. Moreover, a role for TSPO regulating $Ca^{2+}$ homoeostasis has been figured out in isolated rat heart mitochondria. Protoporphyrin IX (PPIX), a high-affinity TSPO ligand, decreases mitochondrial $Ca^{2+}$ uptake dose-dependently. Another study by the same group showed PPIX affecting the function of VDAC. A VDAC-TSPO-ANT complex reconstruction into lipid bilayers, which was then exposed to PPIX, showed decreased VDAC conductance. This finding provides first evidence that

TSPO may modulate mitochondrial $Ca^{2+}$ homeostasis, and thereby other mitochondrial processes (Tamse et al, 2008).

## 2.3 TSPO in mitochondrial respiration

While only 2% of the total body weight is occupied by our brain, the brain requires up to 20% of the energy - even in the resting state. This energy is necessary for the neurotransmitter inclusion in synaptic vesicles, the presynaptic vesicle transfer and the postsynaptic signaling (Ly et al., 2006). Furthermore, energy is used for the maintenance of ion gradients across neuronal membranes, intracellular signaling and gene transcription as well as epigenetic gene regulation (Mattson et al., 2008).
Being the main producers of energy in form of ATP, mitochondria are the powerhouse of the cell (Campanella et al., 2009).
The first step of aerobic respiration is the aerobic glycolysis of glucose into pyruvate and the conversion of fatty acids into fatty-acyl-CoA. Due to this permeability of the OMM, pyruvate and fatty-acyl-CoA are transferred to the mitochondrial intermembrane space (IMS) and then imported into the mitochondrial matrix (Lodish et al., 2013). In the mitochondrial matrix, the pyruvate and fatty-acyl-CoA are converted into acetyl CoA, which is necessary to drive the citric acid cycle (Lodish et al., 2013). The electrons, gathered from this conversion are then moving through a series of IMM bound electron carriers, called electron transport chain (ETC) to $O_2$, thereby regenerating $NAD^+$ and FAD (Lodish et al., 2013). This stepwise movement of electrons is coupled to a proton ($H^+$) pumping activity across the inner membrane, which results in an electrochemical $H^+$ gradient crossing the IMM (Lodish et al., 2013).
The gradient forms a proton motive force which powers ATP synthesis and generates most of the ATP resulting from aerobic oxidation of glucose (Lodish et al., 2013). The proton motive force (pmf) across the IMM depends on a combination of two factors, a pH gradient and a membrane potential ($\Delta\psi m$). The pmf is necessary for oxidative phosphorylation (OXPHOS), electron transport and ATP formation (Lodish et al., 2013).
On their way from NADH and $FADH_2$ to the electron acceptor $O_2$ electrons pass four large multiprotein complexes.These complexes form the ETC (Gatliff et al., 2012). Energy sourced from the ETC is used to pump protons outward the matrix generating the pH gradient and the membrane potential (Lodish et al., 2013). As described by

Peter Mitchell in his chemiosmotic hypothesis, the proton-motive force is the ultimate source of energy for ATP synthesis. The enzyme, which ensures the ATP production, ATP synthase or $F_0F_1$ complex, is highly conserved across species (Lodish et al., 2013).

Findings of VDAC reconstitution into planar phospholipid membranes provide compelling evidence that voltage-gating via VDAC selectively controls ATP/ADP flow between mitochondria and cytosol (Colombini, 2012). VDAC voltage-gating also controls the mitochondrial import of inorganic phosphate (Hodge & Colombini, 1997). As a result it is assumed that VDAC facilitates the transport of ADP, ATP, respiratory substrates, inorganic phosphate, organic anions as well as small cations like $K^+$, $Na^+$ and $Ca^{2+}$ thereby enabling the mitochondrial function and energy supply (Lemasters & Holmuhamedov, 2006). However, the regulatory mechanisms of VDAC remain controversial. A long missing player in the regulation of VDAC's OMM permeability was tubulin, a cytoskeleton protein. Carre et al. showed an association of mitochondrial tubulin with VDAC. It has already been published that, depending on VDAC`s phosphorylation state and applied voltage, nanomolar concentrations of dimeric tubulin induce functionally important reversible blockage of VDAC reconstituted into planar phospholipid membranes (Carre et al., 2002). A later analysis demonstrated that the VDAC-blocked state is impermeable to ATP and other multi-charged anions (Rostovtseva et al., 2012) and it reduces the respiration rate (Rostovtseva et al., 2008). According to this, the tubulin-VDAC interaction can be regulated through a competition with other proteins, correlated to VDAC (Gatliff & Campanella, 2012). An example for this is the OMM protein TSPO, localized in close proximity to VDAC, and prevalent at IMM-OMM contact sites. In primary microglia TSPO knock-out cells it has been demonstrated that the basal oxygen consumption was significantly reduced in comparison to wild-type cells. Consequently, TSPO might function as a modulator of cellular energy metabolism (Banati et al., 2014).

There is evidence demonstrating TSPO's involvement in mitochondrial metabolism. The respiration of mouse C1300 neuroblastoma cells was analyzed using TSPO ligands. In a study cells were incubated with Ro 5-4864 and PK11195 which resulted in a dose dependent reduction of oxygen consumption in these cells (Larcher et al., 1989).

Another group isolated rat kidney mitochondria to treat each sample 24h with nine different TSPO ligands to investigate the respiratory function. The applied TSPO ligands, in particular Ro 5-4864 and PK11195 decreased the rate of oxidative phosphorylation (OXPHOS, triggered by addition of ADP) and increased the rate of state IV respiration (the rate arising when all available ADP is phosphorylated to ATP) (Hirsch et al., 1989). As a result, these findings corroborate a mitochondrial energy metabolism model in the outer mitochondrial membrane. In this model TSPO might interact with VDAC, altering VDAC permeability to ADP, $P_i$ and ATP (Gatliff & Campanella, 2012).

Recent studies using cells or mitochondria of genetic TSPO knock-out mice achieved different results. Šileikytė et al. compared the oxygen consumption rates (OCRs) of mitochondria from liver-specific $Tspo_{c\Delta/\Delta}$ mice and control $Tspo_{fl/fl}$ mice which showed no differences in the OCR's of those cells (Šileikytė et al., 2014). Another group analyzed the OCR of embryonic fibroblasts from $Tspo_{-/-}$ mice which showed decreased values compared to $Tspo_{fl/fl}$ mice (Zhao et al. 2016). Tu et al. showed that the OCR in steroidogenic MA-10 leydig cells (expressing very high levels of TSPO) showed no difference when compared to TSPO-deleted MA-10 cells (Tu et al. 2016).

First evidence of a TSPO oxygen regulation in brain cells was found in isolated primary microglia cells of TSPO knock-out mice. The OCR was significantly lower in TSPO knockout cells compared to control microglia (Banati et al. 2014).

These studies indicate that the change in OCR is a cell-type dependent effect which might correlate with the energetic status of cell, mitochondrial ion signaling or ROS damage. Interestingly, mitochondria of brain cells were particularly affected by TSPO knock out (Banati et al. 2014), indicating a special role of TSPO in brain microglia metabolism.

### 2.4 TSPO in mitochondrial energy metabolism, inflammation and protection

With regard to several recent studies indicating that TSPO has no physiological function in steroidogenesis raises the critical question of the reason for its high expression level in mitochondria of steroidogenic tissue. Tu et al. identified TSPO affecting fatty acid oxidation (FAO) by investigating different mitochondrial properties in TSPO-deficient steroidogenic MA-10 cells. Further they observed an up-regulation of genes involved in mitochondrial FAO in the adrenal glands of TSPO knock-out mice. These recent findings might indicate a novel TSPO function in modulating

mitochondrial metabolism which is important for lipid storage and metabolism (Tu et al., 2016). Moreover, the recent increase in obesity research and the associated use of quantitative trait loci analysis between inbred mouse strains identified TSPO 18 kDa as one of the 6 possible genes which are able to influence mice triglyceride metabolism (Leduc et al., 2011).

Not only for lipid metabolism, but also for the whole energy metabolism, maintained through the ETC, TSPO is important. Liu et al. successfully transfected TSPO in Jurkat cells which show a low to absent endogenous TSPO expression. They figured out that a set of genes which is involved in the ETC of mitochondrial energy production are up-regulated in the transfected Jurkat cells. Furthermore, this up-regulation correlates with an increased mitochondrial ATP synthesis and an increase in cell excitability by decreased rectified $K^+$ channel currents and with an increase in cell proliferation and motility. This increased cell metabolism, energy production, cell cycle, motility and cell membrane excitability is assumed by the regulatory effect of TSPO (Liu et al., 2017).

Furthermore, TSPO is linked to inflammatory bowel diseases (IBL). Ostuni et al. early showed a TSPO overexpression in ulcerative colitis and Crohn's disease and dysplasia (Ostuni et al., 2010). In 2016 the same group found a TNF-induced interleukin (IL)-8 expression induces reactive oxygen species (ROS) production and is followed by TSPO expression. TNF also alters mitochondrial ultrastructure thereby inducing apoptotic cell death. PK11195 treatment maintained the mitochondrial ultrastructure, prevented IL-8 and ROS production and thus the cell death (Issop et al., 2016). This assumes a TSPO function in mitochondrial membrane integrity, the control of mitochondrial ROS production and probably in tissue regeneration.

A lot of studies characterized TSPO as a target which prevents ROS production, thereby preventing mitochondria induced cell death. This makes TSPO a particularly interesting drug target for future investigations (Veenman et al., 2008), (Gatliff et al., 2014), (Selvaraj & Stocco, 2015), (Gut P., 2015), (Joo et al., 2015), (Tu et al., 2016), (Liu et al., 2017).

Another possible regulatory role of TSPO is suggested for the cardio system. Studies showed a critical regulatory role of the physiological cardiac function by TSPO to protect the heart under pathological conditions. TSPO might further represent an alternative strategy to develop new pharmacological agents to protect the myocardium against ischemia–reperfusion injury (Morina et al., 2016). Also, Motloch

et al. discussed the role of TSPO in arrhythmogenesis in regard to acute ischemia-reperfusion injury and myocardial infarction. The recent observations of TSPO as a regulator of mitochondrial energy metabolism pathways might enlarge its use from a diagnostic inflammatory marker to a therapeutic target of multiple cardiovascular disorders, including ischemic heart disease (Motloch et al., 2015).
The current discussion of TSPO involves various mitochondrial pathways. The new insights in recent years changed the scientific landscape of TSPO and opened a new way for diagnostic and therapeutic investigations with the primary focus on mitochondrial metabolism and protection.

## 2.5 TSPO in the brain

Despite experiments connecting TSPO function to the possible regulation of mitochondrial metabolism, the best described process in which TSPO is dynamically regulated is the activation of resident microglia in response to brain injury or neuro-inflammation (Rupprecht et al., 2010), (Albrecht et al., 2016). Only a few cell types in the CNS express TSPO under physiological conditions. TSPO is mainly found in glial cells (Casellas et al., 2002), reactive astrocytes (Maeda et al., 2007), and in neurons (Chen & Guilarte, 2008). TSPO in the brain is highly upregulated in regions of injury and inflammation. The observed higher expression of TSPO in injured brain regions is defining TSPO as a good marker for neuropathological processes (Setiawan et al., 2015a,b), (Albrecht et al., 2016). The high affinity and selective ligand PK11195 can be labeled with various radio isotopes and is therefore a detecting ligand. Using imaging techniques, labeled PK11195 makes injured areas visible. Available techniques are the positron emission tomography (PET) and the single photon emission computed tomography (SPECT) (Chen & Guilarte, 2008). Under neuropathological conditions such as stroke or neurodegenerative disorders, e.g. Alzheimer's disease (Edison et al., 2008), Parkinson's disease (Ghadery et al., 2017), Huntington's disease (Chen & Guilarte, 2008), Multiple sclerosis (Rissanen et al., 2014) and amyotrophic lateral sclerosis (Zürcher et al., 2015), TSPO expression is increased in reactive microglia and astrocytes (Maeda et al., 2007).
Furthermore, an antidepressive (Qui et al., 2016), (Zhang et al., 2017), (Li et al., 2016a), (Li et al., 2016b) and an axiolytic (Schüle et al., 2014), (Nothdurfter et al., 2012) effect of TSPO is assumed, according to recent *in vivo* and *in vitro* studies. TSPO is also located in neuronal cells of the spinal cord as well. In comparison to

placebo treated animals, a neuropathic pain model in rats showed that progesterone administration improved the recovery from neuropathic pain and modulated the TSPO expression in the spinal cord. These data suggest that steroid hormones probably modulate TSPO levels in the brain (Liu et al., 2014b). Another finding showed that estradiol activates TSPO expression in hypothalamic astrocytes due to a calcium-mediated pathway, resulting in enhanced progesterone synthesis (Chen et al., 2014).

# 3 Aim of the Thesis

The fundamental basis of this thesis was the development of a reliable and reproducible method to characterize the TSPO function in neurosteroid synthesis and mitochondrial metabolism. The requirement for the needed method was to facilitate a variety of experiments and thereby excluding non-specific side effects. Previous TSPO observations, only obtained by the use of TSPO ligands, led to the assumption that ligand-induced pharmacological effects could be non-specific or unrelated to TSPO. Therefore, I decided to design a TSPO-knock-down in mouse microglia cells (BV-2 cells) by means of small interfering RNA (siRNA). This TSPO-gene-silencing model gives me the opportunity to perform experiments in presence and absence of TSPO.

Since the recent in vivo and in vitro studies using TSPO knock-out models refuted the role of TSPO in steroidogenesis, there is still an open question of the involvement of TSPO in neurosteroidogenesis. Therefore, a possible role for TSPO in neurosteroid synthesis has to be analyzed in a comparative experiment by means of the $TSPO_{knock\text{-}down}$ model and Scramble cells. Levels of pregnenolone, the precursor molecule of neurosteroids have to be analyzed in TSPO-knock-out-cells and after drug-treatment by means of two different techniques: ELISA (enzyme-linked immunosorbent assay) and GC/MS (gas chromatography / mass spectroscopy) technique.

Furthermore, the precise physiological and pathological function of TSPO in mitochondrial metabolism is still unknown, but there is evidence for a role of TSPO in calcium homoeostasis (Gatliff & Campanella, 2012), mitochondrial respiration (Banati et al., 2014), glucose homoeostasis (Tu et al., 2016) and other bioenergetic parameters reflecting mitochondrial health (Gatliff et al., 2014), (Gatliff & Campanella, 2016). Therefore, the role of TSPO in mitochondrial metabolism has to be analyzed in $BV\text{-}2_{scramble}$ and $BV\text{-}2\text{-}TSPO_{knock\text{-}down}$ brain cells to investigate metabolic changes with regard to calcium homoeostasis, respiration and mitochondrial membrane potential. This observation might help to characterize the role of TSPO in this new field of mitochondrial metabolism and gives a deeper insight in the precise function.

# 4 Materials and Methods

## 4.1 Cell culture procedure of BV-2 mouse microglia cells

BV-2 mouse microglia cells were a generous gift from Dr. Marcus Karlstetter (Center of Ophthalmology, Experimental Immunology of the Eye, University of Cologne, Germany). BV-2 cells were cultured in Roswell Park Memorial Institute Medium (RPMI 1640 Medium, PAA Laboratories, Cölbe, Germany) supplemented with 10% fetal calf serum (FCS), 1% L-glutamine, 1% (v/v) penicillin-streptomycin and 195 nM mercaptoethanol. Cells were cultured at 37 °C, 95% humidity and 5% $CO_2$.

## 4.2 TSPO knock-down in BV-2 mouse microglia cells

*Design of mouse TSPO shRNA*

The design of the mouse TSPO shRNA (mshTSPO) was taken from RNAi Consortioum (Cambridge, UK) for the Gene translocator protein (TSPO) and the Taxon Mus musculus (mouse) with the accession number (NM_009775.2). For the given target sequence, the following hairpin sequence was used:

Target sequence: CCGTGCTCAACTACTATGTAT
Hairpin sequence: 5’-CCGG-CCGTGCTCAACTACTATGTAT-CTCGAG-ATACATAGTAGTTGAGCACGG-TTTTTG-3’

Forward and reverse oligos for mshRNA were established and finally produced by GENEART AG (Regensburg, Germany):

mshTSPO-F: 5'-CCGGCCGTGCTCAACTACTATGTATCTCGAGATACATAGTAGTTGAGCACGGTTTTTG-3'
mshTSPO-R: 5'-AATTCAAAAACCGTGCTCAACTACTATGTATCTCGAGATACATAGTAGTTGAGCACGG-3'

These oligos contain the shRNA sequence flanked by sequences that are compatible with the sticky ends of EcoRI and AgeI. The mshTSPO-F and the mshTSPO-R oligos

were annealed and ligated into the pLKO.1 TRC vector (Addgene, Cambridge, USA), producing a final plasmid, expressing the shRNA for mouse TSPO.

*Cloning of mshTSPO into the pLKO.1 cloning vector*

The pLKO.1-TRC cloning vector contains a 1.9 kb stuffer which was digested with EcoRI and AgeI restriction enzymes. Following the Addgene protocol (Addgene, 2006), the mshTSPO-F and mshTSPO-R oligos were resuspended with demineralized and distilled water ($ddH_20$) to a concentration of 20 µM. 5 µl of each oligo was mixed with 5 µL 10 x NEB buffer 2 (New England Biolabs, Frankfurt a.M., Germany) and 20 µl $ddH_20$. This mixture was incubated for 4 minutes at 90 °C, and then subsequently cooled down in a 70 °C water beaker to allow the oligos gently annealing.

*Digesting the pLKO.1 TRC cloning vector*

During annealing, the pLKO.1 TRC cloning vector was digested, to integrate the construct. According to the protocol (Addgene, 2006), 6 µg of the maxipreparation DNA product of pLKO.1 TRC-cloning vector has to be mixed with 5 µL 10x NEB buffer, 1 µL AgeI enzyme (New England Biolabs, Frankfurt a.M., Germany) to 50 µL $ddH_20$ and incubated for 2 hours at 37 °C. After purification with Qiaquick gel extraction kit (QUIAGEN, Hilden, Germany), the extract, diluted in 30 µL of $ddH_2O$, was mixed with 5 µL 10x NEB buffer 1 and 1 µL EcoRI and 14 µL $ddH_2O$ and was finally incubated at 37 °C for 2 hours. A control Gel (0.8% agarose gel) showed two bands, one 7 kb and one 1.9 kb. The 7 kb band is the linearized vector and has to be cut out, purified with a Qiaquick gel extraction kit and finally eluted in 30 µL of $ddH_2O$.

*Ligation and Transformation of mshTSPO into bacteria*

For ligation, a standard T4 ligation was used. Therefore, 2 µL of the annealed oligos were mixed with 2 µl (20 ng) of the digested pLKO.1 TRC-cloning vector, 2 µL of 10x NEB T4 DNA ligase buffer (New England Biolabs) and 1 µL NEB T4 DNA ligase (New England Biolabs, Germantown, USA) to 20 µL $ddH_2O$ and incubated at 14 °C for 20 hours. 2 µl of this ligation mix was transformed into 20 µl of competent DH5α

cells (Thermo Fischer Scientific, Darmstadt, Germany) following manufacturer's protocol. The mixture was placed on LB agar plates, containing 100 µg/ml ampicillin and incubated at 37 °C overnight. Once positive clones were by blue-white selection, the insert of these clones was verified by a sequencing reaction. Finally, one clone with proper sequence was selected and a maxipreparation with QIAGEN Plasmid Kit was performed, getting a mshTSPO plasmid with a concentration of 1 µg/µl.

*Producing lentiviral particles of the mshTSPO plasmid*

On the first day, $1x10^6$ HEK-293T cells were seeded in one well of a 6 well plate and incubated at 37 °C, 5% $CO_2$ overnight. HEK-293T cells were cultured in DMEM + 10% FBS with penicillin/streptomycin. On the second day, a transfection mix was prepared using the calcium-phosphate precipitation. During this process, the desired plasmid was bound to precipitated calcium phosphate and the newly formed complex can be taken up by the cells. HEK cells that were split the day before on a 6 well plate were first treated with chloroquine. Per single well of HEK293T cells, 2 µl chloroquine diphosphate stock solution (25 mM in $H_2O$) was diluted 1:1000 in HEK media and given to the cells, which were then incubated for 1 hour at 37° C. Meanwhile, the transfection mix was assembled in 1.5 ml Eppendorf tubes (table 1). After incubation, the chloroquine containing media was replaced by normal HEK media and 100 µl of transfection mix was added to each well. To produce infectious lentiviruses containing the shRNA against mouse TSPO, HEK cells were left undisturbed, incubating at 37 °C, 95% humidity and 5% $CO_2$ for 2 days in the S2 lab.

| Substance | Amount used for 1 well of HEK cells |
|---|---|
| mshTSPO plasmid | 3 µg |
| psPAX2 plasmid | 2.2 µg |
| pMD2.G plasmid | 0.8 µg |
| $CaCl_2$ (2 M) | 5 µl |
| 2 x HBS | 50 µl |
| $ddH_2O$ | 39 µl |

**Table 1 Transfection mix per well of HEK cells. psPAX2 plasmid (Addgene, Cambridge, USA) is a second-generation lentiviral packaging vector. pMD2.G (Addgene, Cambridge, USA), is an envelope plasmid.**

*Producing lentiviral particles of scramble shRNA plasmid*

On the first day, $1x10^6$ HEK-293T cells were seeded in one well of a 6 well plate and incubated at 37 °C, 5% $CO_2$ overnight. HEK-293T cells were cultured in DMEM + 10% FBS with penicillin/streptomycin. On the second day, a transfection mix was prepared using the calcium-phosphate precipitation. During this process, the desired plasmid was bound to precipitated calcium phosphate and the newly formed complex can be taken up by the cells. HEK cells that were split the day before on a 6 well plate were first treated with chloroquine. Per single well of HEK293T cells, 2 µl chloroquine diphosphate stock solution (25 mM in $H_2O$) was diluted 1:1000 in HEK media and given to the cells, which were then incubated for 1 hour at 37° C. Meanwhile, the transfection mix was assembled in 1.5 ml Eppendorf tubes (table 2). After incubation, the chloroquine containing media was replaced by normal HEK media and 100 µl of transfection mix was added to each well. To produce infectious lentiviruses containing the scramble shRNA plasmid, HEK cells were left undisturbed, incubating at 37 °C, 95% humidity and 5% $CO_2$ for 2 days in the S2 lab.

| Substance | Amount used for 1 well of HEK cells |
|---|---|
| Scramble shRNA plasmid | 3 µg |
| psPAX2 plasmid | 2.2 µg |
| pMD2.G plasmid | 0.8 µg |
| $CaCl_2$ (2 M) | 5 µl |
| 2 x HBS | 50 µl |
| $ddH_2O$ | 39 µl |

**Table 2 Transfection mix per well of HEK cells. Scramble shRNA plasmid (Addgene, #1864) is a 3rd gen lentiviral negative control vector containing scrambled shRNA; psPAX2 plasmid (Addgene) is a second-generation lentiviral packaging vector. pMD2.G (Addgene, Cambridge, USA), is an envelope plasmid.**

*Transduction of the plasmids in BV-2 mouse microglia cells*

The incorporation of foreign DNA into another cell by dint of a viral vector is called transduction. To transduce the BV-2 cells, the supernatant of the HEK cells that were transfected 2 days before with either mshTSPO or scramble plasmid were used, since it contained the infectious lentiviruses. In the S2 lab, the virus containing media was taken off the HEK cells and sterile filtered through a 40 µm filter to remove any remaining virus producing HEK cells, so that only the viral particles themselves were

left in the both flow-throughs. The filtered media were put on 90% confluent BV-2 cells (seeded one day before). To help the BV-2 cells taking up the lentivirus, they were centrifuged for 60 min with 2400 RPM at RT. Afterwards, the virus containing media was substituted with BV-2 media. During the following days, media of the cells was changed daily, including 2 µg/ml puromycin for selection. After five days cells were split into petri dishes and after another 5 days they were transferred to the S1 lab and termed BV-2-TSPO$_{knock-down}$ cells and BV-2$_{scramble}$ cells.

### 4.3 Immunohistochemistry

BV-2$_{scramble}$ cells or BV-2-TSPO$_{knock-down}$ cells were grown for 24 hours on a sterile glass coverslip with 12 mm diameter. Then, cells were washed 3 times with 1 × PBS (Sigma Aldrich, Munich, Germany) and fixed for 10 minutes at room temperature with 4% (wt/vol) paraformaldehyde (Carl Roth GmbH, Karlsruhe, Germany). After three additional washing steps with PBS, cells were permeabilized with blocking/permeabilization solution (10% (vol/vol) normal goat serum and 0.5% (vol/vol) Triton X-100 in 1 × PBS) for 20 minutes. Cells were then labeled overnight, at 8 °C with rabbit-anti-TSPO antibody (ab109497, Abcam, Cambridge, UK) and mouse-anti-ATPB antibody (ab14730, Abcam) both diluted 1:1000 in 2% normal goat serum and 0.1% Triton X-100 in 1 × PBS. The next day, after three additional washing steps with 1 x PBS, cells were incubated for 1 hour with a secondary antibody mixture of CY3 goat-anti-mouse IGG (red) (Life Technologies, Carlsbad, USA) and Alexa Fluor 488 goat-anti-rabbit IGG (green) (Life Technologies) both diluted 1:1000 in 2% normal goat serum and 0.1% Triton X-100 in 1×PBS. During the last 15 minutes of the secondary antibody incubation, DAPI antibody was added in 1:1000 concentration to the antibody mixture. Finally, cells were mounted with Roti®-Mount FluorCare (Carl Roth GmbH) and analyzed using an inverted microscope (Observer.Z1, Zeiss, Jena) equipped with four different objectives (20x, 40x, 63x, 100x). The light source was the high-speed wavelength switch Lambda DG4 (XBO 175 W) from Sutter instruments. Images were taken by a Zeiss AxioCam MRm. Every experiment was conducted using the software ZEN (blue edition, 2012) by Zeiss.

## 4.4 TSPO distribution in different mouse tissues

Western blot analysis was performed on fresh whole cell lysates of 9 various organs from adult wild-type mice. The densitometrically achieved results of TSPO protein expression in these 9 tissue samples were evaluated in relative units (rU) and in relation to β-actin as a loading control. Three measurements, each with fresh tissue, were performed in double determination.

## 4.5 Western Blotting

*Cell preparation*

To prepare the cell lysates of BV-$2_{scramble}$ cells, $5x10^5$ cells were seeded in each well of a 6 well plate. In an additional approach, to prepare BV-2-$TSPO_{knock\text{-}down}$ cell lysates, cells were seeded in each well of another 6 well plate. The cells were incubated for 4 hours at 37 °C, 95% humidity and 5% $CO_2$. Then, substances in table 3 were administered to BV-$2_{scramble}$ cells. Additionally, in the solvent control wells of BV-$2_{scramble}$ and BV-2-$TSPO_{knock\text{-}down}$ cells, as well as in the LPS injected well, 2 µl of ethanol were applied to allow equal conditions. Cells were then incubated 24 hours at 37 °C, 95% humidity and 5% $CO_2$. Media was removed and cells were washed 3 times with 1 x PBS. 100 µl homogenization buffer (20 mM HEPES, 5 mM EDTA, 1 M NaCl) including fresh Protease Inhibitor Cocktail (Sigma Aldrich) was added and cells were scrapped.

| Stimulant | Molecular weight | Solvent | Working concentration. | Incubation time | Company |
|---|---|---|---|---|---|
| XBD173 | 401.50 g/mol | ethanol | 10 µM | 24 h | APAC, Col., USA |
| PK11195 | 352.86 g/mol | ethanol | 100 nM | 24 h | Sigma |
| Ro5-4864 | 319.19 g/mol | ethanol | 100 nM | 24 h | Sigma |
| LPS | 1 mg/ml | media | 100 ng/ml | 24 h | Sigma |

**Table 3 Substances used for Western Blot. All substances which were used for cell incubation are listed in this table. Additional information is their molecular weight in g/mol, the used solvent, the final working concentration, and the contributors.**

After scrapped cells were mechanically homogenized on ice, an additional homogenization step was needed. Cell lysates were treated with an ultrasonic probe (GM 3100 HF, ZEFA, Grasbrunn, Germany) for 30 seconds on ice with 40% power.

*Protein quantification via Bradford assay*

Cell lysates were quantified for their protein concentration by Bradford method (Bradford, 1976) with the Bio-Rad Protein Assay Dye Reagent Concentrate (Bio-Rad Laboratories, Munich, Germany).

*SDS-PAGE procedure*

After quantification, 20 µg of protein lysates were separated by sodium dodecyl sulfate gel electrophoresis (SDS-PAGE) with 15% polyacrylamide gels and were then transferred onto a nitrocellulose membrane. Membranes were blocked with 5% non-fat dry milk in TBST (10 mM TRIS, 150 mM NaCl, 0.1% Tween 20; pH 7.4). The membranes were incubated overnight at 4 °C with a rabbit-anti-TSPO antibody (ab109497, Abcam) and β-actin with a rabbit-anti-β-actin antibody (Sigma-Aldrich), both diluted 1:1000 in 5% non-fat dry milk in TBST. Blots were washed three times with TBST and incubated with secondary horseradish peroxidase (HRP)-conjugated antibodies goat-anti-rabbit IGG-HRP (Santa Cruz) and donkey-anti-goat IGG-HRP (Santa Cruz), both diluted 1:5000 in 5% non-fat dry milk in TBST. Bands were detected with the Chemiluminescence Substrate Super Signal West Pico (Fisher Scientific, Schwerte, Germany) and visualized with a digital imaging system (Image Quant LAS 4000, GE Healthcare Europe). Densitometry analysis was performed with Image J Software (Wayne Rasband, National Institute of Health, USA). TSPO values were normalized to β-actin.

## 4.6 Pregnenolone Quantification

TSPO might play an important role in cholesterol transport and conversion to pregnenolone, the precursor molecule of the neurosteroid synthesis. Therefore, pregnenolone was quantified in both BV-$2_{scramble}$ cells and in BV-2-$TSPO_{knock\text{-}down}$ cells using two different experimental methods.

*Cell preparation*

$1x10^6$ BV-$2_{scramble}$ cells or BV-2-$TSPO_{knock\text{-}down}$ cells were seeded each onto petri dishes and were incubated four hours at 37 °C, 95% humidity and 5% $CO_2$. Cells were treated for 16 hours with substances indicated in table 4. Additionally, in the solvent control wells of BV-$2_{scramble}$and BV-2-$TSPO_{knock\text{-}down}$ cells, as well as in the LPS injected well, 10 µl of ethanol were applied to allow equal conditions. Cells were then incubated at 37 °C, 95% humidity and 5% $CO_2$. After this first period of incubation, plates were washed once with 1 x PBS, and then filled with 10 ml pregnenolone assay buffer (140 mM NaCl, 5 mM KCl, 1.8 mM $CaCl_2$, 1 mM $MgSO_4$, 10 mM glucose and 10 mM HEPES), and 25 µM trilostane (Sigma Aldrich). Trilostane was added to inhibit the further metabolism of pregnenolone to neurosteroids. Cells were treated again with the compounds according to table 4 for further 8 hours. Afterwards, supernatants were stored at -20 °C for further use.

| Stimulant | Molecular weight | Solvent | Working concentr. | Incubation time | Company |
|---|---|---|---|---|---|
| XBD173 | 401.50 g/mol | Ethanol | 10 µM | 24 h | APAC, USA |
| PK11195 | 352.86 g/mol | Ethanol | 100 nM | 24 h | Sigma |
| Ro5-4864 | 319.19 g/mol | Ethanol | 100 nM | 24 h | Sigma |
| LPS | 1 mg/ml | Media | 100 ng/ml | 24 h | Sigma |

**Table 4 Substances used for pregnenolone quantification. Substances used for cell incubation are listed in this table. Additionally, the molecular weight in g/mol, the used solvent, the final working concentration and the contributors were given.**

Two methods were used to quantify pregnenolone concentration, an antibody-based measurement method (ELISA) and a gas chromatography/mass spectrometry method (GC/MS). In contrast to the ELISA assay, the GC/MS analysis is 20 times cheaper and more reliable. This method allows the quantification of three or more substances out of one sample in a range from 10 ng/ml up to a dimension of gram/milliliter. As the ELISA is more expensive, measurement of just one substance out of one sample was possible and quantification was limited up to a maximal pregnenolone concentration of 25 ng/ml. An advantage of the ELISA technique was its higher sensitivity. The ELISA technique allows pregnenolone quantification

starting from 1 ng/ml, whereas GC/MS analysis allows steroid quantification starting from 5 ng/ml.

### 4.6.1 Enzyme-Linked Immunosorbent Assay (ELISA)

Supernatants of the cells were used and quantified in an enzyme-linked immunosorbent assay (ELISA) for pregnenolone quantification, according to the manufacturer's recommendations (Pregnenolone ELISA, IBL International, Hamburg, Germany). 10 µl of each sample was taken and diluted by 40 µl pregnenolone buffer, to get the required 50 µl of sample template. These 50 µl were pipetted on a rabbit-anti-pregnenolone antibody coated 96-microwell plate. 100 µl of pregnenolone-HRP conjugate was then added. Ready-to-use-calibrators were provided by IBL International. Afterwards 150 µl of tetramethylbenzidine/hydrogen peroxide (TMB) substrate was added. After 15 min, 50 µl of stopping solution was pipetted into each well. Assays were read with a Tecan Spectraphotometer (Tecan, Crailsheim, Germany) at 450 nm. Data were analyzed by Magellan Data Analysis Software (Tecan, Version 2.0).

### 4.6.2 GC/MS analysis

*SPE extraction*

The internal standard, deuterium labeled pregnenolone-d4 (80 ng) (#Q5500-024, Steraloids, Newport, USA) was added to the sample (1 ml of BV-$2_{scramble}$ cells). The mixture was then loaded onto the C18 encapped SPE column (3 ml/500 g, Machery-Nagel, Düren, Germany), previously preconditioned with 3 ml of methanol and 3 ml a 95%/5% water-methanol, successively. After rinsing the samples with the internal standard, the column was washed with 3 ml of the 95%/5% water-methanol mixture. The cartridges were dried for ten minutes under vacuum, and then the steroids were extracted with 3 ml of methanol. The extract was then evaporated to dryness under a nitrogen stream (42 °C). The dry residue was dissolved in 100 µl of ethyl acetate and vortexed.

*Derivatization*

The ethyl acetate extract was derivatized by addition of 20 µl heptafluorobutyric acid anhydride reagent (HFBA, Machery Nagel, Düren, Germany) for 30 minutes. After derivatization at room temperature, the extract was evaporated to dryness under a nitrogen stream (42 °C). The dry residue was then adjusted to 25 µl with toluene and decanted in special GC vials.

*Gas chromatography/mass spectrometry (GC/MS) analysis*

Analyses were performed on an HP 6890+ gas chromatograph (Agilent Technologies, Palo Alto, CA, USA) fitted with a 5%diphenyl-95%dimethylpolysiloxane Optima 5 MS capillary column (25 m × 0.20 mm × 0.20 µm; Machery Nagel, Düren, Germany). Samples were injected (3 µl) into the GC in split less (25 psi; 1 min) mode at 250 °C using an HP 6890+ series injector. The carrier gas was ultrapure helium set at constant flow mode (1.3 ml/min). The reaction gas was methane. The GC temperature program was 90 °C (1 min hold) increased to 290 °C (5 min hold) at a rate of 7.5 °C/min. The gas chromatograph was coupled to an HP 5973 Mass Selective Detector (MSD, Agilent Technologies), operated in negative chemical ionization (NCI) mode at 2024 V under the single ion monitoring mode (SIM) using the molecular ion of each compound or a specific ion fragment scan/s. The initial temperature of the oven was 95°C (1min), followed by a multiple-ramp temperature program: 210°C in 30°C/min steps; hold for 3 min -> 235°C in 2.5°C/min steps; hold for 9 min -> 300°C in 25°C/min steps; hold for 6 min.

| Compound | Abbreviation | Quatification Ion (m/z) | Confirmation Ion (m/z) | Retention time |
|---|---|---|---|---|
| Pregnenolone* | Preg | 472.4 | 492.4 | 27.7 min |
| Allopregnenolone* | AlloPreg | 474.4 | 494.4 | 23.9 min |
| Tetrahydrodeoxy-corticosterone* | THDOC | 515.2 | 490.4 | 28.7 min |
| Pregnenolone-D4* | | 476.4 | 496.4 | 27.6 min |

**Table 5 Quantification and Confirmation Ions (m/z) of the used steroids and the internal standard. Pregnenolone-D4* purchased from Steraloids, Newport, USA.**

The steroids were quantified in relation to the deuterated steroid pregnenolone-d4, used as internal standard. The ions used for quantification (QI, mainly molecular ions) and confirmation (Ci) are listed in table 5. The response factors of the different compounds were measured by injecting a solution of unlabeled standards mixed with deuterated compounds used as internal and syringe standards. No compounds have been found in blank samples.

## 4.7 The relationship of TSPO ligand pharmacology and neurosteroidogenesis

The pharmacological profile of three well established TSPO ligands XBD173, etifoxine and diazepam with regard to TSPO binding affinity, TSPO expression and neurosteroidogenesis was analyzed to figure out any relationship.

### 4.7.1 Western Blot

BV-$2_{wild\text{-}type}$ cells were seeded onto 6-well culture plates until 80% confluence. Cells were treated for 24 h with XBD173, etifoxine or diazepam at concentrations of 0.1 µM, 1 µM, 3 µM and 10 µM. These concentrations were chosen according to concentrations reached in the cerebrospinal fluid of humans treated with diazepam (Kanto et al., 1975). Solvent (ethanol) concentration was 0.5% in each well.
Protein quantification via Bradford assay and SDS-PAGE procedure was performed according to the protocol in 4.5. TSPO values were normalized to β-actin as a loading control.

### 4.7.2 Pregnenolone ELISA

BV-$2_{wild\text{-}type}$ cells were seeded onto 24-well plates. 80% confluent cells were treated for 24 h with etifoxine, XBD173 or diazepam directly added to the medium at concentrations of 0.1 µM, 1 µM, 3 µM and 10 µM, respectively.
The ELISA assay procedure was performed according to the protocol in 4.6.1. Pregnenolone concentrations were normalized to solvent control.

### 4.7.3 [$^3$H]PK11195 radioligand binding assay

[$^3$H]PK11195 saturation binding assays were performed using cell lysates of BV-$2_{wild\text{-}type}$ cells, prepared as previously described. Lysates were homogenized with assay buffer (50 mmol/l TRIS; pH = 7.4) and pipetted into a 96-well plate at a final volume

of 100 µl containing 35 µg total protein per well. Saturation binding assays included the following concentrations: 0.1 nM, 0.5 nM, 1 nM, 2 nM, 3 nM, 4 nM, 5 nM and 6 nM of [$^3$H]PK11195 (Perkin Elmer, Downers Grove, IL, USA) with a specific activity of 82–83 Ci/mmol. Samples were incubated with 10 µmol/l unlabeled PK11195 (Sigma-Aldrich). Competitions were performed with [$^3$H]PK11195 at a concentration of 1 nM for each sample. The competitors etifoxine, XBD173 or diazepam were added at concentrations of 0.1 nM, 0.5 nM, 1 nM, 5 nM, 10 nM, 15 nM and 20 nM, respectively. The concentrations of competing compounds were chosen according to the $K_d$ value of [$^3$H]PK11195, which had a high binding affinity already at nanomolar concentrations (data not shown). Assays were incubated at 25°C for 60 min and then terminated by vacuum filtration through a UniFilter-96 GF/C with 1.2 µm pore size (PerkinElmer) with ice-cold assay buffer. The amount of bound [$^3$H]PK11195 was determined using a Mikroszint 20 (Perkin Elmer) and the Tri-Carb 2900TR Liquid Scintillation Analyzer (Perkin Elmer). Data (disintegration per minute) were transformed to fmol [$^3$H]PK11195 bound per mg protein (fmol/mg). Specific binding values were calculated and saturation binding data were analyzed by nonlinear regression with GraphPad Prism 5.0 (San Diego, CA, USA). $B_{max}$ and $K_D$ values, respective measures of [$^3$H]PK11195 binding capacity (indicating PBR/TSPO density), were also measured with Graph Prism 5.0.

## 4.8 Analysis of intracellular $Ca^{2+}$ levels with FURA-2 dye

*Imaging setup and application system*

A Zeiss inverted microscope (Observer.Z1) equipped with four different objectives (20x, 40x, 63x, 100x; see supplements) was used (figure 2). As light source the high-speed wavelength switch Lambda DG4 (XBO 175 W; Sutter instruments, Novato, USA) was used, and images were taken with AxioCam (MRm; Carl Zeiss Microscopy) with a special filter for FURA-2, explained in the next paragraph. Every experiment was conducted using the software ZEN (Blue Edition, 2012; Carl Zeiss Microscopy). The custom-made perfusion system consists of ten 10 ml glass syringes connected to an adjustable pressure source via plastic tubes. The glass syringes were filled with ringer solution and substances, used for stimulation, explained and listed later. From each syringe, a single small-diameter plastic tube

leads to the mixing chamber, where the different channels meet to form the inflow. The tubes can be individually opened and closed by dint of electromagnetic pinch valves, controlled via the associated panel. The inflow is then placed in the bathing chamber and provides constant application of the experimental solutions. A suction device is placed at the other end of the chamber to circumvent overflow.

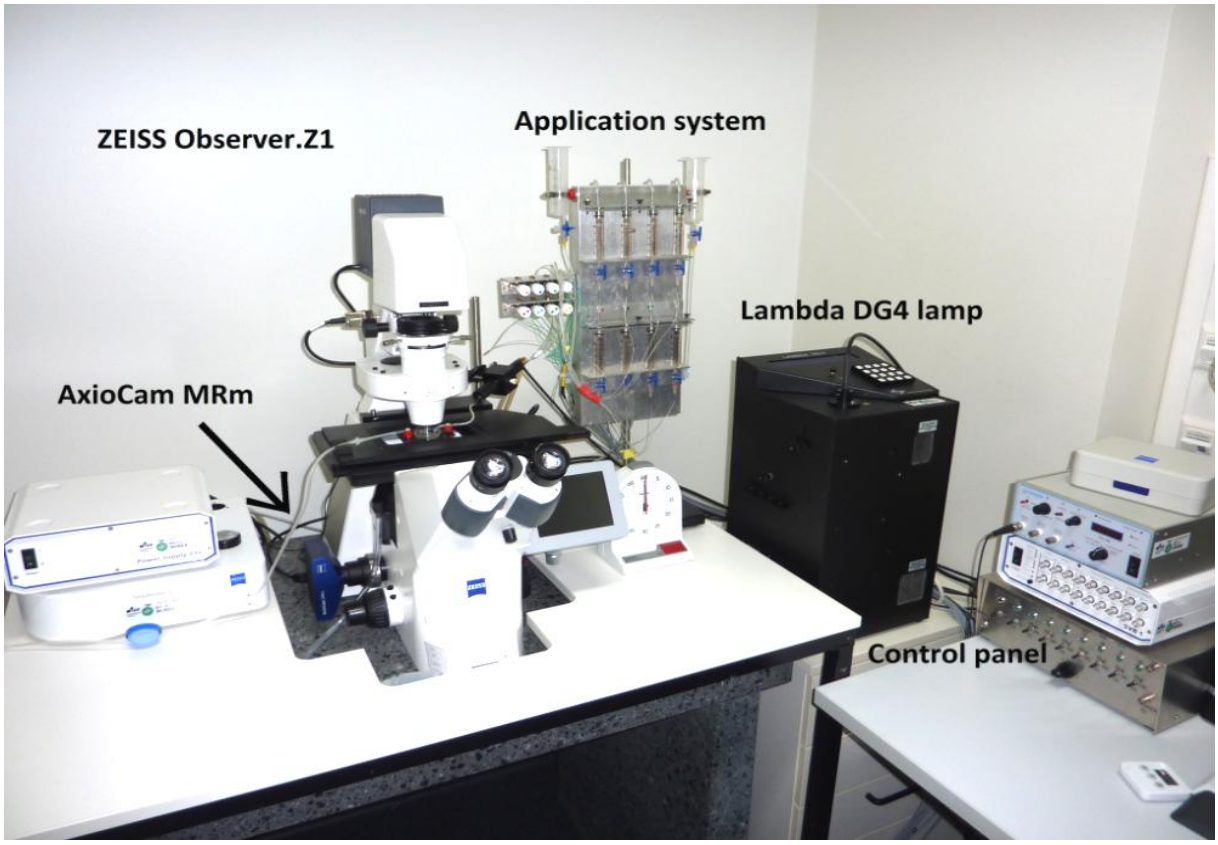


**Figure 2 Calcium Imaging Setup.**
**The calcium imaging setup consists of a Zeiss inverted microscope (Observer.Z1) with four different objectives (20x, 40x, 63x, 100x). The light source is the high-speed wavelength switch Lambda DG4 (XBO 175 W, Sutter instruments). Images are taken by a AxioCam MRm (Zeiss). On the right is the application system and the control panel.**

*FURA-2-AM fluorescence dye and stimulants used within the calcium imaging setting*

FURA-2-acetoxymethyl ester (FURA-2-AM; Invitrogen/Life technologies, Karlsruhe, Germany) is a membrane permeable aminopolycarboxylic acid with a molar mass of 636.50 g/mol. FURA-2-AM is widely used as a fluorescent, ratiometric dye for the quantitative measurement of free cytosolic $Ca^{2+}$ concentrations in living cells (Tsien et

al., 1985). FURA-2-AM crosses the cell membrane and once inside the cell, the acetoxymethyl groups are removed by cellular esterases. Removal of these esters regenerates "FURA-2", the pentacarboxylate calcium indicator and a $Ca^{2+}$ chelating agent. FURA-2 in non-bound state has maximal absorbance at 363 nm, which shifts to 335 nm when $Ca^{2+}$ is available and bound to FURA-2. Excitation with both wavelengths leads to emission of light at around 510 nm (512 nm as free molecule, 505 nm as complex with $Ca^{2+}$). It is a great advantage to use FURA-2 as a ratiometric dye. Confounding factors such as cell thickness or loading concentrations are annulled automatically (Tsien et al., 1985). All substances for stimulation, used within the $Ca^{2+}$ imaging setting to investigate the involvement of TSPO in $Ca^{2+}$ signaling, are listed in table 6.

*Cell preparation*

$2x10^5$ BV-$2_{scramble}$ cells and BV-2-$TSPO_{knock\text{-}down}$ cells were seeded each on ø 25 mm sterile glass coverslips, placed in 6 well plates, and incubated over night at 37 °C, 95% humidity and 5% $CO_2$. Then, cells were incubated with the substances of table 6 by pipetting into cell media to achieve the final working concentration. Additionally, to achieve comparable experiments, 2 µl ethanol was pipetted in the media for the control of BV-$2_{scramble}$ and BV-2-$TSPO_{knock\text{-}down}$ cells and in the LPS well. Then, cells were incubated 24 h at 37 °C, 95% humidity and 5% $CO_2$.

| Stimulant | Molecular Weight | Solvent | Working conc. | Field of Application | Company |
|---|---|---|---|---|---|
| ATP | 507.18 g/mol | ringer | 100 µM | acute (perfusion) | Roth, GER |
| FCCP | 254.17 g/mol | ethanol | 10 µM | acute (pipette) | Biomol, GER |
| XBD173 | 401.50 g/mol | ethanol | 10 µM | 24 h incubation | APAC |
| PK11195 | 352.86 g/mol | ethanol | 100 nM | 24 h incubation | Sigma |
| Ro5-4864 | 319.19 g/mol | ethanol | 100 nM | 24 h incubation | Sigma |
| LPS | 1 mg/ml | media | 100 ng/ml | 24 h incubation | Sigma |

**Table 6 Substances used in calcium imaging experiment. All substances used for $Ca^{2+}$ imaging are listed in this table. Additional information is their molecular weight in g/mol, the used solvent and the final working concentration, as well as the contributors and the field of application.**

*FURA-2 imaging procedure*

After 24 h, cells have been prepared the following way: FURA-2 working solution was prepared (2 µl of FURA-2/AM and 2 µl of Pluronic (10% in $H_2O$; Pluronic® F-127, Sigma, Seeze, Germany)) Pluronic is a nonionic, surfactant polyol (molecular weight approx. 12,500 Da) that has been found to facilitate the solubilization of dyes and other materials in physiological media (Malgaroli et al., 1987). This mixture was diluted in 1 ml of Opti-MEM® to obtain a final FURA-2 concentration of 2 µM. For cell incubation, media of 6 well plates, containing coverslips was substituted by the prepared solution and cells were allowed to take up the dye for 30 min at 37 °C, 95% humidity and 5% $CO_2$. Afterwards, the coverslip was taken out of the fluid and placed into a bath chamber, washed with classic ringer solution, and mounted onto the Zeiss inverted microscope, where they were perfused permanently with ringer for at least 2 minutes before the start of the experiment. 1 ml of the prepared solution is usually reused for incubation of cells up to three times. Therefore, 1 ml of Opti-MEM® containing FURA-2 was sufficient to conduct up to 3 single measurements.

After ensuring that no more agglomerated pieces of FURA-2/AM dye were floating in the field of view, measuring of intracellular free and bound $Ca^{2+}$ was carried out. Therefore, a high-speed polychromator system, switching the wavelength of excitation light between 340 and 380 nm at a 2 s interval, was used. The emitted light was filtered with a FT409 nm and BF510/90 nm filter and detected by the attached digital camera. Experiments were executed using the 40x objective, exposure times of 30 ms, and a binning of 4x4.

In the beginning of the experiments (a typical experimental pattern is shown in figure 14) ATP was applied extracellularly by means of the perfusion system for 60 seconds. Sill vital cells should now show an increase of intracellular $Ca^{2+}$, because ATP stimulates purinergic receptors (P2X and P2Y), which are present in almost all mammalian tissues (Abbracchio et al., 2009). P2Y is a Gq protein-coupled receptor, activating phospholipase C (PLC), which then cleaves the phospholipid phosphatidylinositol-4,5-bisphosphate ($PIP_2$) into diacyl glycerol (DAG) and inositol-1,4,5-trisphosphate ($IP_3$). DAG remains bound to the membrane, and $IP_3$ is released as a soluble molecule into the cytosol. $IP_3$ then binds to $IP_3$ receptors, which are, as mentioned above, particular $Ca^{2+}$ channels in the endoplasmic reticulum (ER). These channels are specific to $Ca^{2+}$ and only allow $Ca^{2+}$ to move through. After another

washing step $Ca^{2+}$ concentration returned to basal levels and the intracellular $Ca^{2+}$ stores recovered, before the p-trifluoromethoxy-phenylhydrazone (FCCP) application was carried out. FCCP is an ionophore and an uncoupling agent, meaning that it disrupts the mitochondrial membrane potential and therefore interrupts the ATP synthesis (Heytler, 1962). The resulting depolarization of the mitochondrial membrane potential and the loss of ATP further lead to an efflux of $Ca^{2+}$ from mitochondrial stores (Duchen, 1990). Due to the fact that FCCP is highly lipid soluble and to avoid that it is absorbed by the plastic/silicon tubules of the perfusion system, we decided to apply it directly via pipette to the chamber. Therefore, perfusion was stopped when cells were slightly covered with ringer solution. The FCCP stock was solved in ringer solution to reach a concentration of 10 µM and an ethanol concentration less than 1 promille. Finally, 300 µl of the FCCP (10 µM) solution was added to the perfusion bath, still in stop-mode, for 60 seconds to provoke any reaction. Subsequently washing with ringer solution, until the reaction went back to the baseline, was done.

FURA-2 ratio ($F_{ratio}$ 340/380) images were displayed and the $F_{ratio}$ values from the regions of interest (ROIs) drawn on individual cells were monitored during the experiments and analyzed later offline with IgorPro (Wavemetrics, Portland, USA).

## 4.9 Mitochondrial membrane potential analysis with JC-1 dye

JC-1 staining technique is used to detect the mitochondrial membrane potential (in intact, viable cells (Zamzami et al., 2000). The mitochondrial membrane potential is generated by the mitochondrial electron transport chain, which drives a proton flow from matrix through inner mitochondrial membrane to cytoplasm, thus creating an electrochemical gradient. This gradient is in turn responsible for the formation of ATP molecules by the ATP synthase and therefore, the mitochondrial membrane potential is an important parameter for mitochondrial functionality and an indirect parameter for energy status of the cell.

*Imaging setup and application system*

The imaging setup of JC-1 was used in the same way as above in imaging setup and application system of FURA-2 $Ca^{2+}$imaging (figure 2). A Zeiss inverted microscope was equipped with four different objectives, the high-speed wavelength switch

Lambda DG4 as light source and the AxioCam MRm for taking images with a special filter for JC-1. The experiments were conducted by using the ZEN software.

*JC-1 fluorescence dye and stimulants used within the mitochondrial membrane potential measurement setting*

JC-1 (5, 5', 6, 6'-tetrachloro-1, 1', 3, 3'-tetraethyl-benzimidazolcarbocyanineiodide; Biomol, Hamburg, Germany) is a cationic dye that exhibits potential-dependent accumulation in mitochondria, indicated by a fluorescence emission shift from green (~ 525 nm) to red (~ 590 nm). On the one hand, a high mitochondrial membrane potential in cells leads to the formation of JC-1-aggregates, thus showing red fluorescence. On the other hand, cells with a low mitochondrial membrane potential are those in which JC-1 maintains in the monomeric form, thus showing green fluorescence (Smiley et al., 1991). During JC-1 usage, all reagents must be at room temperature and carefully checked for pH (7.4), due to the fact that the mitochondrial membrane potential is very sensitive to alterations of both parameters. Due to the light sensitivity of JC-1, staining procedure must not be carried out under direct light and therefore cells were incubated in the dark.

*Cell preparation*

$2x10^5$ BV-$2_{scramble}$ cells and BV-2-$TSPO_{knock\text{-}down}$ cells were seeded each on ø 25 mm sterile glass coverslips, placed in 6 well plates, and incubated overnight at 37 °C, 95% humidity and 5% $CO_2$. Then, cells were incubated with the substances listed in table 7 by pipetting into cell media to achieve the final working concentration. Additionally, to achieve comparable experiments, 2 µl ethanol was pipetted into the media for the solvent control and for LPS. Then, cells were incubated 24 h at 37 °C, 95% humidity and 5% $CO_2$.

| Stimulant | Molecular Weight | Solvent | Working concentration | incubation | Company |
|---|---|---|---|---|---|
| XBD173 | 401.50 g/mol | ethanol | 10 µM | 24 h | APAC,Columbia, USA |
| PK11195 | 352.86 g/mol | ethanol | 100 nM | 24h | Sigma, Seeze, GER |
| Ro5-4864 | 319.19 g/mol | ethanol | 100 nM | 24 h | Sigma, Seeze, GER |
| LPS | 100µg/ml | Media | 100 ng/ml | 24 h | Sigma, Seeze, GER |

**Table 7 Substances used for the mitochondrial membrane potential analysis. All substances used for cell stimulation in the JC-1 measurement are listed in this table. Additional information is their molecular weight in g/mol, the used solvent and the final working concentration, as well as the contributors.**

*JC-1 imaging procedure*

After 24 hours, the JC-1 procedure was performed the following way: after freshly preparing the JC-1 working solution (1 µl of JC-1 dye plus 1 µl Pluronic; diluted in 100 µl of Opti-MEM® to obtain a 1:100 pre-dilution), 20 µl of this pre-dilution were mixed with 2 ml of Opti-MEM® to achieve a JC-1 working concentration of 2 µM. For cell incubation media of 6 well plates containing coverslips was substituted with the prepared JC-1 working solution and cells were allowed to take up the dye for 30 min at 37 °C, 95% humidity and 5% $CO_2$. Afterwards, the coverslip was taken out of the solution and placed into a bath chamber, washed with classic ringer solution, and mounted onto the Zeiss inverted microscope, where they were analyzed. Therefore, a high-speed polychromator system, switching the wavelength of the excitation light between 485 and 590 nm was used. Every two seconds a pair of pictures has been taken. The emitted light was filtered with a 515-545 nm filter for the green aggregate and 575-625 nm for the red aggregate and finally detected by the attached digital camera. Experiments were performed with a 40x objective, an exposure time of 15 ms, and a binning of 4x4. For a precise detection of the cells regions of interest (ROI's) were selected and the fluorescence was measured within these ROIs.

## 4.10 Mitochondrial respiration experiments

To figure out TSPO's involvement in the respiratory control, there are many methods to analyze mitochondrial function and dysfunction in a system of isolated mitochondria, permeabilized cells or even intact cells.

### 4.10.1 Analysis of mitochondrial respiration in intact cells

*The Oxygen consumption rate (OCR)*

The mitochondria in intact cells are present in their physiological environment. They are exposed to a relevant mix of substrates and ions. They interact with the cytoplasm, plasma membrane and other organelles and cell structures. The oxygen consumption rate (OCR) in BV-$2_{scramble}$ cells and BV-2-$TSPO_{knock\text{-}down}$ cells were determined by using the Seahorse XFp Flux Analyzer (Agilent Technologies, Santa Clara, USA). OCR is an indicator of mitochondrial respiration in a special experimental layout which informs about respiratory control of the cells (Gerencser et al., 2009). Chemical compounds and Seahorse XFp-consumables (Seahorse cartridges and Seahorse miniplates) in this experiment were purchased from Agilent Technologies.

*The Cell preparation in XFp miniplate and preparation of the XFp sensor cartridge*

$7x10^4$ BV-$2_{scramble}$ cells and BV-2-$TSPO_{knock\text{-}down}$ cells were seeded each in XFp 8 well miniplates and stored for 4 hours at 37 °C, 95% humidity and 5% $CO_2$, allowing the cells to attach. Then, cells were incubated with substances, shown in table 8, for 24 h at 37 °C, 95% humidity and 5% $CO_2$. 24 hours before the experiment, 200 µl of the Seahorse XF Calibrant (pH 7.4) was added to each well of the XFp 8 well utility plates and the sensor cartridge was placed on top of the utility plate and hydrated for 16 h at 37 °C in a non-$CO_2$ incubator. 1 hour before measurement assays were initiated by replacing the growth medium from the XFp-miniplates with assay buffer, prepared according to the manufactures recommendations. After three additional washing steps cells were incubated again at 37 °C, 95% humidity and 5% $CO_2$ for 60 minutes to allow temperature and pH of the media to reach equilibrium.

| Stimulant | Molecular weight | Stock Solvent | 1:100 Solvent | Working concentr. | applied volume | Company |
|---|---|---|---|---|---|---|
| XBD173 | 401.50 g/mol | Ethanol | Media | 10 µM | 2 µl | APAC |
| PK11195 | 352.86 g/mol | Ethanol | Media | 100 nM | 2 µl | Sigma |
| Ro5-4864 | 319.19 g/mol | Ethanol | Media | 100 nM | 2 µl | Sigma |
| DAA-1106 | 395.42 g/mol | Ethanol | Media | 10 nM | 2 µl | Clearsyn, Can |

**Table 8 Substances used in the Seahorse respiration analysis of intact cells. All substances, which were used for stimulation in the Seahorse respiration experiment are listed in this table. Additional information is their molecular weight in g/mol, the used solvent and the final working concentration, as well as the contributors.**

*Loading the stimulants of the XFp Cell Mito Stress Kit in the XFp sensor cartridge*

Before running the protocol, the XFp sensor cartridge with the utility plate was removed from the non-$CO_2$ incubator. Simultaneously, the mitochondrial stress compounds, oligomycin (1 µM), FCCP (2 µM) and rotenone/antimycin (1 µM), delivered within the XFp Cell Mito Stress Test Kit were prepared according to the manufactures recommendations. Substances were immediately pipetted into the respective application ports in the XFp sensor cartridge.

*Analysis of mitochondrial respiration in intact cells*

The XFp sensor cartridge was placed on top of the XFp 8-well miniplate and the protocol for basal measurements at 37 °C was started (start, calibration, equilibration, mixing 2 min, 1 min delay and 3 min measurement) and repeated three times. As illustrated in figure 3 each modulator targets a specific component of the ETC.

Oligomycin inhibits the ATP synthase and thereby the oxygen consumption until the LEAK state of respiration is reached. This represents a non-phosphorylating resting state when ATP synthase is not active.

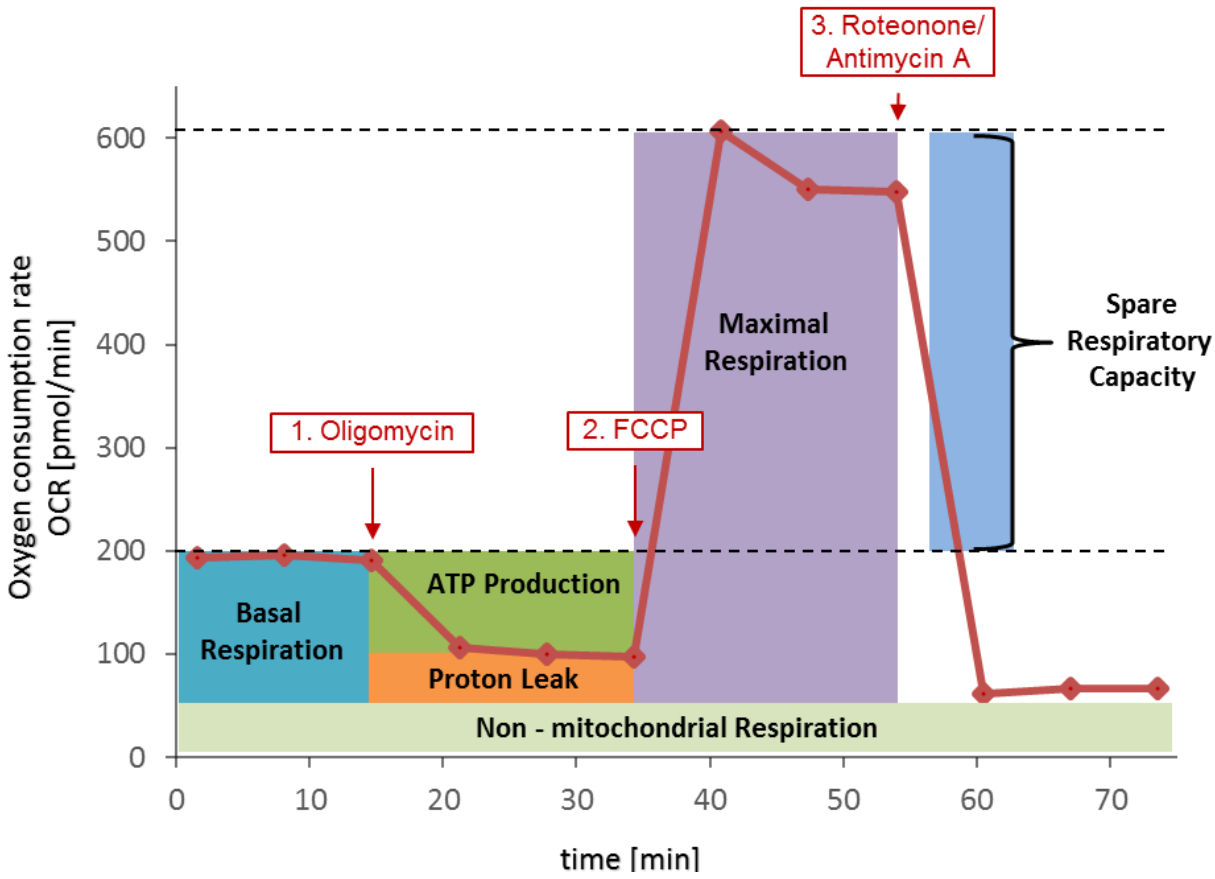


**Figure 3 A classic Seahorse measurement of mitochondrial respiration in intact cells. Basal respiration is the $O_2$ consumption of the cells under basal conditions. It is described as the sum of $O_2$ consumption from ATP demand and the proton leak. ATP production is the difference of basal respiration a resulting proton leak after application of the ATP synthase inhibitor oligomycin. H+ (Proton) Leak is the remaining basal $O_2$ consumption, which is not coupled to ATP production. It is also a mechanism to regulate the mitochondrial ATP production. Maximal respiration is the maximal $O_2$ consumption of the cells as a result of the addition of the uncoupler FCCP. FCCP mimics physiological "energy demand" by stimulating the respiratory chain to operate at maximum capacity. Therefore, it shows the maximal respiration rate of the cell. Spare Respiratory Capacity is the cells ability to respond to spontaneous energetic demands. Non-mitochondrial Respiration is the $O_2$ consumption due to other cellular enzymes that continue respiring after rotenone and antimycin A addition.**

This correlates to the mitochondrial respiration, which is associated with cellular ATP production. FCCP as an uncoupling agent collapses the proton gradient and disrupts the mitochondrial membrane potential resulting in an unlimited electron flow through the ETC whereby $O_2$ is maximally consumed by complex IV. This state of maximal respiration can be used to calculate spare respiratory capacity, defined as the difference between maximal respiration and basal respiration. Spare respiratory

capacity is defined as the cells' ability to respond to an increased energy demand. Finally, a mix of rotenone (complex-I-inhibitor) and antimycin A (complex-III-inhibitor) is injected and shuts down the mitochondrial respiration. Thereby it allows the calculation of non-mitochondrial respiration driven by processes outside the mitochondria (Gerencser et al., 2009). The data for each reported parameter reflect three independent Seahorse XFp measurement series.

### 4.10.2 High resolution respirometry (HRR) with the oxygraph-2k (O2k)

High-resolution respirometry (HRR) protocols are termed substrate–uncoupler–inhibitor titration (SUIT) protocols and are available for analysis of mitochondrial respiratory control and the pathophysiology of mitochondrial diseases. The aim of the experiment was to gain insight into mitochondrial respiration of permeabilized cells and which respiratory chain complex might be influenced by a loss of TSPO. This was analyzed by comparing BV-2-TSPO$_{knock-down}$ cells to BV-2$_{scramble}$ cells.

*Cell preparation*

1x10$^6$ BV-2$_{scramble}$ cells and 1x10$^6$ BV-2-TSPO$_{knock-down}$ cells were seeded each in 10 cm petri dishes and stored at 37 °C, 95% humidity and 5% $CO_2$. One petri dish was used for one experiment. After two days of regular media change, growth media was removed and cells were washed two times with MIR05 media (0.5 mM EGTA, 3 mM $MgCl_2x6H_2O$, 60 mM lactobionic acid, 20 mM taurine, 10 mM $KH_2PO_4$, 20 mM HEPES, 110 mM D-sucrose, 1 g/L fatty acid free BSA) (Gnaiger, et al., 2000). Cells were harvested in 2 ml of MIR05 media, centrifuged 3 minutes at 1200 RPM and resuspended in 1 ml MIR05 media. Cells were counted and the required amount was added to the Oxygraph-2k chambers.

*High resolution respirometry procedure*

1x10$^6$ cells were transferred into each calibrated Oxygraph-2k (O2k, OROBOROS INSTRUMENTS) 2 ml-chambers. BV-2$_{scramble}$ cells were pipetted into chamber A and BV-2-TSPO$_{knock-down}$ cells into chamber B. Oxygen polarography was performed at 37 ± 0.001 °C (electronic peltier regulation) in O2k-chambers and oxygen concentration (µM) as well as oxygen flux per tissue mass (pmol $O_2$ x $s^{-1}$ x $mg^{-1}$)

were recorded in real-time using DatLab software (Oroboros Instruments). In the used SUIT protocol, cells were permeabilized by administration of 4 µl digitonin. Non-phosphorylating LEAK-respiration was induced by adding complex-I-linked substrates malate (0.5 mM) and glutamate (10 mM) but no ADP. If no ADP was phosphorylated by ATP synthase, the low oxygen consumption during this non-phosphorylating LEAK-respiration relates to the proton leak and proton slip.

A saturating ADP concentration (2.5 mM; previously tested) was then applied to the chambers. Complex-I-linked oxidative phosphorylation (OXPHOS) capacity was investigated as a result of phosphorylating complex-I-activity. This gives an insight into any complex-I-linked alteration in BV-$2_{scramble}$ cells in comparison with BV-2-$TSPO_{knock\text{-}down}$ cells.

After addition of the complex-II-linked substrate succinate (10 mM), the combined complex-I and complex-II-linked OXPHOS-capacity was analyzed. As a consequence, with this technique complex-I and complex-II-linked $O_2$ consumption was detectable separately.

Further injection of the ATPase inhibitor oligomycin (2.5 µM) inhibits $O_2$ consumption until the LEAK state of respiration is reached, representing again the non-phosphorylating resting state when ATP synthase is not active.

In the next step FCCP (2 µM), as an uncoupling agent, was applied and collapses the proton gradient, thereby disrupting the mitochondrial membrane potential. As a result, electron flow through the ETC is uninhibited and oxygen is maximally consumed by complex IV. This condition was used to measure the maximal respiratory capacity of the electron transfer system (ETS). The ETS capacity is the non-coupled state at optimum uncoupler concentration.

Subsequent inhibition of complex-I by rotenone (0.5 µM) allowed measurement of complex-II-linked ETS capacity. To control whether other oxygen-consuming processes are involved in mitochondrial respiration, complex III was inhibited by antimycin A (2.5 µM). The resulting residual oxygen consumption (ROX) reflected oxygen consumption from undefined sources and was subtracted from mitochondrial respiratory states (Gnaiger, 2014). Respiratory fluxes were corrected automatically by DatLab for instrumental background according to the manufactures recommendations.

# 5 Results

## 5.1 Confirmation of the BV-2-TSPO$_{knock-down}$

The designed mouse TSPO shRNA (mshTSPO) and the scramble shRNA (lentiviral negative control containing scrambled shRNA) were successfully cloned into pLKO.1 vectors and further stable transfected via lentiviral particles into BV-2 mouse microglia cells. The final cells were termed BV-2-TSPO$_{knock-down}$ and BV-2$_{scramble}$ cells. To prove the silenced target gene expression via RNA interference, western blot analysis of TSPO expression and immunohistological staining against TSPO was performed.

*Western Blot analysis of BV-2-TSPO$_{knock-down}$ and BV-2$_{scramble}$ cells*

Western Blot analysis shows a successful 95.5% knock-down in BV-2-TSPO$_{knock-down}$ cells, compared to BV-2$_{wild-type}$ and BV-2$_{scramble}$ cells ten days after lentiviral knock-

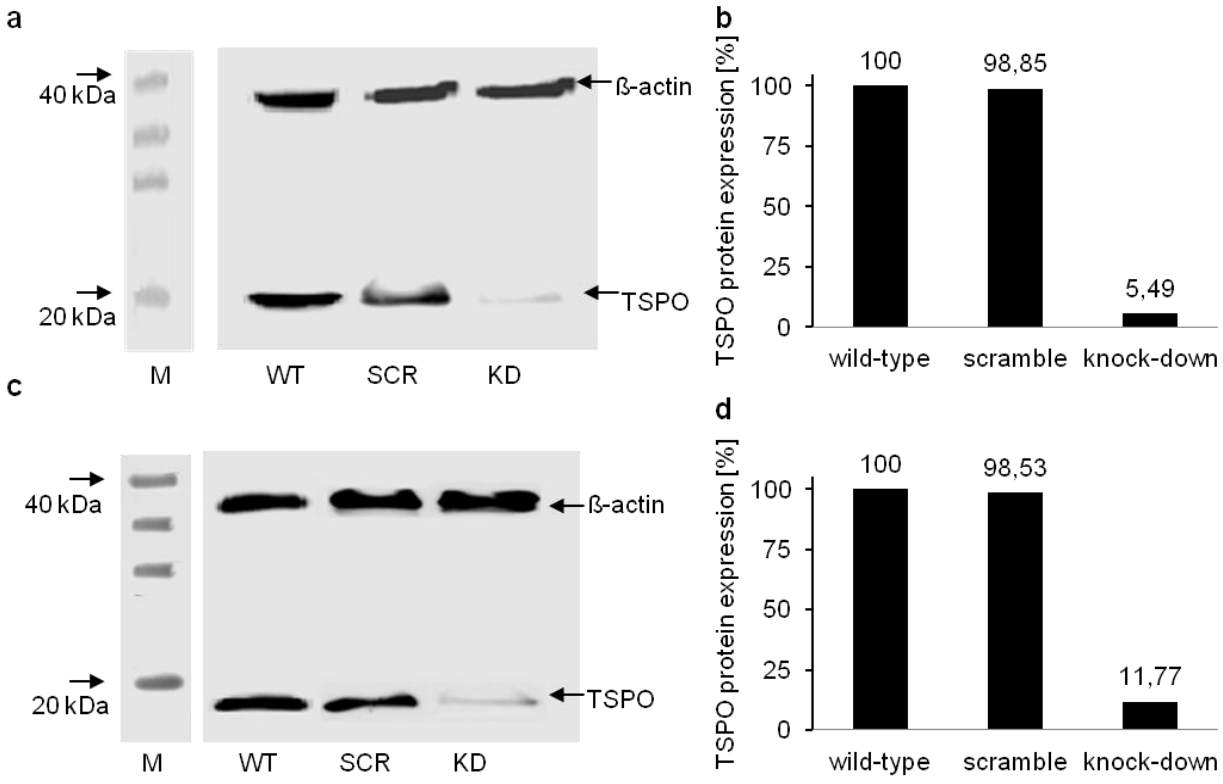


**Figure 4 TSPO protein expression of BV-2$_{wild-type}$ (WT) cells, BV-2$_{scramble}$ cells (SCR) and BV-2-TSPO$_{knock-down}$ (KD) cells after 10 days (a-b) and 25 days (c-d) lentiviral knock-down procedure.**

down procedure (figure 4a-b). Western Blot analysis 25 days after lentiviral knock-down showed a significant reduction of TSPO protein expression levels of 88.2 % (figure 4 c-d). There was no change in level of TSPO expression in BV-$2_{wild\text{-}type}$ and BV-$2_{scramble}$ cells after 10 and 25 days.

*Immunofluorescence analysis of BV-2-TSPO$_{knock\text{-}down}$ and BV-$2_{scramble}$ cells*

An anti-TSPO antibody staining showing presence of TSPO (green) in the BV-2-TSPO$_{scramble}$ cells and its absence in the BV-2-TSPO$_{knock\text{-}down}$ cells (figure 5a). Additional antibody staining of mitochondria (target: mitochondrial membrane ATP synthase) (orange; figure 5b) and DAPI staining of nuclei (blue; figure 5c) were used in BV-$2_{scramble}$ and BV-2-TSPO$_{knock\text{-}down}$ cells for normalization. The merged picture is shown in figure 5d.

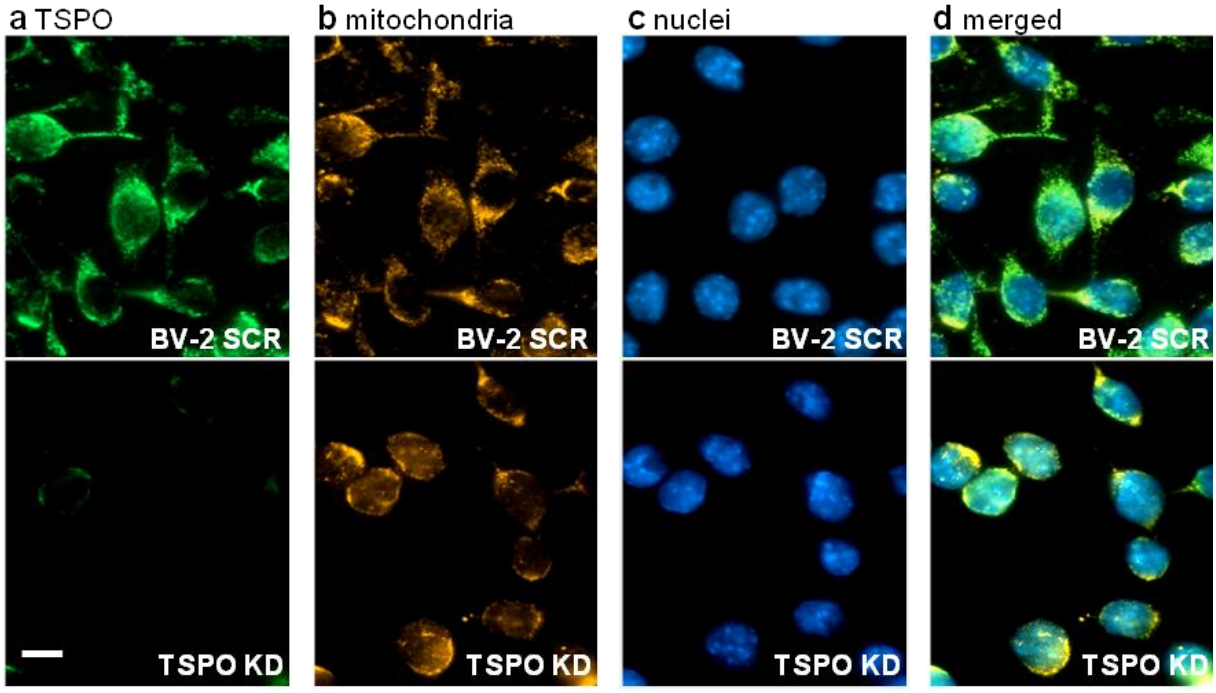


**Figure 5 The anti-TSPO antibody staining shows the presence of TSPO (green) in BV-$2_{scramble}$ cells (SCR) and its absence in BV-2-TSPO$_{knock\text{-}down}$ cells (KD) (5a). Additional antibody staining of mitochondria (target: ATPsynthase; orange; 5b) and DAPI staining of nuclei (blue; 5c) were used in BV-$2_{scramble}$ and BV-2-TSPO$_{knock\text{-}down}$ cells for normalization. The merged picture is shown in figure 5d. green=TSPO; orange =mitochondria; blue=nuclei; yellow =merged image; white scale bar: 10 µm.**

## 5.2 Low TSPO expression in mouse wild-type brain

TSPO is a ubiquitous expressed protein in mammals, but the lowest expression levels are detected in the brain. To get an overview of the percentage distribution of TSPO in a mouse body western blot analysis was performed on whole cell lysates of 9 different organs from adult wild-type mice (figure 6b). The TSPO protein expression in these 9 tissue samples was presented as arbitrary units (rU) in relation to β-actin as a loading control (figure 6a). Three independent experiments were performed. The average and the standard error of the mean were calculated and the TSPO protein expression is shown in figure 6a. While the highest levels of TSPO were observed in lysates from liver (27.4%) and the abdominal visceral fat (18.3%), TSPO protein was also detectable at moderate levels in samples from kidney (11.2%), testis (10.4%), lung (10.2%) and heart (9.5%). The lowest levels were detected in cerebellum (2.9%) and brain lysates (1.6%).

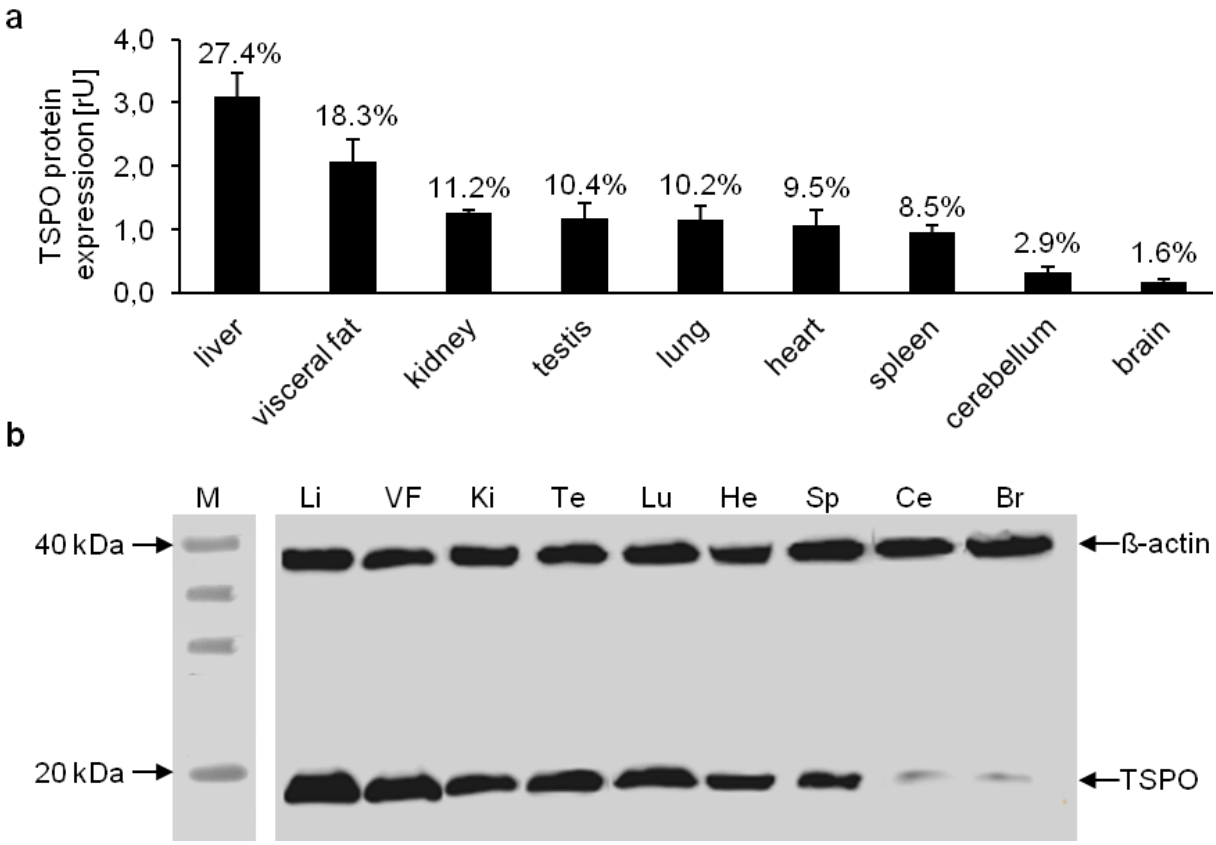


**Figure 6 TSPO protein expression in nine different mouse tissues. (b) Western Blot analysis on whole cell lysates from 9 various organs of adult wild-type mice (a). Results were normalized to β-actin as a loading control and the data are shown in ratio to loading control (a). n=3; mean and standard error of the mean) (Li=liver; VF=visceral fat; KI=kidney; Te=testis; Lu=lung; He=heart; Sp=spleen; Ce=cerebellum; Br=brain)**

## 5.3 Regulation of TSPO protein expression

The effect of 24 hour TSPO ligand incubation on TSPO protein expression in BV-$2_{scramble}$ cells was analyzed by Western blot (figure 7b), to figure out if one of the drugs, used in this thesis, is able to influence the TSPO expression and if there is a correlation to the resulting TSPO function.

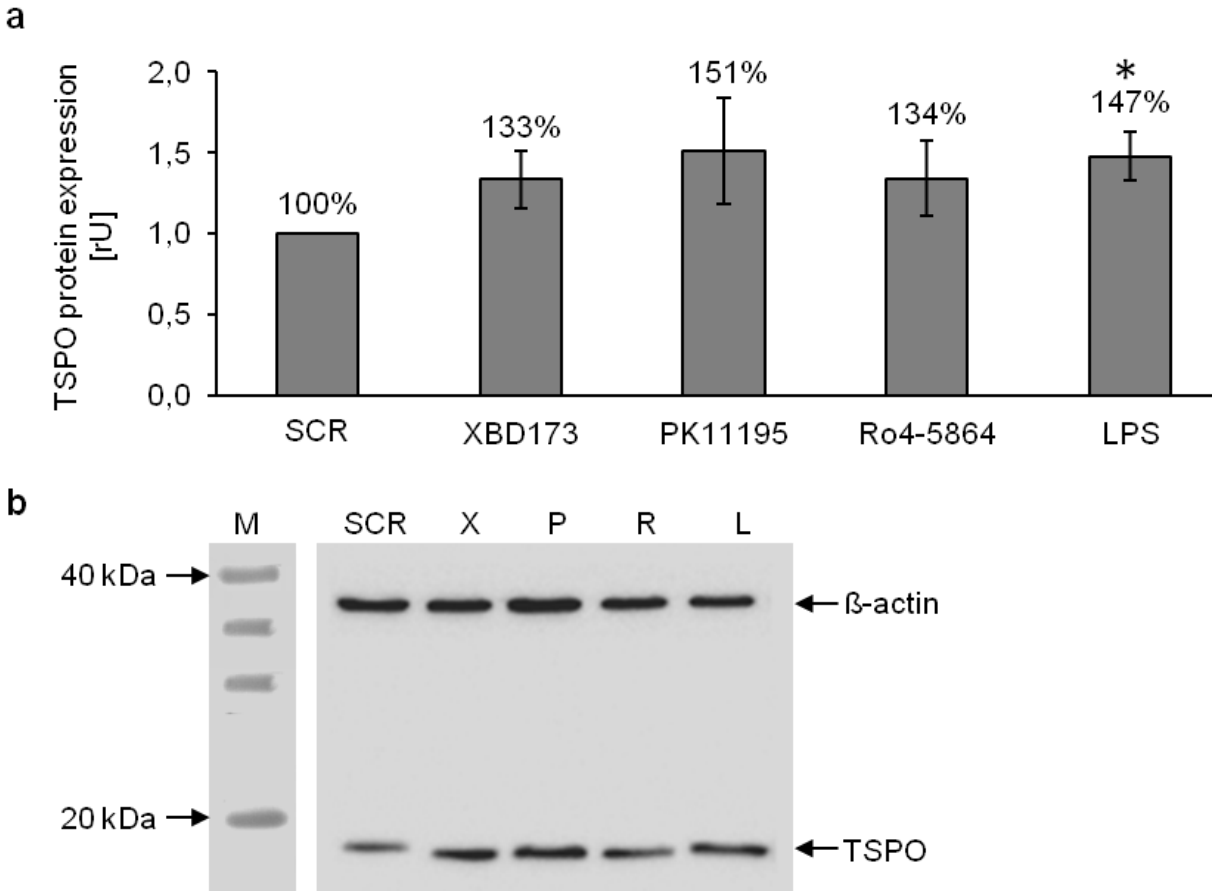


**Figure 7 TSPO protein expression after drug administration and 24 h incubation. Seven independent experiments were performed, results are presented as arbitrary units (rU), normalized to β-actin and in relation to solvent control.**

Seven independent experiments were performed in duplicates on BV-$2_{scramble}$ cell lysates after 24 h treatment with XBD173 (10 µM), PK11195 (100 nM), Ro5-4864 (100 nM) and LPS (100 ng/ml). The average of the duplicates was used to determine the average and standard error of the mean. The results were presented as arbitrary units (rU), normalized to β-actin (figure 7a) and in relation to solvent control. The TSPO expression in percent over solvent control is shown over each column.

PK11195 treatment showed the highest, but not significant TSPO protein expression with 51%, followed by a significant 47% increase of TSPO protein expression after LPS treatment (t-test, p=0.00793). XBD173 and Ro5-4864 showed a moderate increase of TSPO expression with 33% and 34%.

Furthermore, the effect of 24 hour TSPO drug incubation on TSPO protein expression in BV-2-TSPO$_{knock-down}$ cells was analyzed by Western blot (figure 8b), to investigate if the drug incubation has the same effect on BV-2-TSPO$_{knock-down}$ cells.

Six independent experiments were performed in duplicates on BV-2-TSPO$_{knock-down}$ cell lysates after 24 h treatment with XBD173 (10 µM), PK11195 (100 nM), Ro5-4864 (100 nM) and LPS (100 ng/ml). The results were presented as the average and the standard error of the mean as arbitrary units (rU), normalized to β-actin (figure 8a) and in relation to solvent control.

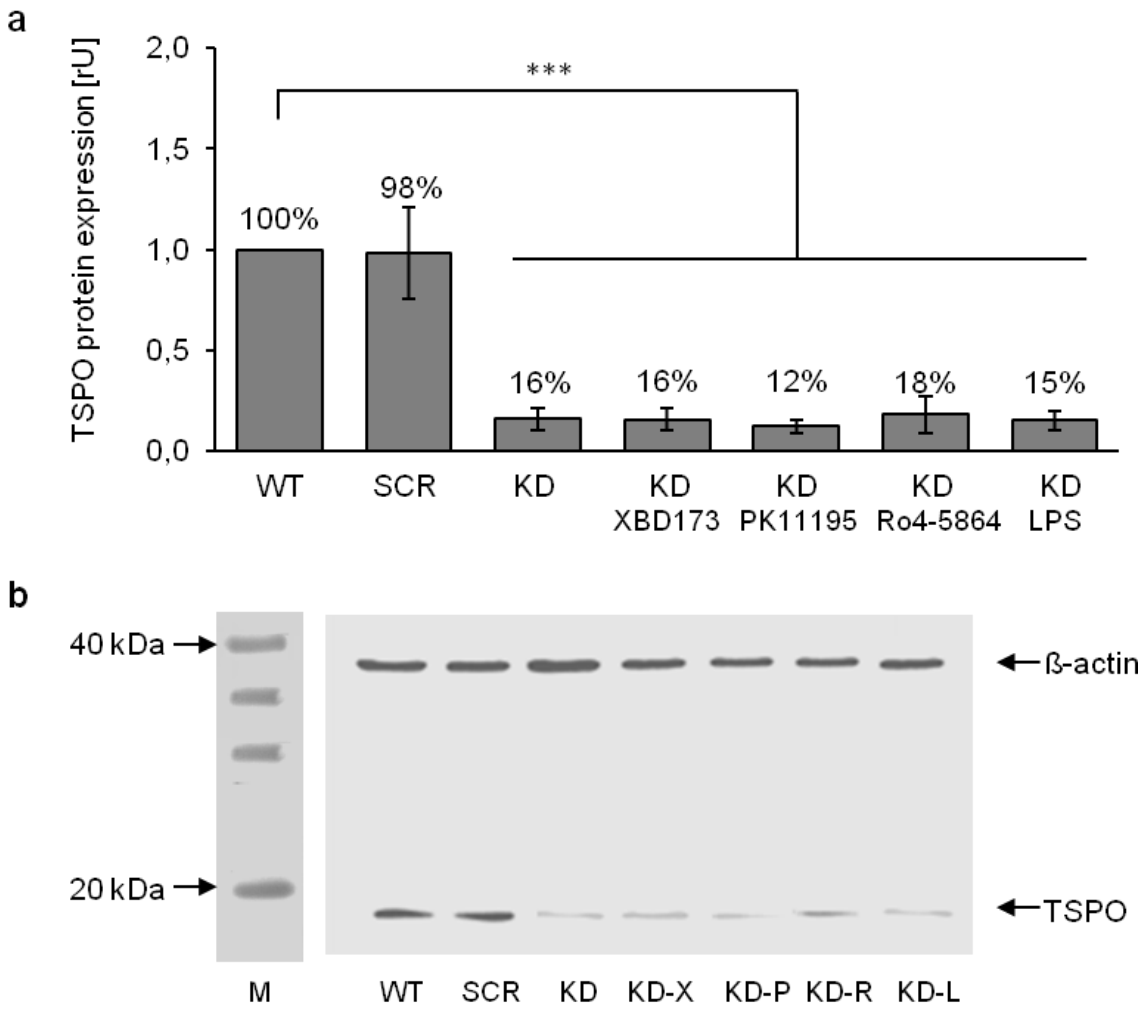


**Figure 8 TSPO protein expression in BV-2-TSPO$_{knock-down}$ cells after drug administration and 24 h incubation. Six independent experiments were performed, results are presented as arbitrary units (rU), normalized to β-actin and in relation to solvent control.**

XBD173, PK11195, Ro5-4864 and LPS treatment of BV-2-TSPO$_{knock-down}$ cells showed a significant decrease in TSPO protein expression when compared to BV-2$_{scramble}$ solvent control (t-test; p<0.0001; SCR=100%, KD$_{XBD173}$=16%, KD$_{PK11195}$=12%, KD$_{Ro5-4864}$=18%, KD$_{LPS}$=15%) (figure 8a). XBD173, PK11195, Ro5-4864 and LPS treatment of BV-2-TSPO$_{knock-down}$ cells showed no significant differences in TSPO protein expression when compared to BV-2-TSPO$_{knock-down}$ cell solvent control (KD$_{solvent\ control}$=16%, KD$_{XBD173}$=16%, KD$_{PK11195}$=12%, KD$_{Ro5-4864}$=18%, KD$_{LPS}$=15%). Figure 8 shows that TSPO specific drugs do not affect TSPO protein expression in BV-2-TSPO$_{knock-down}$ cells. In conclusion, this result clearly confirms the TSPO knock-down in BV-2 mouse microglia cells.

## 5.4 Pregnenolone quantification with ELISA technique

TSPO-specific drugs are assumed to develop an anxiolytic effect by their ability to enhance or reduce neurosteroid synthesis. Therefore, pregnenolone (precursor molecule of all neurosteroids) was quantified after treatment with XBD173 (10 µM), PK11195 (100 nM), Ro5-4864 (100 nM) and LPS (100 ng/ml) in cell culture supernatants of BV-2$_{scramble}$ cells and BV-2-TSPO$_{knock-down}$ cells by ELISA technique (figure 9).

Four independent experiments were performed in duplicates and normalized to solvent control. The average of the duplicates was used to determine the average and standard error of the mean shown in figure 9a-c.

A pregnenolone concentration of 14.30 ng/ml was detected in XBD173 treated BV-2$_{scramble}$ cells. This significant increase (t-test; p=0.0032) when compared to BV-2$_{scramble}$ solvent control (7.79 ng/ml) indicates a putative TSPO-specific effect (figure 9a). All other treatments led in a decrease of pregnenolone concentration when compared to BV-2$_{scramble}$ solvent control. This decrease in pregnenolone concentration was significant after PK11195 (5.30 ng/ml; t-test: p= 0.0261) and Ro4-5684 (5.96 ng/ml; t-test: p=0.015) treatment (figure 9a). A non-significant decrease in pregnenolone concentration (4.48 ng/ml) was detected in LPS treated cells (figure 9a). BV-2-TSPO$_{knock-down}$ cells show no significant differences after drug treatment when compared to BV-2-TSPO$_{knock-down}$ solvent control (figure 9b).

BV-2-TSPO$_{knock-down}$ cells showed a significant decrease in pregnenolone concentration (4.75 ng/ml; t-test: p=0.0002) when compared to BV-2$_{scramble}$ cells (7.79 ng/ml), (figure 9c) which demonstrates a functional role for TSPO in

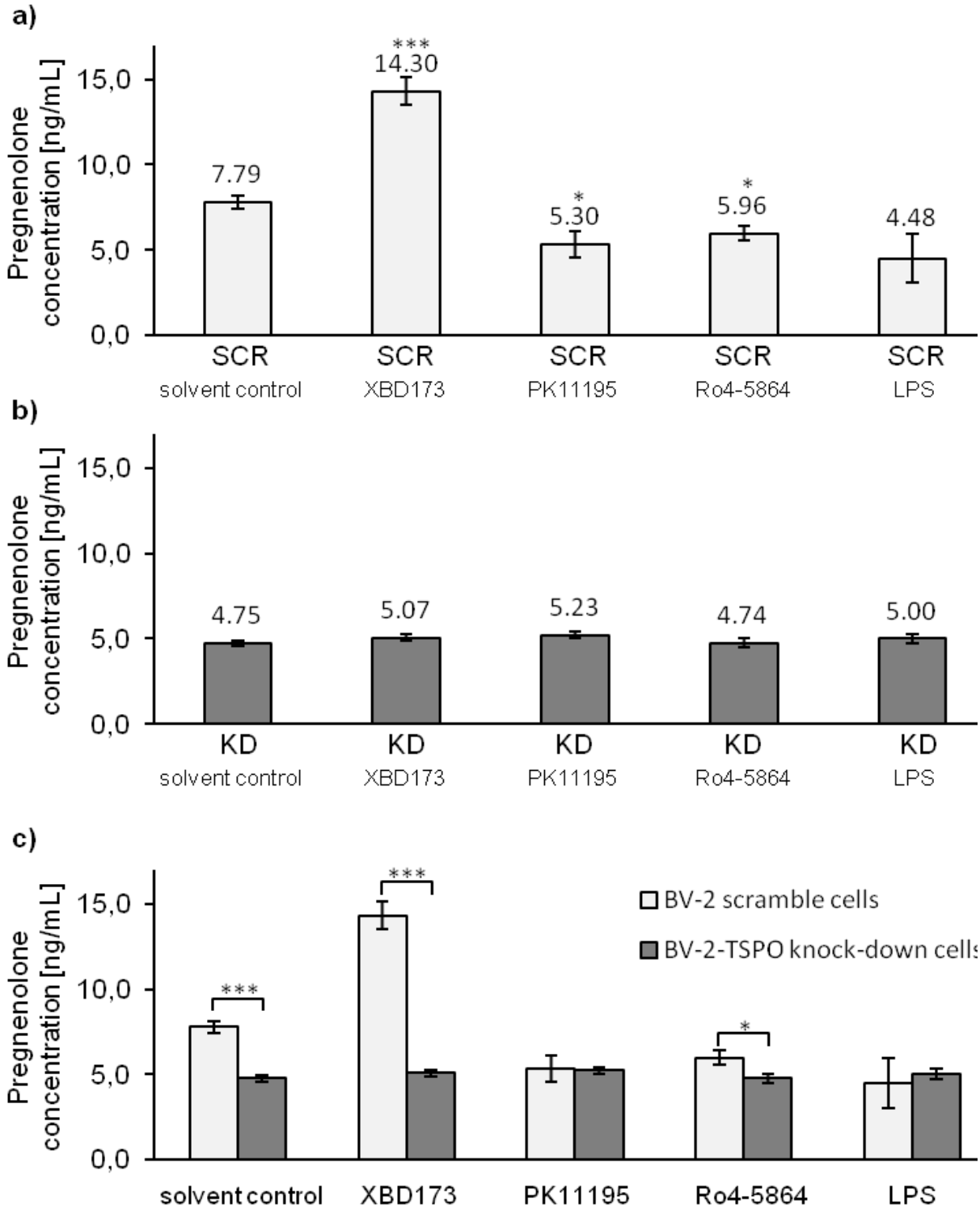


**Figure 9 Pregnenolone quantification of BV-2$_{scramble}$ cells and BV-2-TSPO$_{knock-down}$ cells with ELISA technique after 24h drug incubation. Four independent experiments were performed and normalized to solvent control. The average and the standard error of the mean were calculated. 9a) Pregnenolone quantification of BV-2$_{scramble}$ cells after 24h drug incubation. 9b) Pregnenolone quantification of BV-2$_{scramble}$ cells after 24h drug incubation. 9c) The direct comparison of 24h treated XBD173, PK11195, Ro5-4864 and LPS BV-2-TSPO$_{knock-down}$ cells with BV-2$_{scramble}$ cells.**

neurosteroidogenesis. The direct comparison of XBD173, PK11195, Ro5-4864 and LPS treated BV-2-TSPO$_{knock-down}$ and BV-2$_{scramble}$ cells is shown in figure 9c. A significant decrease of pregnenolone concentration in XBD173 and Ro5-4864 treated BV-2-TSPO$_{knock-down}$ cells (SCR_XBD: 14.30 ng/ml; KD_XBD: 5.07 ng/ml; ttest; p>0.001), (SCR_Ro: 5,96 ng/ml; KD_XBD: 4,74 ng/ml; ttest; p>0.05) when compared to XBD173 and Ro5-4864 treated BV-2$_{scramble}$ cells supports the hypothesis of a functional role for TSPO in neurosteroidogenesis. Moreover, it indicates that XBD173 is a direct TSPO agonist, showing a putative TSPO-specific effect.

### 5.4.1 Neurosteroid quantification with GC/MS analysis

The pregnenolone concentration was determined in either BV-2-TSPO$_{knock-down}$ cells or in BV-2-TSPO$_{scramble}$ cells after treatment with XBD173 (10 µM), PK11195 (100 nM), Ro5-4864 (100 nM) and LPS (100 ng/ml) with GC/MS analysis. THDOC and allopregnanolone concentration was also determined, however the results were below the detection limit of 5 ng/ml. Four independent experiments were performed in duplicates and normalized to the internal standard pregnenolone-d4. The average and the standard error of the mean are shown in figure 10a-c.

XBD173 treated BV-2-TSPO$_{scramble}$ cells show a significantly increased pregnenolone concentration (19.47 ng/ml) (t-test: p=0.048) when compared to solvent control (10.56 ng/ml) (figure 10a). All other treatments induced a decrease in pregnenolone concentration of BV-2$_{scramble}$ cells (figure 10a): LPS treated cells show a significant decrease in pregnenolone concentration (6.74 ng/ml) (t-test: p=0.029) when compared to BV-2$_{scramble}$ solvent control. PK11195 and Ro5-4864 treatment led to decrease in pregnenolone concentration (PK11195: 8.52 ng/ml and Ro5-4864: 9.30 ng/ml) without any significance when compared to BV-2$_{scramble}$ solvent control (figure 10a).

XBD173, PK11195, Ro5-4864 and LPS treated BV-2-TSPO$_{knock-down}$ cells show no significant changes in pregnenolone concentration after drug treatment when compared to BV-2-TSPO$_{knock-down}$ solvent control (figure 10b).

BV-2-TSPO$_{knock-down}$ cells show a significant decrease in pregnenolone concentration (5.25 ng/ml; t-test: p<0.05) when compared to BV-2$_{scramble}$ cells (10,56 ng/ml), (figure 10c) which is in line with my hypothesis as a functional role for TSPO in neurosteroidogenesis. The direct comparison of XBD173, PK11195, Ro5-4864 and

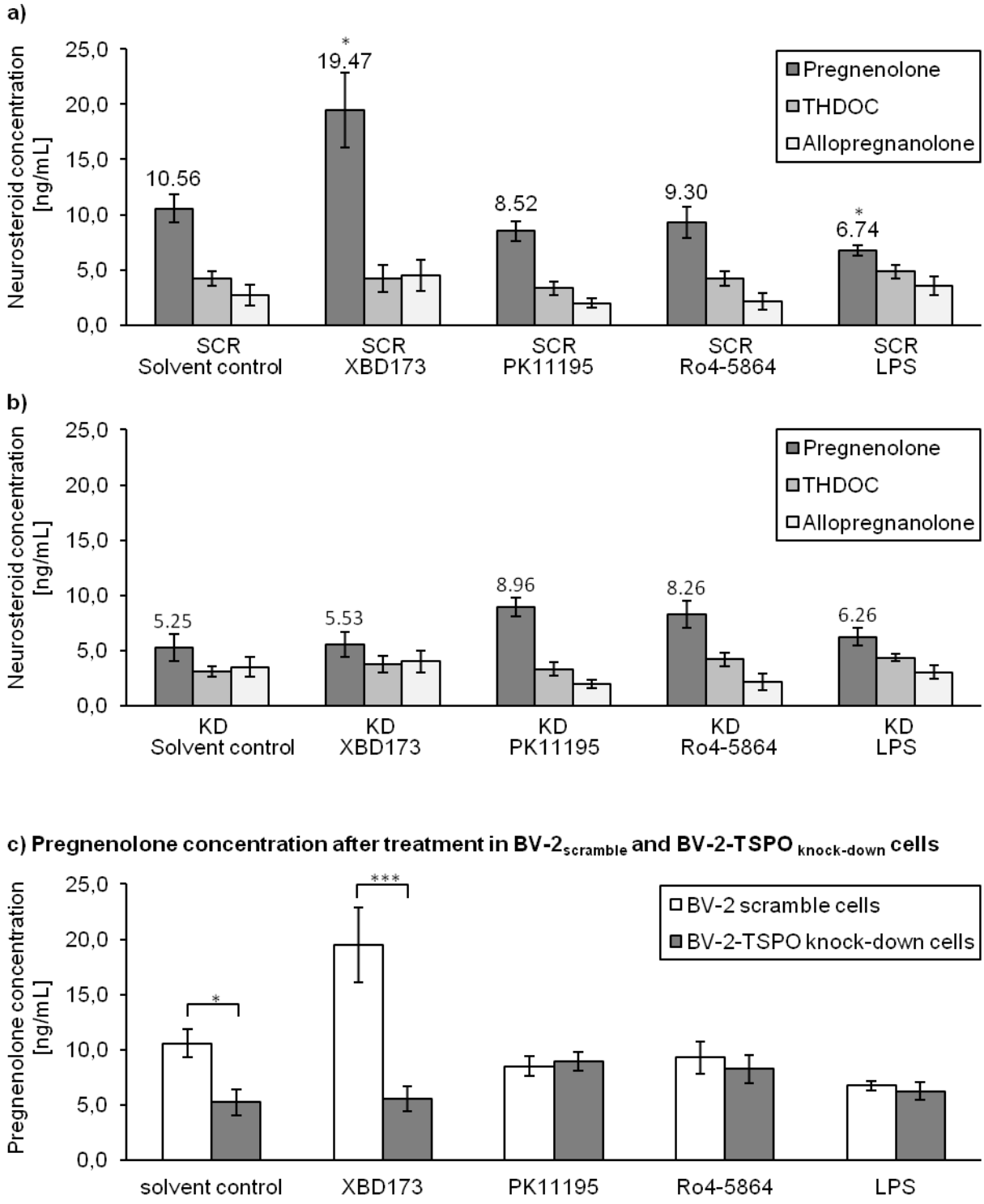


**Figure 10 GC/MS Quantification of neuroactive steroids and pregnenolone. Pregnenolone concentration was determined in either cell culture supernatants of BV-2$_{scramble}$ (SCR) cells or in BV-2-TSPO$_{knock-down}$ (KD) cells after treatment with XBD173 (10µM), PK11195 (100nM), Ro5-4864 (100nM) and LPS (100ng/ml). Levels of THDOC and allopregnanolone were also determined. Four independent experiments were performed in duplicates and normalized to the internal standard pregnenolone-d4. The average and standard error of the mean are shown in [ng/ml].**

LPS treated BV-2-TSPO$_{knock-down}$ cells and BV-2$_{scramble}$ cells are shown in figure 10c. A significant decrease of pregnenolone concentration in XBD173 treated BV-2-TSPO$_{knock-down}$ cells (WT_XBD: 19.47 ng/ml; KD_XBD: 5.53 ng/ml; ttest; p>0.05), when compared to XBD173 treated BV-2$_{scramble}$ cells supports the hypothesis of a functional role for TSPO in neurosteroidogenesis. Moreover, it indicates XBD173 as a direct TSPO agonist which mediates a TSPO-specific effect.

## 5.5 TSPO ligand pharmacology in relationship to neurosteroidogenesis

The pharmacological profile of three well established TSPO ligands XBD173, etifoxine and diazepam with regard to TSPO binding affinity, TSPO expression and pregnenolone concentration was analyzed to figure out any clear relationship to the TSPO function in neurosteroidogenesis.

### 5.5.1 Analysis of TSPO protein expression after TSPO ligand treatment

BV-2$_{wild-type}$ cells were treated with XBD173, etifoxine or diazepam as described previously to show if the protein expression after TSPO ligand incubation has any significant effect which may correlate with a significant effect in the TSPO function of neurosteroid synthesis. The effect of 24 h drug incubation on TSPO protein expression in BV-2 cells is presented in figure 11.

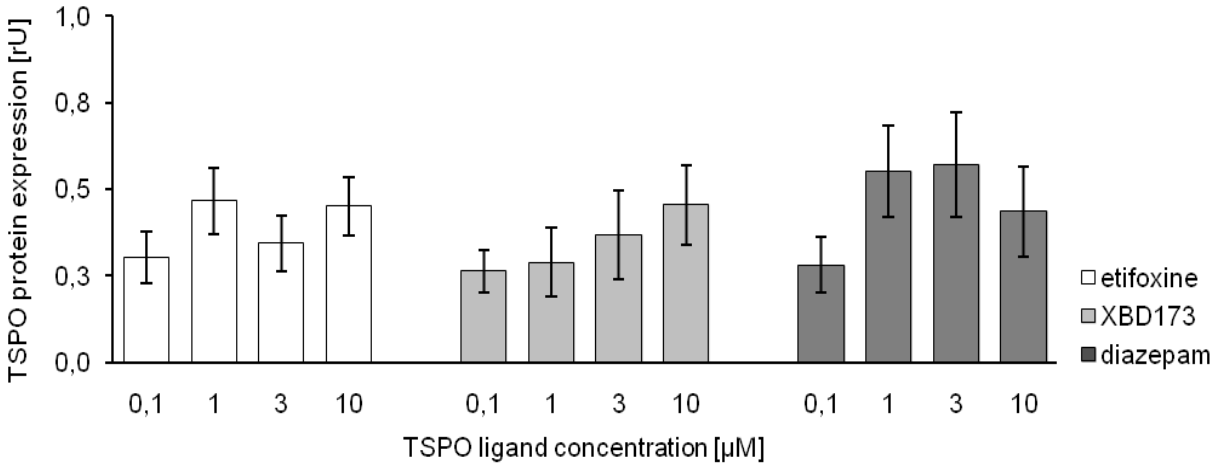


**Figure 11 TSPO protein expression in BV-2$_{wild-type}$ cells after ligand administration and 24 h incubation. Seventeen independent experiments were performed, results are presented as arbitrary units (rU), normalized to β-actin and in relation to solvent control.**

XBD173, etifoxine and diazepam significantly increased TSPO protein expression already at the lowest concentration applied when compared to solvent control (t-test; $p<0.05$). However, there were no significant concentration-related effects on TSPO expression after XBD173, etifoxine or diazepam treatment (ANOVA; $F = 1.452$, $df = 3, 230$, $p = 0.228$). Moreover, there was no significant difference between the different drugs on TSPO protein expression (ANOVA; $F = 1.284$, $df = 2, 230$, $p = 0.279$) and no significant interaction effect between the different compounds and concentrations used (ANOVA; $F = 0.728$, $df = 6, 230$, $p = 0.627$). Within the used concentrations (0.1 µM to 10 µM) the drugs did not show toxic effects.

### 5.5.2 Analysis of the TSPO binding affinity after TSPO ligand treatment

The binding affinity of XBD173, etifoxine and diazepam to TSPO in BV-$2_{wild\text{-}type}$ cells was analyzed by means of a competitive [$^3$H]PK11195 radioligand binding assay to figure out if there is a correlation of the ligand binding affinity and the ligand induced TSPO function. The binding affinity of each ligand is shown as $IC_{50}$, which shows the concentration of a drug at 50% of [$^3$H]PK11195 displacement (figure 12).

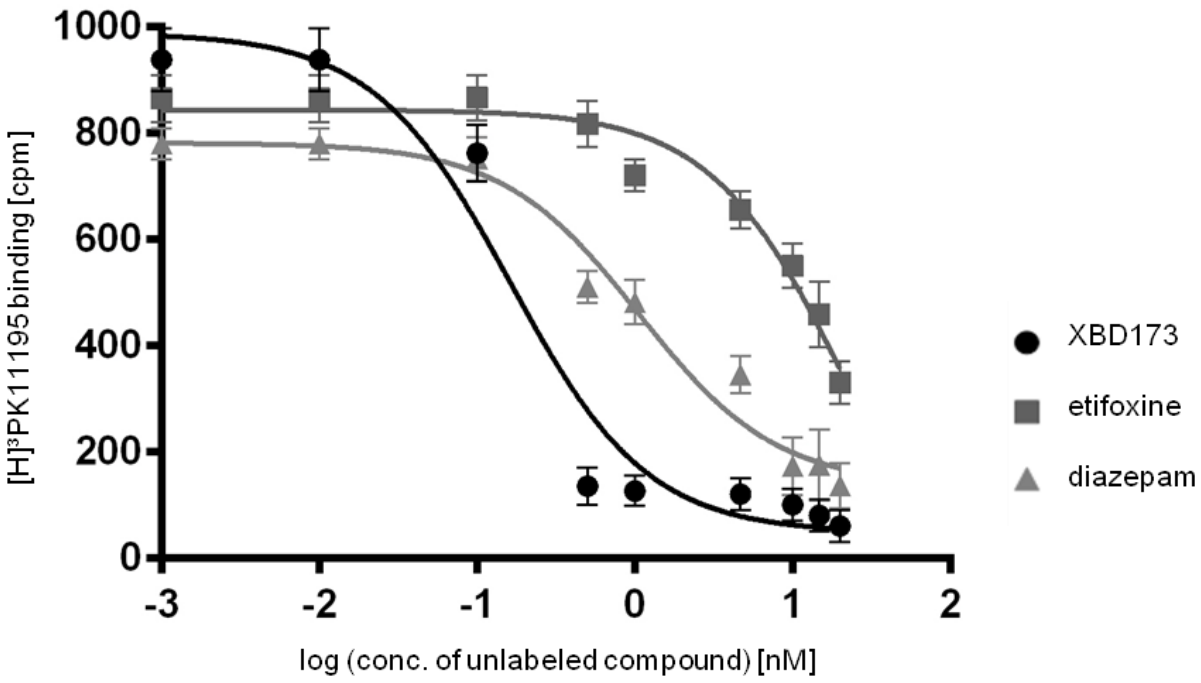


**Figure 12 Displacement of [$^3$H]PK11195 binding to TSPO by XBD173, etifoxine, or diazepam. Data represent the mean values of three independent experiments (each measured in triplicate). The competition of [$^3$H]PK11195 binding by increasing concentrations of incubated compounds in logarithmic representation is shown.**

$IC_{50}$ values appeared sufficient to compare binding affinities of these TSPO ligands, because experimental conditions were identical for all three TSPO ligands. XBD173 showed the highest binding affinity ($IC_{50}$ of 0.16 nM), diazepam showed an intermediate $IC_{50}$ of 1.07 nM and etifoxine had the lowest binding affinity by an $IC_{50}$ of 22.78 nM.

### 5.5.3 Neurosteroid synthesis

Because the anxiolytic efficacy of TSPO ligands is assumed to be determined by their potency to enhance neurosteroid synthesis, pregnenolone levels after treatment with XBD173, etifoxine or diazepam were measured in BV-$2_{wild\text{-}type}$ cells by means of ELISA. Effects of drug incubation on pregnenolone synthesis in BV-2 cells are presented in figure 13. Etifoxine turned out to be the most potent compound, which significantly upregulated pregnenolone levels dose-dependently (ANOVA; $F = 9.471$, $df = 3, 95$, $p<0.001$). However, upon treatment with the highest concentration (10 µM), there was a marked drop of pregnenolone synthesis. Also, XBD173 showed a significant enhancement of pregnenolone synthesis with a significant dose-response-relationship (ANOVA; $F = 3.247$, $df = 3, 95$, $p = 0.025$). Diazepam did not show a significant enhancement of pregnenolone synthesis at all concentrations.

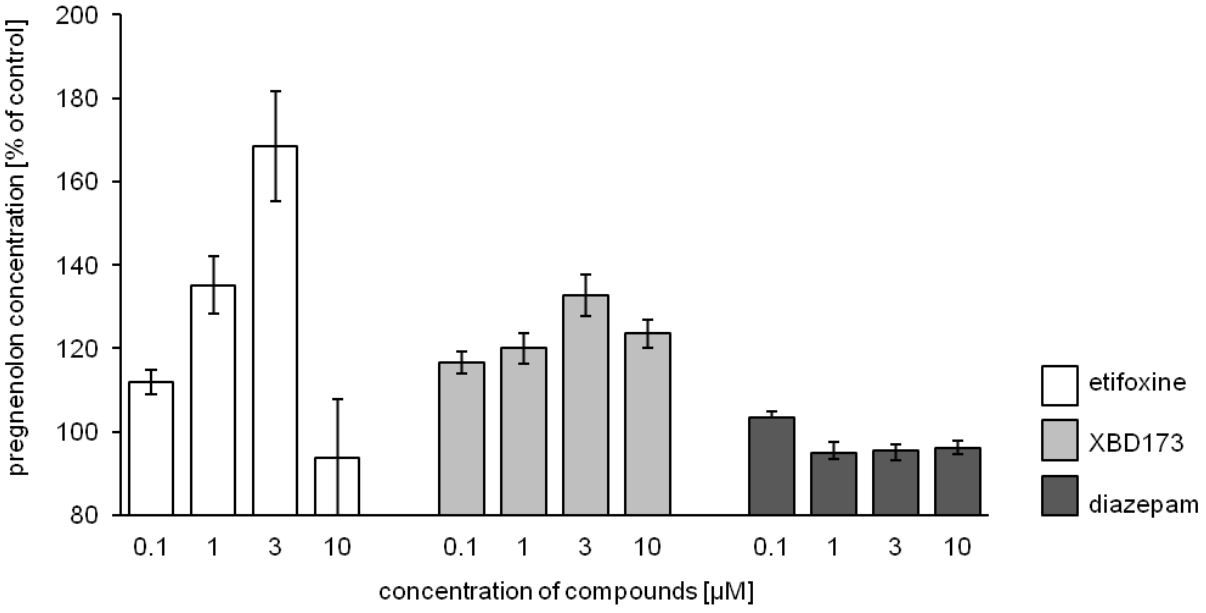


**Figure 13 Pregnenolone concentration after 24 h treatment with XBD173, etifoxine or diazepam. Six independent experiments were performed and normalized to solvent control. The average and the standard error of the mean were calculated.**

## 5.6 $Ca^{2+}$ levels via FURA-2 fluorescence technique

TSPO is assumed to be involved in $Ca^{2+}$ homeostasis but only rare data is available about a role in regulation of cytosolic and mitochondrial $Ca^{2+}$ concentration. Therefore, a $Ca^{2+}$ imaging experiment was performed to compare $Ca^{2+}$ levels in ER and mitochondrial of BV-$2_{scramble}$ (SCR) and BV-2-$TSPO_{knock\text{-}down}$ (KD) cells.

### 5.6.1 $Ca^{2+}$ imaging of BV-$2_{scramble}$ cells

A typical experimental pattern of BV-$2_{scramble}$ cells responding to ATP and FCCP can be seen in figure 14. The According to experimental pattern, FURA-2 based $Ca^{2+}$ imaging was performed on BV-$2_{scramble}$ cells and BV-2-$TSPO_{knock\text{-}down}$ cells after 24 h incubation with 10 µM XBD173, 100 nM PK11195, 100 nM Ro5-4864 and 100 ng/ml LPS. FURA-2 fluorescence ratio values ($F_{ratio(340/380)}$ values) from the regions of interest (ROIs) were analyzed (figure 15) and presented as arbitrary units (rU).

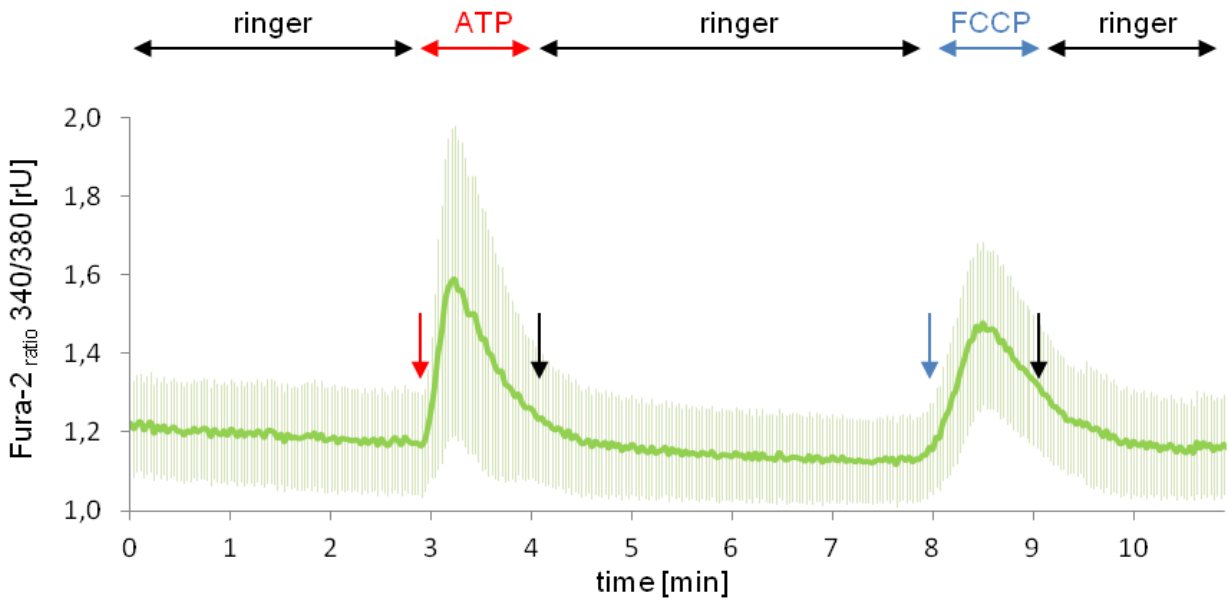


**Figure 14 A typical response curve of BV-$2_{scramble}$ cells to ATP (100 µM) and FCCP (10µM) application. BV-$2_{scramble}$ cells were stimulated using ATP (100µM), to release $Ca^{2+}$ from intracellular ER stores into the cytosol. ATP was applied for 60 seconds (red arrow). Cells were perfused 4 additional minutes with ringer, before they were stimulated with FCCP (10µM), which leads to an efflux of $Ca^{2+}$ from mitochondrial stores. FCCP was applied for 60 seconds, (blue arrow). The green graph shows the ratio of the FURA-2 fluorescence signals (340/380nm) in relative units [rU] plottet against the time in minutes [min]. Light green bars show the negative and positive standard deviation of each measured value.**

The fluorescence ratios of basal relative $Ca^{2+}$ concentration ($\Delta F_{ratio(340/380)basal}$) were measured in BV-$2_{scramble}$ (dark green) and BV-2-$TSPO_{knock\text{-}down}$ cells (light green) during ringer perfusion and normalized to solvent control. Results are presented in figure 15a.

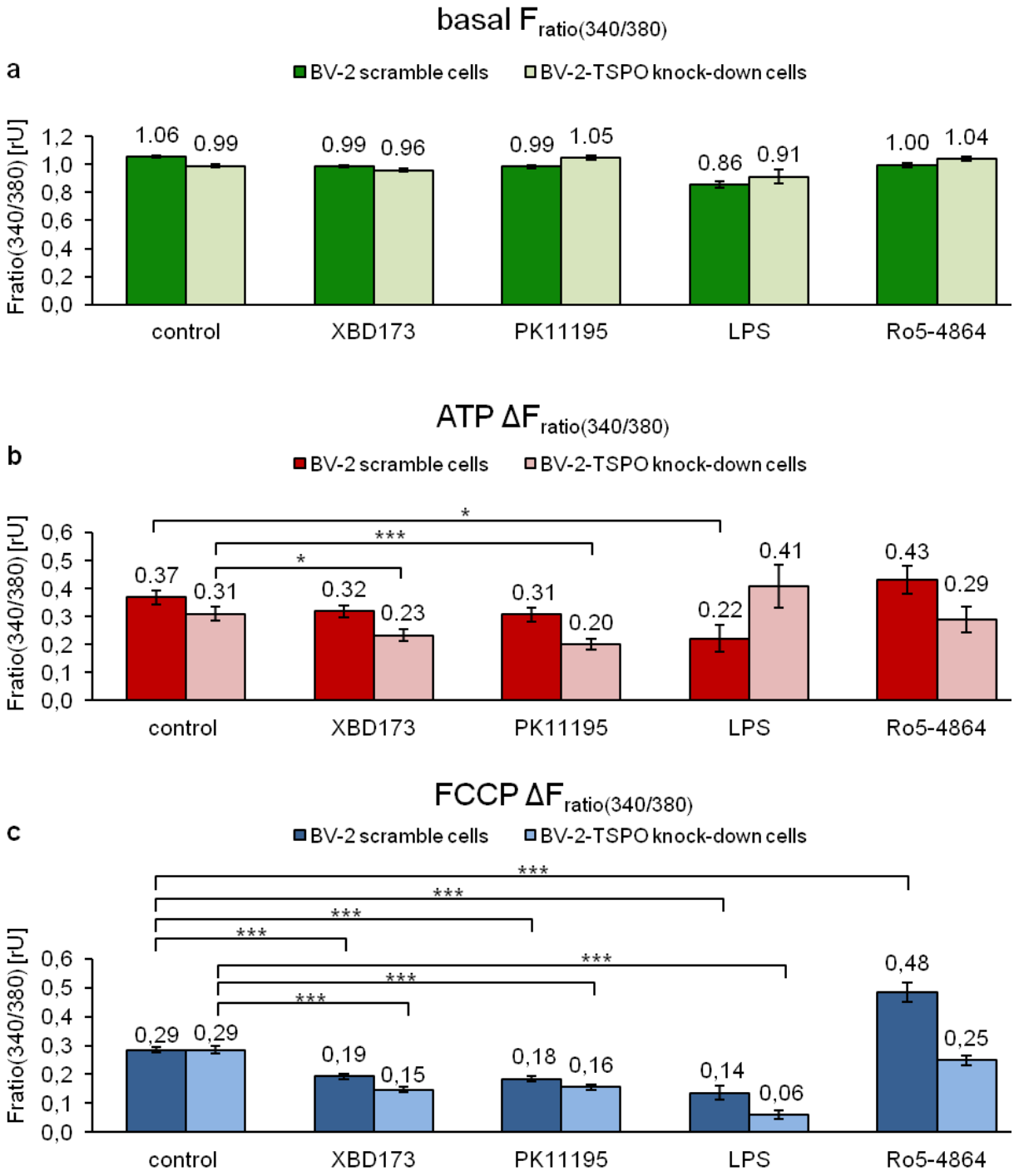


**Figure 15 FURA-2 based $Ca^{2+}$ imaging was performed on BV-2 scramble and BV-2-$TSPO_{knock\text{-}down}$ cells after 24 h incubation with 10 µM XBD173, 100 nM PK11195, 100 nM Ro5-4864 and 100 ng/ml LPS. FURA-2 fluorescence ratio values are presented as arbitrary units (rU).**

The fluorescence ratios after 100 µM ATP application ($\Delta F_{ratio(340/380)ATP}$) were also examined in BV-$2_{scramble}$ (dark red) and BV-2-$TSPO_{knock\text{-}down}$ cells (light red) and normalized to basal ratio. Results are presented in figure 15b and show the $Ca^{2+}$ which is released from ER stores. The FCCP-induced fluorescence ratios $\Delta F_{ratio(340/380)FCCP}$ were investigated in in BV-$2_{scramble}$ (dark blue) and BV-2-$TSPO_{knock\text{-}down}$ cells (light blue) after FCCP application and normalized to basal ratio. The results are presented in figure 15c, and show the $Ca^{2+}$ which is released from mitochondrial stores.

The basal fluorescence ratios $\Delta F_{ratio(340/380)basal}$ (figure 15a) showed no significant changes in the basal $Ca^{2+}$ signal of BV-$2_{scramble}$ cells (XBD173: 0.99; PK11195: 0.99; LPS: 0.86; Ro5-4864: 1.00) compared to BV-$2_{scramble}$ solvent control (SCR: 1.06) and of BV-2-$TSPO_{knock\text{-}down}$ cells (XBD173: 0.96; PK11195: 1.05; LPS: 0.91; Ro5-4864: 1.04) when compared to BV-2-$TSPO_{knock\text{-}down}$ solvent control (SCR: 0.99) after drug treatment.

The ATP-induced $Ca^{2+}$ signal $\Delta F_{ratio(340/380)ATP}$ (figure 15b; dark red) in BV-$2_{scramble}$ cells was increased in Ro5-4864 treated BV-$2_{scramble}$ cells (0.43), but without any significance when compared to BV-2 $_{scramble}$ solvent control (0.37). XBD173 and PK11195 treatment of BV-$2_{scramble}$ cells lead to a slightly, non-significantly decreased $Ca^{2+}$ signal (XBD173: 0.32; PK11195: 0.33), compared to BV-$2_{scramble}$ solvent control. Only LPS treated BV-$2_{scramble}$ cells showed a significant decreased $Ca^{2+}$ signal (0.22; t-test: $p=0.021$) compared to BV-$2_{scramble}$ solvent control.

The ATP-induced $Ca^{2+}$ signal $\Delta F_{ratio(340/380)ATP}$ in BV-2-$TSPO_{knock\text{-}down}$ cells (figure 15b; light red) was non-significantly increased in LPS treated BV-2-$TSPO_{knock\text{-}down}$ cells (LPS: 0.41) when compared to BV-2-$TSPO_{knock\text{-}down}$ solvent control (KD: 0.31). XBD173 (0.23; t-test: $p<0.05$) and PK11195 (0.20; t-test: $p<0.001$) treatment in BV-2-$TSPO_{knock\text{-}down}$ cells led to significantly decreased ATP-induced $Ca^{2+}$ signals when compared to BV-2-$TSPO_{knock\text{-}down}$ solvent control. Only Ro5-4864 treatment showed no changes of the ATP-induced $Ca^{2+}$ signal in BV-2-$TSPO_{knock\text{-}down}$ cells compared to BV-2-$TSPO_{knock\text{-}down}$ solvent control.

The FCCP-induced $Ca^{2+}$ signal $\Delta F_{ratio(340/380)FCCP}$ (figure 15c; dark blue) in BV-$2_{scramble}$ cells showed a high $Ca^{2+}$ signal in Ro5-4864 treated BV-$2_{scramble}$ cells, which is significantly increased when compared to BV-$2_{scramble}$ solvent control (Ro5-4864: 0.48; SCR solvent control: 0.22; t-test: $p<0.001$). The FCCP-induced $Ca^{2+}$ signal in XBD173, PK11195 and LPS treated BV-$2_{scramble}$ cells was low and significantly

decreased when compared to BV-$2_{scramble}$ solvent control (XBD173: 0.19; PK11195: 0.18; LPS: 0.14; t-test: $p<0.001$).

The FCCP-induced $Ca^{2+}$ signal $\Delta F_{ratio(340/380)FCCP}$ (figure 15c; light blue) in BV-2-$TSPO_{knock-down}$ cells was significantly decreased in XBD173 (0.15; t-test: $p<0.001$), PK11195 (0.16; t-test: $p<0.001$) and LPS (0.06; t-test: $p<0.01$) treated BV-2-$TSPO_{knock-down}$ cells when compared to BV-2-$TSPO_{knock-down}$ solvent control (0.29). Only Ro5-4864 treated BV-2-$TSPO_{knock-down}$ cells did not show any difference in the FCCP-induced $Ca^{2+}$ signal when compared to BV-2-$TSPO_{knock-down}$ solvent control.

Summarizing this experiment, the relative basal cytosolic $Ca^{2+}$ concentration is unaltered BV-2-$TSPO_{knock-down}$ cells when compared to BV-$2_{scramble}$ cells and the drug treatment did neither affect the relative basal cytosolic $Ca^{2+}$ concentration in BV-$2_{scramble}$ cells nor in BV-2-$TSPO_{knock-down}$ cells (figure 15a).

However, the ATP-induced $Ca^{2+}$ signal (indirect determination of ER $Ca^{2+}$ release) was increased in Ro5-4864 treated BV-$2_{scramble}$ cells, but decreased in XBD173, PK11195 and LPS treated BV-$2_{scramble}$ cells. The same pattern had become appearent with the FCCP-induced $Ca^{2+}$ signal (indirect determination of mitochondrial $Ca^{2+}$ release) in BV-$2_{scramble}$ cells: it was increased in Ro5-4864 treated BV-$2_{scramble}$ cells, but decreased in XBD173, PK11195 and LPS treated BV-$2_{scramble}$ cells. It is conceivable, that a high relative ER- $Ca^{2+}$ concentration correlates with high relative mitochondrial $Ca^{2+}$ concentration and vice versa. This assumption would lead to a direct ER-mitochondrial link – the mitochondrial associated membranes (MAM) which allow a rapid transmission of $Ca^{2+}$ signals between the ER and mitochondria thereby regulating mitochondrial bioenergetics (van Vilet et al., 2014). Another possibile explanation is a drug induced altered $Ca^{2+}$ storage capacity in ER and mitochodria: XBD173, PK11195 and LPS treatment appears to reduce $Ca^{2+}$ storage capacity in mitochondria and ER of BV-$2_{scramble}$ cells and Ro5-4864 treatement might lead to an increased $Ca^{2+}$ storage capacity in mitochondria and ER of BV-$2_{scramble}$ cells. Furthermore, it was neccesary to proof whether the obtained effects were TSPO mediated. Therefore, the same experiment was performed with BV-2-$TSPO_{knock-down}$ cells.

Direct comparison of the ATP-induced $Ca^{2+}$ signal (indirect determination of ER $Ca^{2+}$ release) and of the FCCP-induced $Ca^{2+}$ signal (indirect determination of mitochondrial $Ca^{2+}$ release) in BV-$2_{scramble}$ cells and BV-2-$TSPO_{knock-down}$ cells showed no significant

differences. This assumes, that a knock-down of TSPO has no effect on the ATP-induced and FCCP-induced $Ca^{2+}$ signal in BV-2 mouse microglia cells.

XBD173 and PK11195 treatment led to a decreased ATP-induced and to a decreased FCCP-induced $Ca^{2+}$ signal in BV-2-$TSPO_{knock\text{-}down}$ cells. This result underlines the prior statement of a drug induced alteration of $Ca^{2+}$ storage capacity in mitochondria and ER, which is unrelated to TSPO.

Furthermore, the ATP-induced $Ca^{2+}$ signal was decreased after LPS treatment in BV-$2_{scramble}$ cells, but increased in LPS treated BV-2-$TSPO_{knock\text{-}down}$ cells. This indicates a $Ca^{2+}$ regulating role of TSPO during inflammation caused by LPS. LPS treated TSPO knock-down cells and BV-$2_{scramble}$ cells showed a significantly decreased FCCP-induced $Ca^{2+}$ signal which indicates a TSPO independent effect.

A similar result was observed after Ro5-4864 treatment. The ATP-induced and the FCCP-induced $Ca^{2+}$ signal was reduced in BV-2-$TSPO_{knock\text{-}down}$ cells compared to BV-$2_{scramble}$ cells. This observation is in favor of the hypothesis` TSPO related effect.

## 5.7 Analysis of the mitochondrial membrane potential

BV-$2_{scramble}$ cells were loaded with the JC-1 dye as described in materials and methods. If the mitochondrial membrane potential is low (less hyperpolarized), JC-1 is predominantly a monomer yielding in green fluorescence. If the mitochondrial membrane potential is high, the dye aggregates which yields in a red to orange colored emission. Therefore, a decrease in the aggregate fluorescent count was an indicator for depolarization of the mitochondrial membrane potential whereas an increase was an indicator for hyperpolarization of the mitochondrial membrane potential.

The basal values in figure 16a show a significantly increased basal mitochondrial membrane potential in XBD173 treated cells (0.33; t-test: $p<0.05$), when compared to solvent control (0.30). PK11195, Ro5-4864 and LPS treatment resulted in a lower mitochondrial membrane potential, which is significantly decreased when compared to solvent control (PK11195: 0.21; t-test: $p<0.001$; Ro5-46864: 0.18; t-test: $p<0.001$; LPS: 0.15; t-test: $p<0.001$). BV-2-$TSPO_{knock\text{-}down}$ cells showed also a significantly decreased mitochondrial membrane potential (0.25; t-test, $p<0.01$) when compared to BV-$2_{scramble}$ solvent control.

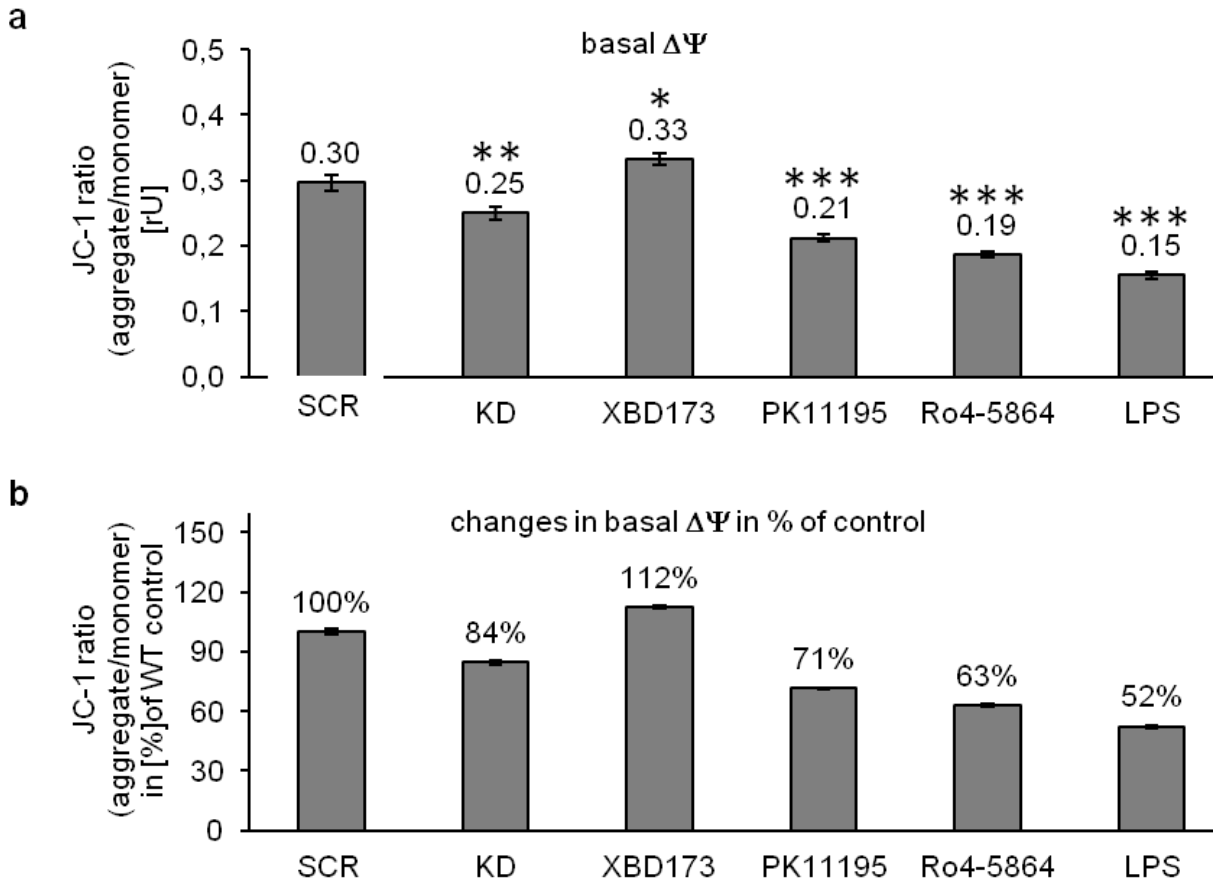


**Figure 16 BV-2-TSPO$_{knock-down}$ cells and BV-2$_{scramble}$ cells after 24h treatment with XBD173 (10 µM), PK11195 (100 nM), Ro5-4864 (100 nM) and LPS (100 ng/mL) were analyzed. JC-1 fluorescence ratios (JC-1 ratio $_{(aggregate/monomer)}$) were detected, normalized to solvent control and are presented in arbitrary units [rU] (a) / percent over solvent control (b).**

A decrease in the fluorescence ratio is an indicator for depolarization (low mitochondrial membrane potential ΔΨ) whereas an increase of fluorescence ratios is an indicator for hyperpolarization (high mitochondrial membrane potential ΔΨ). In BV-2$_{scramble}$ cells, the basal ΔΨ was increased in XBD173 treated cells but decreased in PK11195, Ro5-4864 and LPS treated cells and in BV-2-TSPO$_{knock-down}$ cells (without any treatment). According to Piccoli et al. the highest ΔΨ in XBD173 treated BV-2$_{scramble}$ cells indicates a high energetic status and thereby a low energy demand of these cells (Piccoli et al., 2006). PK11195, Ro5-4864 and LPS treatment and as well BV-2-TSPO$_{knock-down}$ cells showed a constantly lower ΔΨ, indicating a lower energetic status and a higher energy demand of these cells when compared to the BV-2$_{scramble}$ solvent control.

## 5.8 The bioenergetic profile of intact BV-2$_{scramble}$ cells

Cell respiration was analyzed in intact BV-2$_{scramble}$ cells and after 24 h treatment with either 10 µM XBD173, 100 nM PK11195, 100 nM Ro5-4864 or 100 nM LPS with the Seahorse Biosciences Extracellular Flux (XFp) Analyzer as described in material and methods. A typical Seahorse measurement pattern (figure 17) was used to analyze the bioenergetic function of BV-2$_{scramble}$ cells.

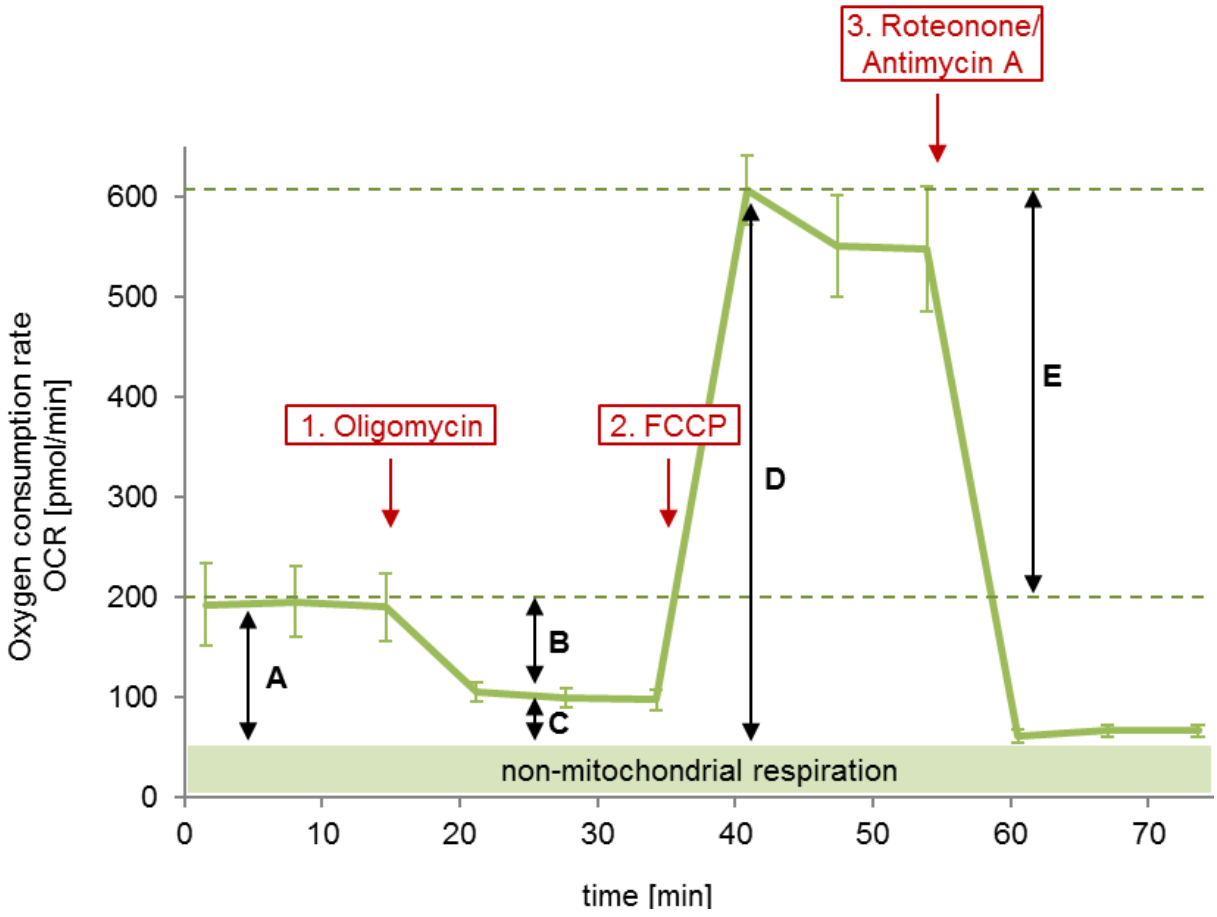


**Figure 17 The oxygen consumption rate (OCR) of BV-2$_{scramble}$ cells was analyzed with the Seahorse Bioscience XFp flux analyzer. Following the manufactures recommendations of the Seahorse Bioscience mito stress test, the basal oxygen consumption rate (A), the non-phosphorylating resting state (LEAK respiration) (C), the ATP turnover (B), the maximal respiration (D) and the Spare respiratory capacity (E) was analyzed in intact BV-2 $_{scrambe}$ cells after 24h treatment with various drugs.**

The obtained OCR data for basal respiration (A), uncoupled, non-phosphorylating LEAK respiration (B), ATP turnover (C), maximal respiration (D) and spare respiratory capacity (E) are shown in figure 18 a-d reported as OCR in pmol per

minute. In the simplified representation of the data (figure 18e), respiratory changes in each experimental setup are shown in ratio solvent control (100% baseline).

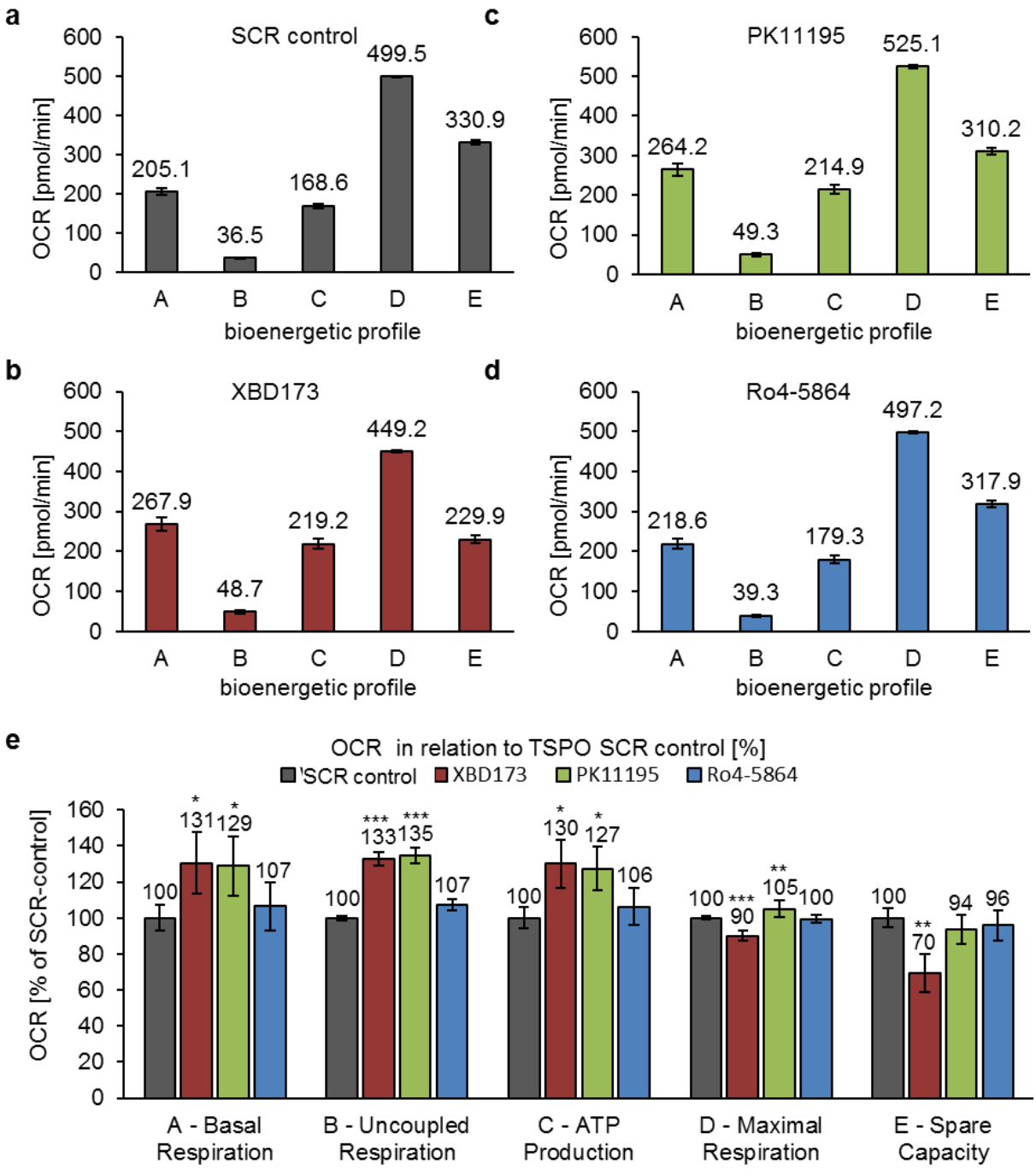


**Figure 18 The basal respiration (A), the leak respiration (B), the calculated ATP turnover (C), the maximal respiration (D) and the spare respiratory capacity (E) were analyzed in drug treated BV-2$_{scramble}$ cells and normalized to BV-2$_{scramble}$ cells solvent control.**

The basal respiration in XBD173 (267.9 pmol/min), PK11195 (264.2 pmol/min) and Ro4-45864 (218.6 pmol/min) treated BV-2$_{scramble}$ cells was enhanced when compared

to BV-$2_{scramble}$ solvent control (205.1 pmol/min), XBD173 (t-test: $p< 0.05$) and PK11195 (t-test: $p< 0.05$) increase was significant (figure 18e).

Then, oligomycin was applied to inhibit the ATP-synthase and induce the non-phosphorylating, uncoupled leak respiration of the cells. XBD173 (48.7 pmol/min; t-test: $p>0.001$) and PK11195 (49.3 pmol/min; t-test: $p>0.001$) treated cells show a significantly increased leak respiration, whereby Ro5-4864 (39.3 pmol/min) treatment led to a non-significant increase when compared to solvent control (36.5 nmol/min).

On the basis of these oligomycin-induced leak respiration results ATP turnover can be calculated. This calculation led to a significant increase of ATP turnover in both, XBD173 (219.2 pmol/min; t-test: $p>0.5$) and PK11195 (214.9 pmol/min; t-test: $p<0.05$) treated cells and to a non-significant increase of ATP turnover after Ro5-4864 (179.3 pmol/min) treatment when compared to solvent control (168.6 pmol/min).

Following the protocol procedure, FCCP as an uncoupling agent collapses the proton gradient and disrupts the mitochondrial membrane potential resulting in an unlimited electron flow through the ETC. This leads to an increase of electron flow and thereby an increase in oxygen consumption. XBD173 treatment led to a significant decrease in maximal respiration (449.2 pmol/min; t-test; $p<0.001$), whereby PK11195 (525.1 pmol/min; t-test: $p<0.01$) treatment provides a significant increase in maximal respiration when compared to solvent control (499.5 pmol/min). This presumably leads to a higher maximal respiratory capacity of XBD173 treated cells and a lower maximal respiratory capacity of PK11195 treated cells compared to solvent control. No significant changes in maximal respiration were detected Ro5-4864 (497.2 pmol/min) treated cells compared to solvent control.

The spare respiratory capacity is defined as maximal respiratory capacity minus basal respiratory capacity. All treated BV-$2_{scramble}$ cells led to a lower spare respiratory capacity (PK11195: 310.2 pmol/min; Ro5-4864: 317.9pmol/min) compared solvent control (330.9 pmol/min), however only XBD173 treated BV-$2_{scramble}$ cells showed a significant decrease (229.9 pmol/min; t-test; $p<0.001$).

### 5.9 The bioenergetic profile of intact BV-$2_{scramble}$ and BV-2-$TSPO_{knock-down}$ cells

In order to show a direct involvement of TSPO in mitochondrial respiration, intact BV-$2_{scramble}$ cells and BV-2-$TSPO_{knock-down}$ cells were analyzed by using the Seahorse Biosciences Extracellular Flux (XFp) Analyzer as described in materials and

methods. The method allows the real-time analysis of bioenergetic changes depending on the presence or absence of TSPO in the cells.

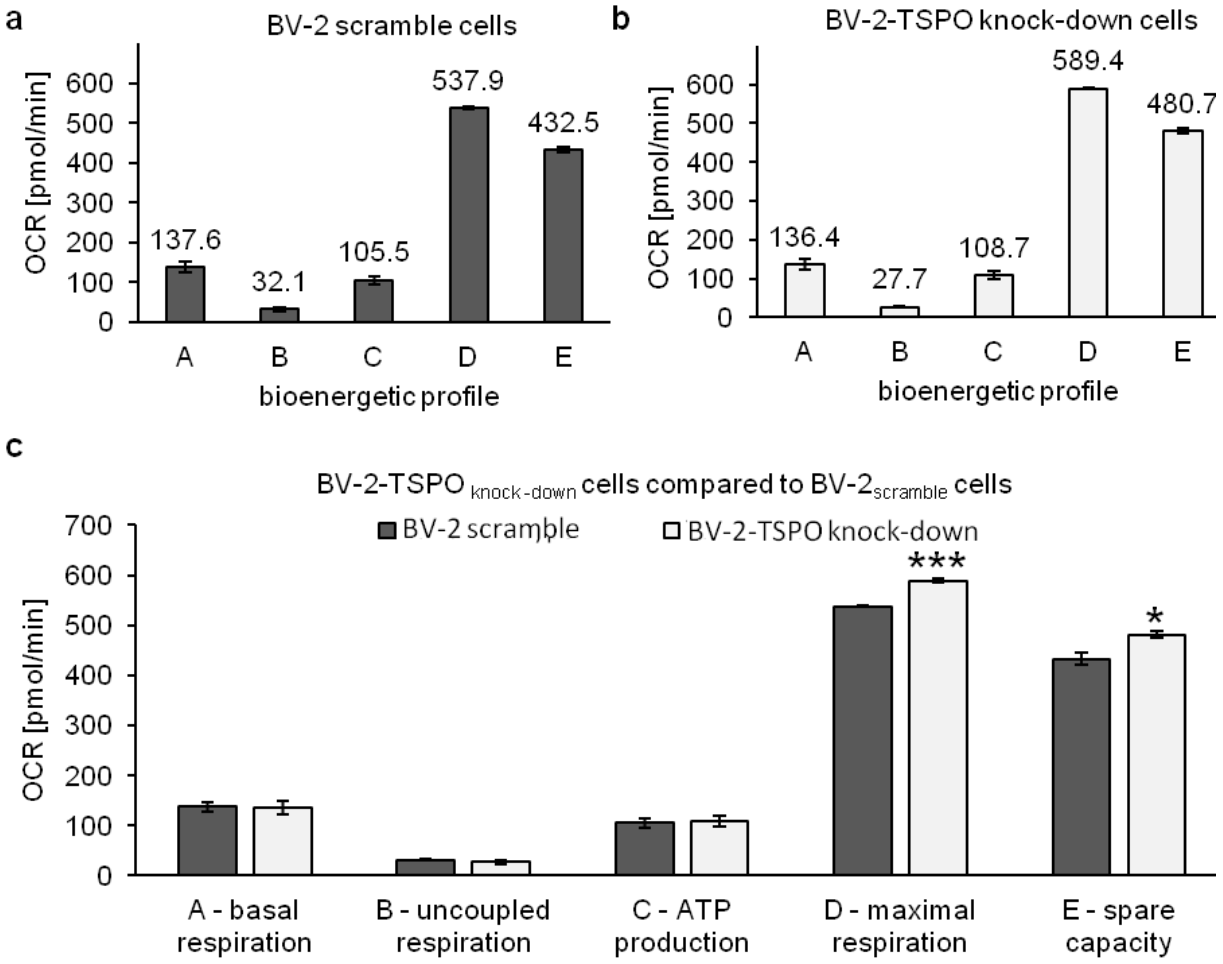


**Figure 19 The bioenergetic profile of BV-2-TSPO$_{knock-down}$ cells and BV-2$_{scramble}$ cells.**
**(a)-(b) Basal respiration (A), non-phosphorylating LEAK respiration (B), ATP turnover (C), maximal respiration (D) and spare respiratory capacity (E) are presented as OCR in pmol per minute. (c) Respiratory changes in BV-2-TSPO$_{knock-down}$ cells statistically compared to BV-2$_{scramble}$ cells.**

The OCR data for basal respiration (A), non-phosphorylating LEAK respiration (B), ATP turnover (C), maximal respiration (D) and spare respiratory capacity (E) are shown in figure 19a and 19b presented as pmol per minute. In figure 19c respiratory changes in BV-2-TSPO$_{knock-down}$ cells are statistically compared to BV-2$_{scramble}$ cells.
The basal respiration (A) of both, BV-2$_{scramble}$ (137.6 pmol/min) and BV-2-TSPO$_{knock-down}$ cells (136.4 pmol/min) showed no significant differences. After oligomycin application, the remaining cell respiration reflected the non-phosphorylating leak respiration (B) of the cells. The leak respiration of BV-2$_{scramble}$ cells (32.1 pmol/min)

did not show significant changes when compared to the leak respiration of BV-2-TSPO$_{knock-down}$ cells (27.7 pmol/min). Then, the ATP turnover (C) was calculated as the difference between basal respiration and leak respiration. The ATP turnover of BV-2-TSPO$_{knock-down}$ cells (108.7pmol/min) did not differ significantly from the one of BV-2$_{scramble}$ cells (105.5 pmol/min). The following FCCP injection led to dissipation of the mitochondrial membrane potential. As a result, BV-2-TSPO$_{knock-down}$ cells showed a significantly increased maximal respiration (D) (589.4 pmol/min; t-test: $p<0.001$) compared to BV-2$_{scramble}$ cells (537.9 pmol/min). Thus, BV-2-TSPO$_{knock-down}$ cells appear to have a higher maximal respiratory capacity when compared to BV-2$_{scramble}$ cells. The spare respiratory capacity (E) of BV-2-TSPO$_{knock-down}$ cells (480.7 pmol/min; t-test: $p<0.05$) is significantly higher than the one of BV-2$_{scramble}$ cells (432.5 pmol/min).

## 5.10 High resolution respirometry in permeabilized cells

The respiration (oxygen flux) of either $1x10^6$ BV-2$_{scramble}$ or $1x10^6$ BV-2-TSPO$_{knock-down}$ cells was analyzed in separated O2k-chambers and recorded in real-time using the Oroboros O2k oxygraph. The used SUIT protocol is visualized in figure 20. The routine respiration of untreated cells (A) was measured before the injection of 4 µl digitonin led to permeabilization of the cells, resulting in the basal respiration of permeabilized BV-2 cells (B). In a following step, the non-phosphorylating LEAK-respiration was induced by adding the complex-I-linked substrates malate (0.5 mM) and glutamate (10 mM), but not ADP. After that, complex-I-linked oxidative phosphorylation (OXPHOS) capacity (C) was investigated separately by addition of a saturating concentration of ADP (2.5 mM). After addition of the complex-II-linked substrate succinate (10 mM), it was possible to analyze the combined complex-I and complex-II-linked OXPHOS-capacity (E). Oligomycin (ATPase synthase inhibitor) injection (2.5 µM) inhibited the $O_2$ consumption until the LEAK state of respiration was reached, representing again the non-phosphorylating resting state when ATP synthase is not active (F). Further inhibition of complex-I by rotenone (0.5 µM) led to the measurement of complex-II-linked ETS capacity. In order to figure out whether there were further oxygen-consuming processes, complex-III was inhibited by antimycin A (2.5 µM). The resulting residual oxygen consumption (ROX) reflects oxygen consumption from undefined sources (Gnaiger, 2014).

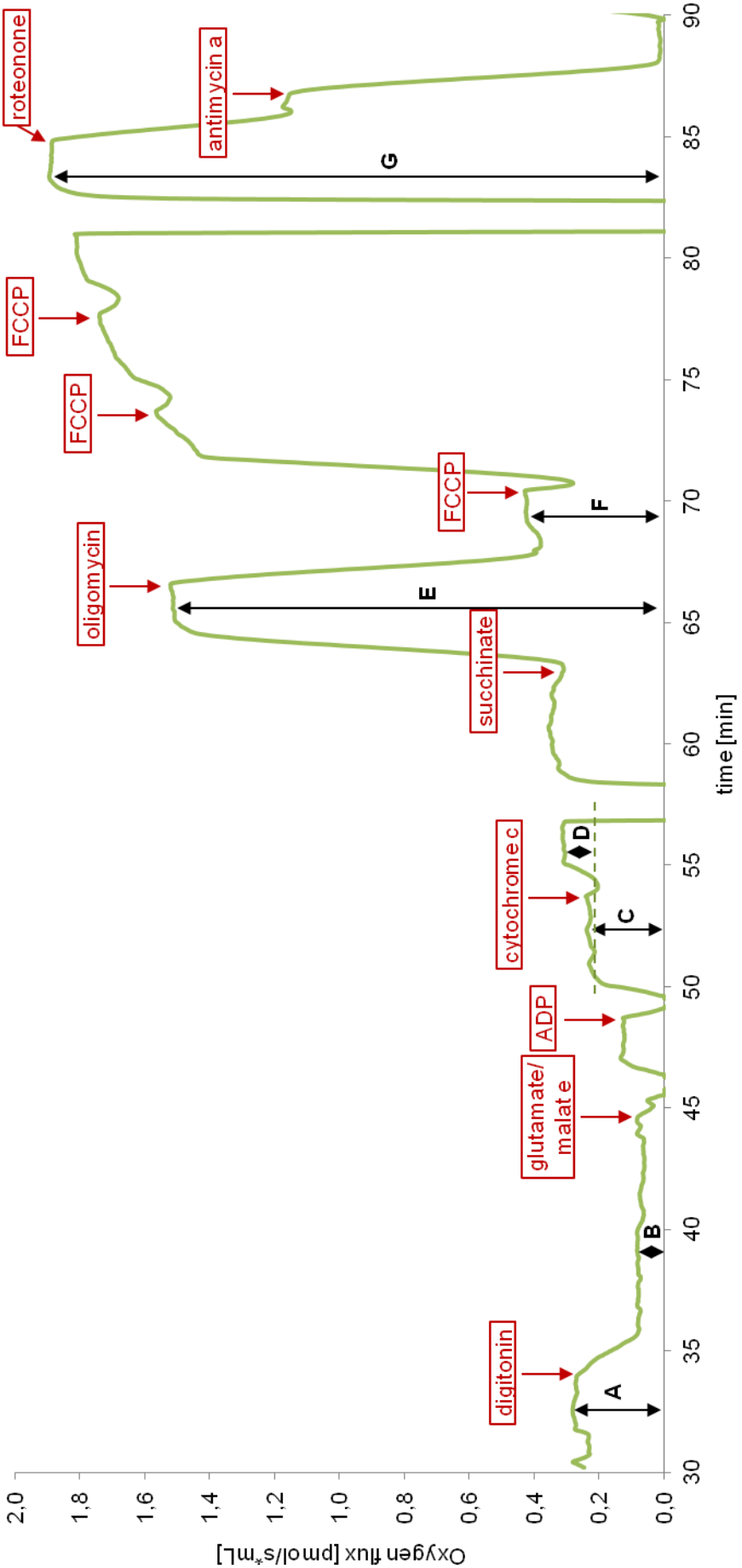


**Figure 20 The SUIT protocol for permeabilized mouse microglia cells for high resolution respirometry analysis with the OROBOROS O2k. Oxygen flux of BV-2-TSPO$_{wild\text{-}type}$cells (green line) was determined using an O2k oxygraph. Cells with a stable routine respiration (A) were permeabilized by addition of 4µl digitonin to measure the oxygen flux in permeabilized cells (B). Then, complex-I-linked substrates malate (0.5 mM) and glutamate (10 mM) were added, followed by 2.5 mM ADP, which is now able to enter through the cell membrane. This allows to measure complex-I-linked oxidative phosphorylation (OXPHOS) capacity (C). In the next step, cytochrome C was iniected to measure the cytochrome C effect (D).**

The statistical analysis of the high resolution respirometry experiment of $10^6$ BV-2-TSPO$_{knock\text{-}down}$ cells and $10^6$ BV-2$_{scramble}$ cells is shown in figure 21 according to the SUIT protocol (figure 20).

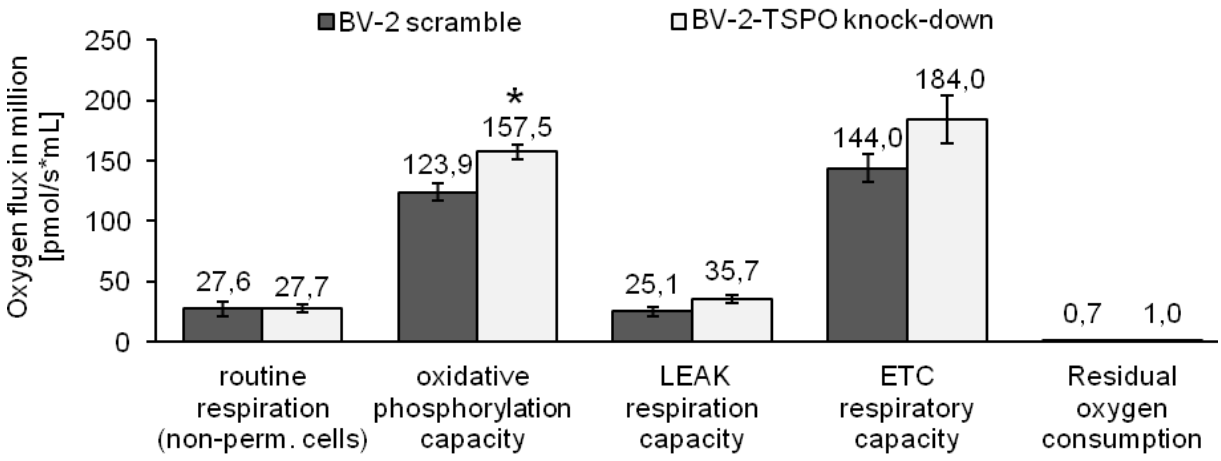


**Figure 21 The bioenergetic profile of BV-2-TSPO$_{knock\text{-}down}$ cells (light grey bars) compared to BV-2$_{scramble}$ ells (dark grey bars). The used SUIT protocol is described in figure 20. The analysis was performed using the same amount of BV-2$_{scramble}$ and BV-2-TSPO$_{knock\text{-}down}$ cells.**

BV-2-TSPO$_{knock\text{-}down}$ cells (light grey bars) show a routine respiration comparable to BV-2$_{scramble}$ cells (dark grey bars). OXPHOS, LEAK and ETC respiratory capacity are increased in BV-2-TSPO$_{knock\text{-}down}$ cells (OXPHOS: 157.5 pmol/s*mL; LEAK: 35.7 pmol/s*mL; 184.0 pmol/s*mL) when compared to BV-2$_{scramble}$ cells (OXPHOS: 123.9 pmol/s*mL; LEAK: 25.1 pmol/s*mL; 144.0 pmol/s*mL), whereby the increase of OXPHOS capacity is significant (t-test, $p<0.05$).

A specific OXPHOS examination of permeabilized cells was performed in $10^6$ BV-2-TSPO$_{knock\text{-}down}$ cells and $10^6$ BV-2$_{scramble}$ cells (figure 21). BV-2-TSPO$_{knock\text{-}down}$ cells showed a higher complex-I (43.5 pmol/s*mL) and complex-II (114.1 pmol/s*mL) - linked OXPHOS capacity than BV-2$_{scramble}$ cells (cI: 33.2 pmol/s*mL; cII: 90.7 pmol/s*mL). However, only the total OXPHOS (sum of complex-I and complex-II-linked OXPHOS capacity) showed a significant (t-test; $p<0.05$) increase in BV-2-TSPO$_{knock\text{-}down}$ cells (157.5 pmol/s*mL) compared to BV-2$_{scramble}$ cells (123.9 pmol/s*mL).

Summarizing this experiment, the presence of TSPO (BV-2$_{scramble}$) leads to a lower ATP utilization and a lower oxidative phosphorylation, which is decreased in both to complex-I and complex-II respiratory capacity. Regarding the mitochondrial

membrane potential experiments, BV-$2_{scamble}$ cells showed a higher energy state of the cell indicating a reduced energy demand which indeed correlates with the lower ATP utilization.

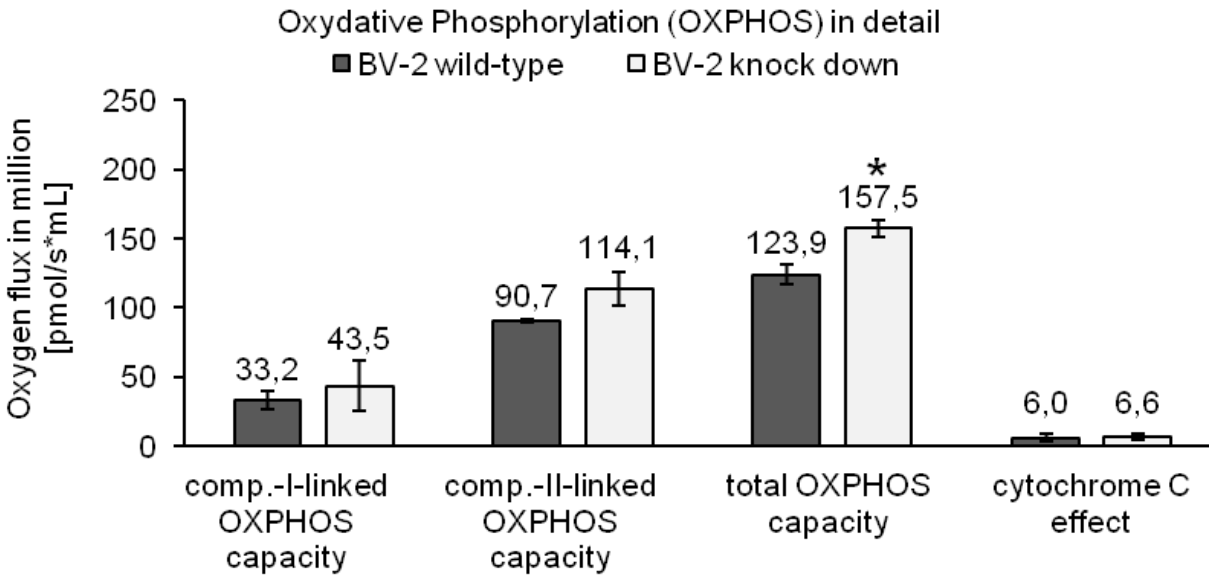


**Figure 22 A specific OXPHOS examination of permeabilized cells was performed in $10^6$ BV-2-$TSPO_{knock-down}$ cells and $10^6$ BV-$2_{scramble}$ cells.**

# 6 Discussion

TSPO is a highly conserved protein, which is expressed in every species (Li et al., 2015) from bacteria to mammals (Yeliseev & Kaplan, 1995). Due to its expression in steroid synthesizing cells and the given high affinity cholesterol binding property, numerous studies have been attempting a putative functional role of TSPO in cholesterol translocation and neurosteroidogenesis (Papadopoulos et al., 1997), (Li et al., 2015). Moreover, TSPO has been suggested to be a component of the mPTP (McEnery et al., 1992), thereby regulating mPTP opening. Recent studies now question the role of TSPO in steroidogenesis, its involvement in the mPTP and the physiological role related to PPIX and heme biosynthesis (Zhao et al. 2016), (Morohaku et al., 2014), (Tu et al., 2014), (Banati et al., 2014), (Šileikytė et al., 2014), (Selvaraj & Stocco, 2015), (Gatliff & Campanella, 2016), (Selvaraj & Tu, 2016). Whereby recent studies are based on genetic TSPO deletions, the early studies only used TSPO ligands to detect any pharmacological effects, which now are purported to be non-specific or related on secondary responses unrelated to TSPO (Tu et al., 2015), (Šileikytė et al., 2014). Therefore, it seems that the precise physiological and pathological function of TSPO is still unknown (Selvaraj & Stocco, 2015), (Gatliff & Campanella, 2016), (Selvaraj & Tu, 2016).

It is a common assumption that ancient, evolutionarily highly conserved gene should be essential for the proper regulation of precise, fundamental physiological processes (McLean et al., 2011). Regarding the possible new role of TSPO in mitochondrial metabolism, neurosteroidogenesis and involvement in ROS generation (Gut et al., 2015), (Selvaraj & Tu, 2016), (Selvaraj & Stocco, 2015), it is still necessary and indispensable to work with genetic TSPO deletions, avoiding any artefacts or secondary effects of TSPO ligands unrelated to TSPO. To get deeper insight in this relationship of TSPO and neurosteroid synthesis, and the role of TSPO in brain mitochondrial metabolism with regard to calcium homoeostasis, respiration and mitochondrial membrane potential a BV-2-TSPO$_{knock\text{-}down}$ model was performed and used in this thesis.

*TSPO is a regulatory protein of neurosteroidogenesis*

The role of TSPO in steroidogenesis is still a frequently discussed and examined topic. Since recent in vivo and in vitro studies using TSPO knock-out models have been refuting its role in steroidogenesis, there is still an open question of TSPO involvement in neurosteroidogenesis (Selvaraj & Tu, 2016). The brain is able to produce neurosteroids *de novo* to regulate neuronal function (Schumacher et al., 2000). In contrast to steroidogenesis, neurosteroidogenesis is not hormone-regulated. Many studies demonstrated TSPO ligands modulating brain neurosteroidogenesis (Papadopoulos et al., 2014), (Selvaraj & Tu, 2016). Neurosteroids are known to evoke anti-inflammatory effects in the brain (Stoffel-Wagner, 2003), (Pinna et al., 2006). Induction of neurosteroid synthesis in the brain by TSPO ligands has already been used to reduce neuropsychiatric disease symptoms in vivo (Rupprecht et al., 2010). There is still an open frame of TSPO involvement in neurosteroidogenesis (Selvaraj & Tu, 2016). And therefore, in order to pursue this issue, the function of TSPO regarding neurosteroid synthesis was analyzed in a comparative study between BV-$2_{scrambled}$ cells and BV-2-$TSPO_{knock-down}$ cells.

*Neurosteroidogenesis in BV-2-$TSPO_{knock-down}$ cells*

A lentiviral TSPO knock-down was performed in BV-2 cells. Western Blot and immunostaining confirmed a significant downregulation of TSPO in BV-2-$TSPO_{knock-down}$ cells when compared to BV-$2_{scramble}$ cells (figure 4 and 5). Two different approaches were used to quantify pregnenolone levels: an antibody-based ELISA and a gas chromatography/mass spectrometry approach. BV-2-$TSPO_{knock-down}$ cells showed a significant decrease in pregnenolone concentration when compared to BV-$2_{scramble}$ cells after analysis with ELISA technique (figure 9c). The GC/MS technique analysis also showed a significant decrease in pregnenolone concentration of BV-2-$TSPO_{knock-down}$ cells when compared to BV-$2_{scramble}$ cells (figure 10c) which is comparable to the ELISA results. This result supports my hypothesis that TSPO plays a regulatory role in neurosteroid synthesis of brain microglia cells.
A further analysis using ELISA and GC/MS technique compared the pregnenolone concentration of BV-2-$TSPO_{knock-down}$ cells and BV-$2_{scramble}$ cells after 24h ligand

treatment (figure 9 and 10). Ligand treatment of BV-$2_{scramble}$ cells shows a significant increase of pregnenolone concentration after XBD173 treatment (figure 9a and 10a), assuming a TSPO-specific effect of XBD173. BV-2-$TSPO_{knock\text{-}down}$ cells showed no enhanced pregnenolone concentration after XBD173 treatment, confirming a TSPO-specific effect of XBD173 in the regulation of neurosteroid synthesis.
A recent study measuring steroid production via pregnenolone concentration was performed by Banati et al. (2014) and showed contrary results. The group was using whole TSPO knock-out mice to analyze the pregnenolone concentration from blood samples via ELISA. They obtained concentration values in a normal range of both TSPO knock-out samples and scramble samples without any significant differences. However, Banati et al. did not directly analyze the pregnenolone concentration in brain cells compared to my experiments based on the single use of brain microglia cells. The use of brain cells allows a better insight in brain neurosteroidogenesis as Banati could just assume by using whole blood samples. The fact that expression of TSPO in the brain is quite low (Daugherty et al., 2013) in ratio to the total body expression makes it even more difficult to have a direct correlation to the neurosteroidogenesis analyzed by whole blood samples.

*How do TSPO ligands influence neurosteroid synthesis?*

Regarding pregnenolone as the precursor of all neurosteroids, the question recently has arised whether TSPO ligands are able to modulate pregenolone production in brain cells. Therefore the relationship between TSPO protein expression, TSPO binding affinity and the resulting effect of neurosteroid synthesis was analyzed in BV-$2_{wild\text{-}type}$ cells (figure 11, 12 and 13). The used TSPO ligands were chosen by their ability to treat anxiety disorders. Etifoxine was the first TSPO ligand with clinical anxiolytic effects, XBD173 exerts potent anxiolytic efficacy in animals as well as in humans and diazepam is a frequently prescribed anxiolytic, also binding to TSPO. XBD173, etifoxine and diazepam all show considerable binding affinities to TSPO in the [$^3$H]PK11195 radioligand binding assay of BV-2-$TSPO_{wild\text{-}type}$ cells (figure 12). XBD173 turned out to be the ligand with the highest binding affinity, followed by diazepam and etifoxine. Furthermore, XBD173, etifoxine and diazepam increased the TSPO protein expression in BV-2-$TSPO_{wild\text{-}type}$ cells, but without showing a clear concentration-dependence (figure 11). The pregnenolone concentration was

significantly increased in BV-2-TSPO$_{wild\text{-}type}$ cells after XBD173 and etifoxine treatment (figure 13). As pointed out before, there is a discrepancy between the binding affinity of a ligand, the effect on TSPO protein expression and finally the enhancement of neurosteroid synthesis as a functional read out. Therefore, a certain TSPO binding affinity - as measured by [$^3$H]PK1195 radio ligand displacement - does not necessarily allow to conclude that the compound has an effect on neurosteroid synthesis just due to its pharmacological affinity.

Due to the results the impact of the selected drugs (XBD, PK11195, Ro5-4864 and LPS) on pregnenolone synthesis was analyzed. By the use of both GC / MS and ELISA technique, we could demonstrate a significant increase in pregnenolone concentration after 24 hours incubation with XBD173. LPS, PK11195 and Ro5-4864 incubation led to a decreased pregnenolone concentration.

The upregulation of the protein expression after 24h incubation with the same drugs XBD173, LPS, PK11195 and Ro5-4864 was confirmed by Western Blot which clearly demonstrates that the upregulation of TSPO is not correlating with an increase in pregnenolone concentration and neurosteroid synthesis.

These results allow to conclude that the effects of TSPO ligands on neurosteroid synthesis are not dependent of the ligand`s binding affinity and the ligand`s protein expression. There is still an open question how the TSPO ligands can be arranged in a certain order due to its effect in pregnenolone production and thereby its effect in neurosteroid synthesis.

The most recent approach from Costa et al. explains the poor relationship between TSPO ligand binding affinities and steroidogenic efficacies with a new finding: the residence time that a compound spends in contact with the target. They found a positive correlation between the period for which a drug interacts with TSPO and the compounds ability to stimulate steroidogenesis. In particular, the specific residence time of a TSPO ligand significantly links the steroidogenic efficacy to the dose-response curve (combined parameter of drug potency and efficacy) (Costa, et al., 2016).

The aspect that TSPO ligands have additional sites of action (Šileikytė et al., 2014) arose with the recently critical consideration of early TSPO studies. Even more, it yielded in the assumption that previous pharmacological effects on steroidogenesis or in mPTP opening, mostly performed by the use of TSPO ligands, could be non-

specific or unrelated to TSPO (Tu et al., 2015), (Šileikytė et al., 2014), (Selvaraj & Tu, 2016).

*TSPO plays a role in Ca2+ homeostasis in inflammatory states*

However, there is only rare data about the role of TSPO in regulation of $Ca^{2+}$ concentration. No genetic TSPO deletion study was performed yet regarding especially $Ca^{2+}$ homoeostasis in brain cells. Therefore, a $Ca^{2+}$ imaging experiment was performed to compare $Ca^{2+}$ in ER and mitochondrial stores of BV-$2_{scramble}$ cells with $Ca^{2+}$ in ER and mitochondrial stores of BV-2-$TSPO_{knock\text{-}down}$ cells. The experimental set up for $Ca^{2+}$ analysis in this thesis was different from actual available TSPO $Ca^{2+}$ studies and allowed a separate analysis of the ER-released $Ca^{2+}$ (ATP-induced $Ca^{2+}$ release) and the mitochondrial-released $Ca^{2+}$ (FCCP-induced $Ca^{2+}$ release).

The relative basal cytosolic $Ca^{2+}$ concentration is unaltered BV-2-$TSPO_{knock\text{-}down}$ cells when compared to BV-$2_{scramble}$ cells and the drug treatment did neither affect the relative basal cytosolic $Ca^{2+}$ concentration in BV-$2_{scramble}$ cells nor in BV-2-$TSPO_{knock\text{-}down}$ cells (figure 15a). This indicates, that TSPO has no effect on the relative basal cytosolic $Ca^{2+}$ concentration in BV-2 mouse microglia cells.

However, the ATP-induced $Ca^{2+}$ signal (indirect determination of ER-$Ca^{2+}$ release) was decreased in XBD173, PK11195 and LPS treated BV-$2_{scramble}$ cells (figure 15b). The same pattern had become appearent with the FCCP-induced $Ca^{2+}$ signal (indirect determination of mitochondrial $Ca^{2+}$ release) in BV-$2_{scramble}$ cells, it was decreased in XBD173, PK11195 and LPS treated BV-$2_{scramble}$ cells (figure 15c). It is conceivable, that the drugs altered the $Ca^{2+}$ storage capacity in ER and mitochodria: XBD173, PK11195 and LPS treatment appears to reduce $Ca^{2+}$ storage capacity in mitochondria and ER of BV-$2_{scramble}$ cells. Furthermore a high ER-$Ca^{2+}$ concentration correlates with high mitochondrial $Ca^{2+}$ concentration and vice versa. This assumption would lead to a direct ER-mitochondrial link – the mitochondrial associated membranes (MAM) which allow a rapid transmission of $Ca^{2+}$ signals between the ER and mitochondria thereby regulating mitochondrial bioenergetics (van Vilet et al., 2014). Studies show that these inter-organelle connections are also involved in $Ca^{2+}$ homeostasis, demonstrating $Ca^{2+}$ transfer from ER to mitochondria (Rodríguez-Arribas et al., 2016). It is conceivable, that MAMs compensate a

$Ca^{2+}$ dysbalance between ER and mitochondria to prevent cell death (Krols et al., 2016). Furthermore, XBD173 and PK11195 treatment led to a decreased ATP-and FCCP- induced $Ca^{2+}$ signal in both, BV-2-$TSPO_{knock\text{-}down}$ cells and BV-$2_{scramble}$ cells. This suggests that the pharmacological XBD173 and PK11195 effect in ER and mitochondria of BV-$2_{scramble}$ and BV-2-$TSPO_{knock\text{-}down}$ cells is not TSPO-mediated. Rearding to the prior statement of an altered the $Ca^{2+}$ storage capacity in ER and mitochodria, this finding underlines that XBD173 and PK11195 have additional sites of action, yielding in a non-specific, TSPO unrelated effect.

The ATP-induced $Ca^{2+}$ signal was decreased in LPS treated BV-$2_{scramble}$ cells, but increased in LPS treated BV-2-$TSPO_{knock\text{-}down}$ cells. This indicates a $Ca^{2+}$ regulating role of TSPO during a LPS-induced inflammation. LPS is a pro-inflammatory stimulus which promotes the secretion of pro-inflammatory cytokines, nitric oxide, and eicosanoids. Cytokines alter intracellular $Ca^{2+}$ levels by depleting $Ca^{2+}$ from the ER leading to protein misfolding and activation of the ER stress response (Yousefi et al., 2013), (Ramadan et al., 2011), (Brozzi et al., 2015). My result leads to the assumption that the presence of TSPO might be necessary to protect the cell from an increased ER-$Ca^{2+}$ release as a response to a pro-inflammatory stimulus.

Ro5-4864 treatment of BV-$2_{scramble}$ and BV-2-$TSPO_{knock\text{-}down}$ cells achieved no significant changes in the ER and mitochondrial $Ca^{2+}$ levels of BV-2-$TSPO_{knock\text{-}down}$ cells, but a great increase in the ER and mitochondrial $Ca^{2+}$ levels of BV-$2_{scramble}$ cells. This describes a TSPO-related enhancing effect in $Ca^{2+}$ buffering and $Ca^{2+}$ storage in both, the ER and the mitochondria after Ro5-4864 treatment.

*TSPO influences the energetic status of the cell*

According to Piccoli et al. a higher mitochondrial membrane potential ($\Delta\Psi$) is correlated with a higher energy state of the cell which can be referred to a lower energy and a lower ATP demand of the cell. If the cell has a lower ATP demand, less ADP is produced. As a result, less ADP is available for the ATP synthase which reduces the rate of oxygen consumption.

Vice versa, a lower mitochondrial membrane potential ($\Delta\Psi$) correlates with a lower energy state of the cell, which indicates a higher energy demand. ATP is then hydrolyzed into ADP, whereby ADP no longer limits the activity of the ATP synthase

and $\Delta\Psi$ immediately changes. This leads to a higher oxygen consumption rate (Piccoli et al., 2006).

$\Delta\Psi$ experiments were performed using the JC-1 fluorescence dye. The highest $\Delta\Psi$ in XBD173 treated BV-$2_{scramble}$ cells indicates a high energetic status and thereby a low energy demand of these cells. PK11195, Ro5-4864 and LPS treated BV-$2_{scramble}$ cells as well as BV-2-$TSPO_{knock\text{-}down}$ cells showed a constantly lower $\Delta\Psi$, indicating a lower energetic status and a higher energy demand of these cells compared to solvent control. This result indicates a reduction in the energy state of the cell, when TSPO is knocked down.

Analysis of the membrane potential led to the result, that the presence of TSPO has a positive effect on the energy state of the cells. Recent studies indicate that TSPO affects mitochondrial energy homeostasis through modulation of the fatty acid oxidation in cell types which are necessary for lipid storage/metabolism (Tu et al., 2016).

Based on the information about the TSPO ability to influence energy states of the cells, a respiration analysis was performed to figure out if the $\Delta\Psi$ result correlates with metabolic changes.

*Respiratory analysis of intact mouse microglia cells showed a TSPO related effect*

A respiration analysis with the Seahorse XFp flux analyzer (figure 18e) showed an enhanced basal respiration in drug treated BV-$2_{scramble}$ cells when compared to BV-$2_{scramble}$ solvent control. XBD173 and PK11195 treated cells showed a significantly increased leak respiration, which might be caused by a higher oxidative stress level in these cells triggered by XBD173 and PK11195. Calculating the ATP turnover, a significant increase was detectable in XBD173 and PK11195 treated cells. Further analysis obtained a significant decrease in maximal respiration of XBD173 treated cells and a significant increase in maximal respiration of PK11195 treated cells compared with solvent control. With regard to the membrane potential analysis, XBD173 treated BV-$2_{scramble}$ cells with an increased $\Delta\Psi$ (higher energy state of the cell) showed the expected decreased maximal respiration. Analogous, PK11195 treated BV-$2_{scramble}$ cells with a decreased $\Delta\Psi$ (lower energy state of the cell) showed the assumed increased maximal respiration. These XBD173 and PK11195 results of

the mitochondrial membrane potential analysis and the respiration experiment are mutually supportive.

In a separate experiment (figure 19) the respiration in intact BV-$2_{scramble}$ cells and BV-2-$TSPO_{knock\text{-}down}$ cells were compared (figure 19c). The basal respiration, leak respiration and the calculated ATP turnover in both, BV-$2_{scramble}$ and BV-2-$TSPO_{knock\text{-}down}$ cells showed no significant differences. The maximal respiration was significantly increased in BV-2-$TSPO_{knock\text{-}down}$ cells when compared to BV-$2_{scramble}$ cells. With regard to the mitochondrial membrane potential analysis BV-2-$TSPO_{knock\text{-}down}$ cells with a lower energy state of the cell achieved the expected increased maximal respiration. Finally, the spare respiratory capacity was also calculated. BV-2-$TSPO_{knock\text{-}down}$ cells showed an increased spare respiratory capacity when compared to BV-$2_{scramble}$ cells. This important factor, defining the vitality of the cells, also shows the cell's ability to respond to stress under conditions of increased energy demand. Certain parameters, such as substrate delivery to the mitochondria or the functional capacity of the enzymes involved in ETC, are able to influence this ability of the cell. For future investigations it is recommended to analyze ROS production in parallel to the respiration. One could figure out whether an altered or lower spare respiratory capacity is accompanied by ROS generation.

*Respiratory analysis showed a TSPO mediated OXPHOS increase*

To gain deeper insight in the metabolism a second comparative respiration analysis with the Oroboros O2k (high resolution respirometry) was performed (figure 20). Both, BV-$2_{scramble}$ and BV-2-$TSPO_{knock\text{-}down}$ cells showed a similar routine respiration of non-permeabilized cells. The same result was found in the Seahorse measurement. OXPHOS, LEAK and ETS respiratory capacity were increased in BV-2-$TSPO_{knock\text{-}down}$ cells, whereby only the enhanced OXPHOS capacity was significant (figure 21). Examining the OXPHOS in detail, high resolution respirometry of permeabilized cells was performed in BV-2-$TSPO_{knock\text{-}down}$ cells and BV-$2_{scramble}$ cells. A higher complex-I and complex-II-linked OXPHOS capacity was detected in BV-2-$TSPO_{knock\text{-}down}$ cells when compared to BV-$2_{scramble}$ cells (figure 22).

Summarizing the respiration experiments, the presence of TSPO (BV-$2_{scramble}$) leads to a lower ATP utilization and a lower oxidative phosphorylation which is decreased in both, complex-I and complex-II-linked OXPHOS capacity. Regarding the

mitochondrial membrane potential experiments, the same cells (BV-$2_{scamble}$) showed a higher energy state of the cell indicating a reduced energy demand which indeed correlates with the lower ATP utilization. The OXPHOS apparatus is the molecular machinery responsible for energy production, but each reduction of oxygen to water by aerobic respiration is accompanied by the formation of reactive intermediates, formerly known as ROS. Generally, complexes I and III are considered the major ROS sources, and complex I is considered to be the primary source of ROS in the brain under both physiological and pathological conditions. BV-2-$TSPO_{knock\text{-}down}$ cells show an increased OXPHOS activity which leads in an increased ATP utilization and thereby in a higher ROS production. It is conceivable, that the presence of TSPO is necessary (BV-$2_{scramble}$ cells), showing a reduced OXPHOS activity, leading in a decreased ATP utilization which finally protects the cell from alterations and cell death.

# 7 Conclusion

In conclusion, the precise function of TSPO 18 kDa is still under investigation. However, my results in this thesis represent a basic characterization of the role of TSPO in mitochondrial brain metabolism. The lentiviral TSPO knock-down in BV-2 mouse microglia cells pointed to a significant influence of TSPO on neurosteroid synthesis which was demonstrated by the use of two different approaches (ELISA and GC/MS) leading to the same results: I was able to figure out a role of TSPO in neurosteroidogenesis in the CNS. But there is still an open question of how exactly TSPO regulates the neurosteroid synthesis. For future investigations it is recommended to either use global KO mice or brain-tissue-specific KO mice in order to gain deeper insight in the detailed mechanism of the cholesterol transport of TSPO in brain mitochondria.

TSPO might play a role in $Ca^{2+}$ homoeostasis. Nevertheles, the basal cytosolic $Ca^{2+}$ level of BV-$2_{scramble}$ and BV-2-$TSPO_{knock\text{-}down}$ cells show no differences. XBD173 and PK11195 treatment in this thesis do not show any TSPO-related effect. But it is conceivable, that the influence of these drugs alter the $Ca^{2+}$ storage capacity in ER and mitochodria of both, BV-$2_{scramble}$ and BV-2-$TSPO_{knock\text{-}down}$ cells. Furthermore, LPS treatment resulted in a decreased ATP-induced $Ca^{2+}$ signal in BV-$2_{scramble}$ cells, but increased ATP-induced $Ca^{2+}$ signal BV-2-$TSPO_{knock\text{-}down}$ cells. This indicates a $Ca^{2+}$ regulating role of TSPO during inflammation (caused by LPS). LPS is a pro-inflammatory stimulus which promotes the secretion of pro-inflammatory cytokines, nitric oxide, and eicosanoids. Cytokines alter intracellular $Ca^{2+}$ levels by depleting $Ca^{2+}$ from the ER leading to protein misfolding and activation of the ER stress response (Yousefi et al., 2013), (Ramadan et al., 2011), (Brozzi et al., 2015). My result leads to the assumption that the presence of TSPO might be necessary to protect the cell from an increased ER $Ca^{2+}$ release as a response to a pro-inflammatory stimulus. Ro5-4864 treatment achieved no significant changes in the ER and mitochondrial $Ca^{2+}$ levels of BV-2-$TSPO_{knock\text{-}down}$ cells, but a great increase in the ER and mitochondrial $Ca^{2+}$ levels of BV-$2_{scramble}$ cells. This describes a TSPO-related increased effect in $Ca^{2+}$ buffering and $Ca^{2+}$ storage in both, the ER and the mitochondria after Ro5-4864 treatment. It has not yet been finally clarified which role TSPO plays in the $Ca^{2+}$ homoeostasis therefore it should be in the focus of further investigations.

Summarizing the respiration analysis and the mitochondrial membrane potential experiment these results indicate that the presence of TSPO increases or probably stabilizes the energy state of the cell, thereby regulating the energy demand of the cell. The following lower ATP utilization results in lower ROS production, which protects the cell from alterations and cell death.

Based on the data presented in this thesis, TSPO influences the mitochondrial metabolism of brain cells, which may be important to control a metabolic dysfunction by physiological modulation. For this reason TSPO is discussed as a regulatory protein and it should be given more attention to TSPO and its regulatory efficacy in mitochondrial metabolism, neurosteroidogenesis and ROS protection for a putative protective role against oxidative stress and mitochondrial metabolic dysfunction.

Furthermore, TSPO is located in the OMM, which is the cytosolic/mitochondrial interface that makes TSPO more accessible as another target / other proteins located within the mitochondrial matrix. This advantage makes TSPO a great pharmacological target for further investigation.

## References

Abbracchio, M. P., Burnstock, G., Verkhratsky, A., & Zimmermann, H. (2009). Purinergic signalling in the nervous system: an overview. Trends in Neuroscience , 32;(1):19-29.

Addgene. (2006, 12). Addgene Plasmid 10878. Protocol Version. Retrieved 11 20, 2015, from www.addgene.org: http://www.addgene.org/tools/protocols/plko/#C

Albrecht, D. S., Granzeria, C., Hooker, J. M., & Loggia, M. L. (2016). In Vivo Imaging of Human Neuroinflammation. ACS Chemical Neuroscience , 7(4):470-83.

Anholt, R. R., De Souza, E. B., Oster-Granite, M. L., & Snyder, S. H. (1985). Peripheral-type benzodiazepine receptors: autoradiographic localization in whole-body sections of neonatal rats. The Journal of pharmacology and experimental therapeutics , 233(2):517-26.

Anholt, R. R., Murphy, K. M., Mack, G. E., & Snyder, S. H. (1984). Peripheral-type benzodiazepine receptors in the central nervous system: localization to olfactory nerves. Journal of Neuroscience , 4, 593–603.

Anholt, R. R., Pederson, P. L., De Souza, E. B., & Snyder, S. H. (1986). The peripheral-type benzodiazepine receptor. Localization to the mitochondrial outer membrane. Journal of Biology and Chemistry , 261, 576–583.

Arbo, B. D., Benetti, F., Garcia-Segurac, L. M., & Ribeiroa, M. F. (2015). Therapeutic actions of translocator protein (18kDa) ligands in experimental models of psychiatric disorders and neurodegenerative diseases. Journal of Steroid Biochemistry & Molecular Biology , 154: 68–74.

Banati, R. B., Middleton, R. J., Chan, R., Hatty, C. R., Kam, W. W., Quin, C., et al. (2014). Positron emission tomography and functional characterization of a complete PBR/TSPO knockout. Nature Communications , 5:5452.

Banati, R. B., Myers, R., & Kreutzberg, G. W. (1997). PK (’peripheral benzodiazepine’)–binding sites in the CNS indicate early and discrete brain lesions: microautoradiographic detection of [3H]PK11195 binding to activated microglia. Journal of Neurocytology , 26, 77–8.

Baty, V., Denis, B., Goudot, C., Bas, V., Renkes, P., Bigard, M. A., et al. (1994). Hepatitis induced by alpidem (Ananxyl). Four cases, one of them fatal. Gastroenterological Clinical Biology , 18:1129–1131.

Bernadi, P. (1999). Mitochondrial transport of cations: channels, exchangers, and permeability transition. Physiological Review , 79:1127–1155.

Bernassau, J. M., Reversat, J. L., Ferrara, P., Caput, D., & Lefur, G. (1993). A 3D model of the peripheral benzodiazepine receptor and its implication in intra mitochondrial cholesterol transport. Journal of Molecular Graphics , 11, 236–244.

Berridge, M. J. (2012). Calcium signalling remodelling and disease. Biochemical Society , 40 (2012), pp. 297–309.

Bose, H. S., Lingappa, V. R., & Miller, W. L. (2002). Rapid regulation of steroidogenesis by mitochondrial protein import. Nature , 417:87–91.

Bradford, M. M. (1976). A rapid and sensitive method for the quantitation of microgram quantities of protein utilizing the principle of protein-dye binding. Analytical Biochemistry , 7;(72):248-54.

Braestrup, C., & Squires, R. (1977, September). Specific benzodiazepine receptors in rat brain characterized by high-affinity (3H)diazepam binding. Proceedings of the National Academy of Sciences , pp. 74(9): 3805–3809.

Brozzi, F., Nardelli, T. R., Lopes, M., Millard, I., Barthson, J., Igiollo-Esteve, M., et al. (2015). Cytokines induce endoplasmic reticulum stress in human, rat and mouse beta cells via different mechanisms. Diabetologia , 58(10):2307-16.

Campanella, M., Parker, N., Tan, C. H., Hall, A. M., & Duchen, M. R. (2009). IF(1): setting the pace of the F(1)F(o)-ATP synthase. Trends in Biochemical Science , 34(7):343-50.

Carre, M., Andre, N., Carles, G., Borghi, H., Brichese, L., Briand, C., et al. (2002). Tubulin is an inherent component of mitochondrial membranes that interacts with the voltage-dependant anion channel. Journal of Biological Chemistry, 277(37): 33664-9.

Casellas, P., Galiegue, S., & Basile, A. S. (2002). Peripheral benzodiazepine receptors and mitochondrial function. Neurochemistry International , 40(6):475-86.

Chauveau, F., Boutin, H., Van, C. N., Dolle, F., & Tavitian, B. (2008). Nuclear imaging of neuroinflammation:a comprehensive review of [11C]PK11195 challengers. European Journal of Neuclear Medicine and Molecular Imaging , 35:2304–2319.

Chen, C., Kuo, J., Wong, P., & Micevych, P. (2014). Estradiol modulates translocator protein (TSPO) and steroid acute regulatory protein (StAR) via protein kinase A (PKA) signaling in hypothalamic astrocytes. Endocrinology , 155;(8):2976–2985.

Chen, M. K., & Guilarte, T. R. (2008). Translocator protein 18kDa (TSPO): molecular sensor of brain injury and repair. Pharmacological Therapy , 118 (1):1–17.

Colombini, M. (2012). Mitochondrial outer membrane channels. Chemical reviews , 112, 6373−6387.

Costa, B., Da Pozzo, E., Giacomelli, C., Barresi, E., Taliani, S., Da Settimo, F., et al. (2016). TSPO ligand residence time: a new parameter to predict compound neurosteroidogenic efficacy. ACS Chemical Neuroscience , 17;7(8):1041-6.

Daugherty, D. J., Selvaraj, V., Chechneva, O. V., Liu, X. B., Pleasure, D. E., & Deng, W. (2013). A TSPO ligand is protective in a mouse model of multiple sclerosis. EMBO molecular medicine , (5) 891-903.

De Souza, E. B., Anholt, R. R., Murphy, K. M., Snyder, S. H., & Kuhar, M. J. (1985). Peripheral-type benzodiazepine receptors in endocrine organs: autoradiographic localization in rat pituitary, adrenal, and testis. Endocrinology , 116(2):567-73.

Delavoie, F., Li, H., Hardwick, M., Robert, J. C., Giatzakis, C., Péranzi, G., et al. (2003). In Vivo and in Vitro Peripheral-Type Benzodiazepine Receptor Polymerization:Functional Significance in Drug Ligand and Cholesterol Binding. Biochemistry , 42, 4506-4519.

Do-Rego, J. L., Mensah_Nyagan, A. G., Feuilloley, M., Ferrara, P., Pelletier, G., & Vaudry, H. (1998). The endozepine triakontatetraneuropeptide diazepam-binding inhibitor [17-50] stimulates neurosteroid biosynthesis in the frog hypothalamus. Neuroscience , 83 555-570.

Duchen, M. R. (1990). Effects of metabolic inhibition on the membrane properties of isolated mouse primary sensory neurones. Journal of Physiology , 424;():387-409.

Edison, P., Archer, H. A., Gerhard, A., Hinz, R., Pavese, N., Turkheimer, F. E., et al. (2008). Microglia, amyloid, and cognition in Alzheimer's disease: An [11C](R)PK11195-PET and [11C]PIB-PET study. Neurobiology of disease , 32(3):412-9.

File, S. E., & Lister, R. G. (1983). The anxiogenic action of Ro 5-4864 is reversed by phenytoin. Neuroscience Letters , 35 (1): 93–6.

Fur, G., Perrier, M. L., Vaucher, N., Imbault, F., Flamier, A., Benavides, J., et al. (1983). Peripheral benzodiazepine binding sites: effect of PK 11195, 1-(2-chlorophenyl)-N-methyl-N-(1-methylpropyl)-3-isoquinolinecarboxamide. I. In vitro studies. Life Science , 32, 1839–1847.

Gatliff, J., & Campanella, M. (2012). The 18Kda Translocator Protein (TSPO): A New Perspective in Mitochondrial Biology. Current Molecular Medicine , 12(4):356-68.

Gatliff, J., & Campanella, M. (2016). TSPO: kaleidoscopic 18-kDa amid biochemical pharmacology, control and targeting of mitochondria. Biochem J , 473(2):107-21.

Gatliff, J., East, D., Crosby, J., Abeti, R., Harvey, R., Craigen, W., et al. (2014). TSPO interacts with VDAC1 and triggers a ROS-mediated inhibition of mitochondrial quality control. Autophagy , 10:2279–2296.

Gehlert, D. R., Yamamura, H. I., & Wamsley, J. K. (1985). Autoradiographic localization of "peripheral-type" benzodiazepine binding sites in the rat brain, heart and kidney. Naunyn-Schmiedeberg's Archives of Pharmacology , 328, 454–460.

Gerencser, A. A., Neilson, A., Choi, S. W., Edman, U., Yadava, N., Oh, R. J., et al. (2009). Quantitative Microplate-Based Respirometry with Correction for Oxygen Diffusion. Analytical Chemistry , 81;(16):6868–6878.

Ghadery, C., Koshimori, Y., Coakeley, S., Harris, M., Rusjan, P., Kim, J., et al. (2017). Microglial activation in Parkinson’s disease using [18F]-FEPPA. Journal of Neuroinflammation , 14: 8.

Gilquin, B., Taillebourg, E., Cherradi, N., Hubstenberger, A., Gay, O., Merle, N., et al. (2010). The AAA + protein ATAD3A controls mitochondrial dynamics at the interface of the inner and outer membranes. Molecular Cell Biology , 30:1984 –1996.

Gincel, D., Zaid, H., & Shoshan-Barmatz, V. (2001). Calcium binding and translocation by the voltage-dependent anion channel: a possible regulatory mechanism in mitochondrial function. Journal of Biochemistry , 358(Pt 1): 147-55.

Gnaiger, E. (2014). Mitochondrial pathways and respiratory control. An introduction to OXPHOS analysis. 4th ed. Inssbruck: OROBOROS MiPNet Publications.

Gnaiger, E., Kuznetsov, A. V., Schneeberger, S., Seiler, R., Brandacher, G., Steurer, W., et al. (2000). Mitochondria in the cold. In K. M. Heldmaier G, Life in the Cold (pp. 431-442). Berlin, Heidelberg, New York: Springer.

Gut P, Z. M., Gut, P., Zweckstetter, M., & Banati, R. B. (2015). Lost in translocation: the functions of the 18-kD translocator protein. Trends in Endocrinology and Metabolism , 26(7):349-56.

Gut, P. (2015). Targeting mitochondrial energy metabolism with TSPO ligands. Biochemical Society Transactions , 43(4):537-42.

Hamon, A., Morel, A., Hue, B., Verleye, M., & Gillardin, J. M. (2003). The modulatory effects of the anxiolytic etifoxine on GABAA receptors are mediated by the beta subunit. Neuropharmacology , 45:293–303.

Hardwick, M., Fertikh, D., Culthy, M., Li, H., Vidic, B., & Papadopouolos, V. (1999). Peripheral-type benzodiazepine receptor (PBR) in human breast cancer: correlation of breast cancer cell aggressive phenotype with PBR expression, nuclear localization, and PBR-mediated cell proliferation and nuclear transport of cholesterol. Cancer Research , 59, 831–842.

Harris, J. R. (2010). Cholesterol Binding and Cholesterol Transport Proteins: Structure and Function in Health and Dissease. Hexham, Northumberland: Science.

Hirsch, J. D., Beyer, C. F., Malkowitz, L., Beer, B., & Blume, A. J. (1989). Mitochondrial Benzodiazepine Receptors Mediate Inhibition of Mitochondrial Respiratory Control. Molecular Pharmacology , 35(1):157-63.

Hodge, T., & Colombini, M. (1997). Regulation of metabolite flux through voltage-gating of VDAC channels. Journal of Membrane Biology , 157(3): 271-9.

Hubstenberger A., (2008). ATAD 3A and ATAD 3B are distal 1p-located genes differentially expressed in human glioma cell lines and present in vitro antioncogenic and chemoresistant properties. Experimental cell research , 314:2870 –2883.

Issop, L., Ostuni, M. A., Lee, S., Laforge, M., Péranzi, G., Justin, P., et al. (2016). Translocator Protein-Mediated Stabilization of Mitochondrial Architecture during Inflammation Stress in Colonic Cells. PLoS One , 11(4).

Jaremko, L., Jaremko, M., Giller, K., Becker, M., & Zweckstetter, M. (2014). Structure of the Mitochondrial Translocator Protein in Complex with a Diagnostic Ligand. Science , 343 (6177): 1363-1366.

Jaremko, L., Jaremko, M., Giller, K., Becker, S., & Zweckstetter, M. (2015b). Conformational Flexibility in the Transmembrane Protein TSPO. Chemistry , 9;21(46):16555-63.

Jaremko, M., Jaremko, L., Jaipuria, G., Becker, S., & Zweckstetter, M. (2015a). Structure of the mammalian TSPO/PBR protein. Biochemical Society Transactions , 43 (4) 566-571.

Jonas, E. (2006). BCL-xL regulates synaptic plasticity. Molecular Interactions , 6, 208–222.

Joo, H. K., Lee, Y. r., Kang, G., Choi, S., Kim, C. S., Ryoo, S., et al. (2015). The 18-kDa Translocator Protein Inhibits Vascular Cell Adhesion Molecule-1 Expression via Inhibition of Mitochondrial Reactive Oxygen Species. Molecules and Cells , 38(12):1064-70.

Kanto J, K. L. (1975). Cerebrospinal-fluid concentration of diazepam and its metabolites in man. Acta Pharmacol Toxicol , 36(4):328-34.

Kelly-Hershkovitz E, W. R. (1998). Effects of peripheral-type benzodiazepine receptor antisense knockout on MA-10 Leydig cell proliferation and steroidogenesis. The Journal of biological chemistry , 273 (5478-5483).

Kita, A., Kinoshita, T., Kohayakawa, H., Furukawa, K., & Akaike, A. (2009). Lack of tolerance to anxiolysis and withdrawal symptoms in mice repeatedly treated with AC-5216, a selective TSPO ligand. Neuropsychophamacology Biology Psychiatry , 33;(6):1040–104.

Kita, A., Kohhayakawa, H., & Kinoshita, T. (2004). Antianxiety and antidepressant-like effects of AC-5216, a novel mitochondrial benzodiazepine receptor ligand. British Journal of Pharmacology , 142;(7):1059–1072.

Korkov, V. M., Sachse, C., Short, J. M., & Tate, C. G. (2010). Three-dimensional structure of TspO by electron cryomicroscopy of helical crystals. Structure , 8(6):677-87.

Korneyev, A., Pan, B. S., Polo, A., Romeo, E., Guidotti, A., & Costa, E. (1993). Stimulation of brain pregnenolone synthesis by mitochondrial diazepam binding inhibitor receptor ligands in vivo. Journal of neurochemistry , 61 1515-1524.

Kozikowski, A. P., Ma, D., Brewer, J., Sun, S., Costa, E., Romeo, E., et al. (1993). Chemistry, binding affinities, and behavioral properties of a new class of "antineophobic" mitochondrial DBI receptor complex (mDRC) ligands. Journal of medicinal chemistry , 36 2908-2920.

Krols, M., Bultynck, B., & Janssens, S. (2016). ER–Mitochondria contact sites: A new regulator of cellular calcium flux comes into play. Journal of Cell Biology , 214 (4): 367.

Langer, S. Z., Arbilla, S., Benavides, J., & Scatton, B. (1990). Zolpidem and alpidem: two imidazopyridines with selectivity for omega 1- and omega 3-receptor subtypes. Advances in Biochemical Psychopharmacology , 46:61–72.

Larcher, J. C., Vayssiere, J. L., Le Marquer, F. J., Cordeau, L. R., Keane, P. E., Bachy, A., et al. (1989). Effects of peripheral benzodiazepines upon the O2 consumption of neuroblastoma cells. European Journal of Pharmacology , 161(2-3):197-202.

Leduc, M. S., Hageman, R. S., Verdugo, R. A., Tsaih, S. W., Walsh, K., Churchill, G. A., et al. (2011). Integration of QTL and bioinformatic tools to identify candidate genes for triglycerides in mice. Journal of Lipid Research , 52, 1672-1682.

Lemasters, J. J., & Holmuhamedov, E. (2006). Voltage-dependent anion channel (VDAC) as mitochondrial governator—Thinking outside the box. Biochimica et Biophysica Acta (BBA) - Molecular Basis of Disease , (1762);(2);p.181–190.

Li, D., Zhen, J., Wang, M., Feng, L., Lu, Y., Yang, N., et al. (2016a). Wuling powder prevents the depression-like behavior in learned helplessness mice model through improving the TSPO mediated-mitophagy. Journal of Ethnopharmacology, 186:181-8.

Li, D., Zheng, J., Wang, M., Feng, L., Ren, Z., Liu, Y., et al. (2016b). Changes of TSPO-mediated mitophagy signaling pathway in learned helplessness mice. Psychiatry research , 245:141-147.

Li, F., Liu, J., Garavito, R. M., & Ferguson-Miller, S. (2015). Evolving understanding of translocator protein 18 kDa (TSPO). Pharmacol Res , 99:404-9.

Li, F., Liu, J., Zheng, Y., Garavito, R. M., & Ferguson-Miller, S. (2015). Crystal structures of translocator protein (TSPO) and mutant mimic of a human polymorphism. Science , 347(6221), 555-558.

Li, H., & Papadopoulos, V. (1998). Peripheral-type benzodiazepine receptor function in cholesterol transport. Identification of a putative cholesterol recognition/ interaction amino acid sequence and consensus pattern. Endocrinology , 139 (12):4991–4997.

Li, H., Yao, Z., Degenhardt, B., Teper, G., & Papadopoulos, V. (2001). Cholesterol binding at the cholesterol recognition/ interaction amino acid con-sensus (CRAC) of the peripheral-type benzodiazepine receptor and inhibition of steroidogenesis by an HIV TAT-CRAC peptide. Pro-ceedings of the National Academy of Sciences of the United States of America , 98:1267–1272.

Liu, G. J., Middleton, R. J., Hatty, C. R., Kam, W. W., Pham, T., Harrison-Brown, M., et al. (2014a). The 18 kDa translocator protein, microglia and neuroinflammation. Brain Pathology , 24, 631–653.

Liu, G. J., Middleton, R. J., Kam, W. W., Chin, D. Y., Hatty, C. R., Chan, R. H., et al. (2017). Functional gains in energy and cell metabolism after TSPO gene insertion. Cell Cycle , 19:0.

Liu, X., Li, W., Dai, L., Zhang, T., Xia, W., Liu, H., et al. (2014b). Early repeated administration of progesterone improves the recovery of neuropathic pain and modulates spinal 18kDa-translocator protein (TSPO) expression. The Journal of Steroid Biochemistry and Molecular Biology , 143:130–140.

Lodish, H., Kaiser, C., Bretscher, A., Amon, A., Berk, A., Krieger, M., et al. (2013). 12.2. Mitochondria and the Citric acid Cycle. In H. Lodish, C. Kaiser, A. Bretscher, A. Amon, A. Berk, M. Krieger, et al., Molecular Cell Biology. 7th edition (pp. 524-532). New York: W.H. Freeman and Company.

Maeda, J., Higuchi, M., Inaji, M., Ji, B., Haneda, E., Okauchi, T., et al. (2007). Phase-dependent roles of reactive microglia and astrocytes in nervous system injury as delineated by imaging of peripheral benzodiazepine receptor. Brain Research , 1157, 100–111.

Malgaroli, A., Milani, D., Meldolesi, J., & Pozzan, T. (1987). Fura-2 measurement of cytosolic free Ca2+ in monolayers and suspensions of various types of animal cells. Journal of Cell Biology , 105(5):2145-55.

Manji, H., Kato, T., Di Prospero, N. A., Ness, S., Beal, M. F., Krams, M., et al. (2012). Impaired mitochondrial function in psychiatric disorders. Nature Reviews Neuroscience , 18;13(5):293-307.

Mattson, M. P., Gleichmann, M., & Cheng, A. (2008). Mitochondria in neuroplasticity and neurological disorders. Neuron , 60, 748–766.

McEnery, M. W., Snowman, A. M., Trifiletti, R. R., & Snyder, S. H. (1992). Isolation of the mitochondrial benzodiazepine receptor: association with the voltage-dependent anion channel and the adenine nucleotide carrier. Proceedings of the National Academy of Sciences , 89, 3170–317.

McLean, C. Y., Reno, P. L., Pollen, A. A., Bassan, A. I., Capelli, T. D., Guenther, C., et al. (2011). Human-specific loss of regulatory DNA and the evolution of human-specific traits. Nature , 471 (7337): 216–219.

Morina, D., Musmana, J., Posna, S., Berdeauxa, A., & Ghaleha, B. (2016). Mitochondrial translocator protein (TSPO): From physiology to cardioprotection. Biochemical Pharmacology , 1;105:1-13.

Morohaku, K., Pelton, S. H., Daugherty, D. J., Butler, W. R., Deng, W., & Selveraj, V. (2014). Translocator protein/peripheral benzodiazepine receptor is not required for steroid hormone biosynthesis. Endocrinology , 155:89–97.

Morrison, E. A., & Henzler-Wildman, K. A. (2012). Reconstitution of integral membrane proteins into isotropic bicelles with improved sample stability and expanded lipid composition profile. Acta Biochimica et Biophysica Sinica , 1818, 814–820.

Motloch, L. J., Hu, J., & Akar, F. G. (2015). The mitochondrial translocator protein and arrhythmogenesis in ischemic heart disease. Oxidative medicine and cellular longevity , 2015:234104.

Murail, S., Robert, J. C., Coic, Y. M., Neumann, J. M., Ostuni, M. A., Yao, Z. X., et al. (2008). Secondary and tertiary structures of the transmembrane domains of the translocator protein TSPO determined by NMR. Stabilization of the TSPO tertiary fold upon ligand binding. Biochimica et Biophysica Acta , 1778, 1375–1381.

Jamin, N., Neumann, J.M., Ostuni, M.A., Vu, T.K., Yao, Z.X., Murail, S., Robert, J.C., Giatzakis, C., Papadopoulos, V., Lacapère, J.J. (2005). Characterization of the cholesterol recognition amino acid consensus sequence of the peripheral-type benzodiazepine receptor. Molecular Endocrinology , 19, 588–594.

Nguyen, N., Fakra, E., Pradel, V., Jouve, E., Alquier, C., Le Guern, M. E., et al. (2006). Efficacy of etifoxine compared to lorazepam monotherapy in the treatment of patients with adjustment disorders with anxiety: a double-blind controlled study in general practice. Hauman Psychopharmacology , 21;(3):139-149.

Nothdurfter, C., Baghai, T. C., Schüle, C., & Rupprecht, R. (2012). Translocator protein (18 kDa) (TSPO) as a therapeutic target for anxiety and neurologic disorders. European archieves of psychiatry and clinical neuroscience , 2:S107-12.

Olson, J. M., Ciliax, B. J., Mancini, W. R., & Young, A. B. (1988). Presence of peripheral-type benzodiazepine binding sites on human erythrocyte membranes. Eur. J. Pharmacol , 152, 47–53.

Ostuni, M. A., Issop, L., Péranzi, G., Walker, F., Faaseu, M., Elbim, C., et al. (2010). Overexpression of translocator protein in inflammatory bowel disease: potential diagnostic and treatment value. Iflammatory Bowel Disseases , 16: 1476–1487.

Ostuni, M., Ducroc, R., Péranzi, G., Tonon, M. C., Papadopoulos, V., & Lacapere, J. J. (2007). Translocator protein (18 kDa) ligand PK 11195 induces transient mitochondrial Ca2+ release leading to transepithelial Cl− secretion in HT-29 human colon cancer cells. Biology of the cell , 99, 639–647.

Owen, D. R., & Matthews, P. M. (2011). Imaging brain microglial activation using positron emission tomography and translocator protein-specific radioligands. International Review of Neurobiology , 101, 19–39.

Palzur, E., Sharon, A., Shehadeh, M., & Soustiel, J. F. (2016). Investigation of the mechanisms of neuroprotection mediated by Ro5-4864 in brain injury. Neuroscience , 329:162-70.

Papadopoulos, V. (2014). On the Role of the Translocator Protein (18-kDa) TSPOin Steroid Hormone Biosynthesis. The Endocrine Society , 155(1):15–20.

Papadopoulos, V., Aghazadeh, Y., Fan, J., Campioli, E., Zirkin, B., & Midzak, A. (2015). Translocator protein-mediated pharmacology of cholesterol transport and steroidogenesis. Molecular Cell Endocrinology , 15;408:90-8.

Papadopoulos, V., Amri, H., Boujard, N., Cascio, C., Culty, M., Garnier, M., et al. (1997). Peripheral benzodiazepine receptor in cholesterol transport and steroidogenesis. Steroids , 62:21–28.

Papadopoulos, V., Baraldi, M., Guilarte, T. R., Knudsen, T. B., Lacapère, J. J., Lindemann, P., et al. (2006). Translocator protein (18kDa): new nomenclature for the peripheral-type benzodiazepine receptor based on its structure and molecular function. Trend in pharmacological science , 27(8):402-9.

Papadopoulos, V., Berkovich, A., Krueger, K. E., Costa, E., & Guidotti, A. (1991). Diazepam binding inhibitor and its processing products stimulate mitochondrial

steroid biosynthesis via an interaction with mitochondrial benzodiazepine receptors. Endocrinology , 129 1481-1488.

Piccoli, C., Scrima, R., Boffoli, D., & Capitanio, N. (2006). Control by cytochrome c oxidase of the cellular oxidative phosphorylation system depends on the mitochondrial energy state. Biochemical Journal , 396(3);573–583.

Pinna, G., Costa, E., & Guidotti, A. (2006). Fluoxetine and norfluoxetine stereospecifically and selectively increase brain neurosteroid content at doses that are inactive on 5-HT reuptake. Psychopharmacology , 186(3):362-72.

Qui, Z. K., He, J. L., Liu, X., Zhang, G. H., Zeng, J., Nie, H., et al. (2016). The antidepressant-like activity of AC-5216, a ligand for 18KDa translocator protein (TSPO), in an animal model of diabetes mellitus. Scientific report , 6:37345.

Qui, Z. K., Zhang, L. M., Zhao, N., Chen, H. X., Zhang, Y. Z., Liu, Y. Q., et al. (2013). Repeated administration of AC-5216, a ligand for the 18kDa translocator protein, improves behavioral deficits in a mouse model of post-traumatic stress disorder. Progress in Neuro-Psychopharmacology & Biological Psychiatry , 45:40-46.

Ramadan, J. W., Steiner, S. R., O'Neill, C. M., & Nunemaker, C. S. (2011). The central role of calcium in the effects of cytokines on beta-cell function: implications for type 1 and type 2 diabetes. Cell Calcium , 50(6):481-90.

Rapizzi, E., Pinton, P., & Szabadkai, G. (2002). Recombinant expression of the voltage-dependent anion channel enhances the transfer of Ca2+ microdomains to mitochondria. Journal of Cell Biology , 159(4): 613-24.

Ratcliffe, S. L., & Matthews, E. K. (1995). Modification of the photodynamic action of delta-aminolaevulinic acid (ALA) on rat pancreatoma cells by mitochondrial benzodiazepine receptor ligands. British Journal of Cancer , (71) 300-305.

Rissanen, E., Tuisku, J., Rokka, J., Paavilainen, T., Parkkola, R., Rinne, J. O., et al. (2014). In vivo detection of diffuse inflammation in secondary progressive multiple

sclerosis using PET imaging and the radioligand11C-PK11195. Journal of Nuclear Medicine , 55;(6):939–94.

Rizzuto, R., De Stefani, D., Raffaello, A., & Mammucari, C. (2012). Mitochondria as sensors and regulators of calcium signalling. Nature Reviews Molecular Cell Biology , 13, 566-578.

Rizzuto, R., Pinton, P., & Carrinfton, W. (1998). Close contacts with the endoplasmic reticulum as determinants of mitochondrial Ca2+ responses. Science , 280(5370): 1763-6.

Rodríguez-Arribas, M., Yakhine-Diop, S. M., Pedro, J. M., Gómez-Suaga, P., Gómez-Sánchez, R., Martínez-Chacón, G., et al. (2016). Mitochondria-Associated Membranes (MAMs): Overview and Its Role in Parkinson's Disease. Molecular Neurobiology , 1-17.

Rone, M. B., Midzak, A. S., Issop, L., Rammouz, G., Jagannathan, S., Fan, J., et al. (2012). Identification of a Dynamic Mitochondrial Protein Complex Driving Cholesterol Import, Trafficking, and Metabolism to Steroid Hormones. Molecular Endocrinology , 26(11):1868–1882.

Rostovtseva, T. K., & Bezrukov, S. M. (2012). VDAC inhibition by tubulin and its physiological implications. Biochimica et Biophysica Acta (BBA) - Biomembranes , 1818(6):1526–1535.

Rostovtseva, T. K., Sheldon, K. L., Hassanzadeh, E., Monge, C., Saks, V., Bezrukov, S. M., et al. (2008). Tubulin binding blocks mitochondrial voltage-dependent anion channel and regulates respiration. Proceedings of the national academy of sciences of the Ubited States of America , 105(48): 18746–18751.

Rupprecht, R., Papadopoulos, V., Rammes, G., Baghai, T. C., Fan, J., Akula, N., et al. (2010). Translocator protein (18 kDa) (TSPO) as a therapeutic target for neurological and psychiatric disorders. Nature Reviews , 9(12):971-88.

Rupprecht, R., Rammes, G., Eser, D., Baghai, T. c., Schüle, C., Nothdurfter, C., et al. (2009). Translocator protein (18kD) as target for anxiolytics without benzodiazepine-like side effects. Science , 325;(5939):490–493.

Schüle, C., Nothdurfter, C., & Rupprecht, R. (2014). The role of allopregnanolone in depression and anxiety. rogress in neurobiology , 113:79-87.

Selvaraj, V., & Stocco, D. M. (2015). The changing landscape in translocator protein (TSPO) function. Trends in Endocrinology and Metabolism , 26(7):341-8.

Selvaraj, V., & Tu, L. N. (2016). Current status and future perspectives: TSPO in steroid neuroendocrinology. Journal of Endocrinology , 231(1):R1-R30.

Serra, M., Madau, P., Chessa, M. F., Caddeo, M., Sanna, E., Trapani, G., et al. (1999). 2-Phenyl-imidazo[1,2-a]pyridine derivatives as ligands for peripheral benzodiazepine receptors: stimulation of neurosteroid synthesis and anticonflict action in rats. British Journal of Pharmacology , 127;(1):177–187.

Setiawan, E., Wilson, A. A., & Mizrahi, R. (2015a). Role of translocator protein density, a markerof neuroinflammation, in the brain during majordepressive episodes. JAMA Psychiatry , 72;(3):268–275.

Setiawan, E., Wilson, A. A., Mizrahi, R., Rusjan, P. M., Miller, L., Rajkowska, G., et al. (2015b). Increased Translocator Protein Distribution Volume, A Marker of Neuroinflammation, in the Brain During Major Depressive Episodes. JAMA Psychiatry , 72(3): 268–275.

Šileikytė, J., Blachly-Dyson, E., Sewell, R., Carpi, A., Menabò, R., Di Lisa, F., et al. (2014). Regulation of the Mitochondrial Permeability Transition Pore by the Outer Membrane Does Not Involve the Peripheral Benzodiazepine Receptor (Translocator Protein of 18 kDa (TSPO)). Journal of Biological Chemistry , 289(20): 13769–13781.

Smiley, S. T., Reers, M., Mottola-Hartshorn, C., Lin, M., Chen, A., Smith, T. W., et al. (1991). Intracellular heterogeneity in mitochondrial membrane potentials revealed by

a J-aggregate-forming lipophilic cation JC-1. Proceedings of the National Academy of Science U S A , 88;(9):3671-5.

Stoffel-Wagner, B. (2003). Neurosteroid Biosynthesis in the Human Brain and Its Clinical Implications. Annals of the New York Academy of Sciences , Vol.1007, p.68-74.

Suzuki, Y., & Yokoyama, K. (2015). Development of Functional Fluorescent Molecular Probes for the Detection of Biological Substances. Biosensors , 5;(2):337-363.

Szabadkai, G., Bianchi, K., & Varnai, P. (2006). Chaperonemediated coupling of endoplasmic reticulum and mitochondrial Ca2+ channels. Journal of Cell Biology , 175(6): 901-11.

Tamse, C. T., Lu, X., Mortel, E. G., Cabrales, E., Feng, W., & Schaefer, S. (2008). The peripheral benzodiazepine receptor modulates Ca2+ transport through the VDAC in rat heart mitochondria. Journal of Clinical Basic Cardiology , 11(1-4): 24-9.

Thomson, M. (2003). Does cholesterol use the mitochondrial contact site as a conduit to the steroidogenic pathway? Bioessays , 25:252– 258.

Tsien, R. Y., Rink, T. J., & Poenie, M. (1985). Measurement of cytosolic free Ca2+ in individual small cells using fluorescence microscopy with dual excitation wavelengths. Cell Calcium , 6(1-2):145-57.

Tu, L. N., Morohaku, P. R., Pelton, S. H., Butler, W. R., Stocco, D. M., & Selvaraj, V. (2014). Peripheral benzodiazepine receptor/translocator protein global knock-out mice are viable with no effects on steroid hormone biosynthesis. Journal of Biology and Chemistry , 289:27444–27454.

Tu, L. N., Zhao, A. H., Hussein, M., Stocco, D. M., & Selveraj, V. (2016). Translocator protein (TSPO) affects mitochondrial fatty acid oxidation in steroidogenic cells. Endocrinology .

Tu, L. N., Zhao, A. H., Stocco, D. M., & Selvaraj, V. (2015). PK11195 effect on steroidogenesis is not mediated through the translocator protein (TSPO). Endocrinology , 156 1033-1039.

van Vilet, A. R., Verfaillie, T., & Agostinis, P. (2014). New functions of mitochondria associated membranes in cellular signaling. Biochimica et Biophysica Acta , 1843(10):2253-62.

Vashington, F. D., & Murphy, J. V. (1962). Ca ion uptake by rat kidney mitochondria and its dependence on respiration and phosphorylation. Journal of Biological Chemistry , 237: 2670-7.

Veenman, L., Shandalov, Y., & Gavish, M. (2008). VDAC activation by the 18 kDa translocator protein (TSPO), implications for apoptosis. Journal of Bioenergetics and Biomembranes , 40:199–205.

Venneti, S., Wagner, A. K., Wang, G., Slagel, S. L., Chen, X., Lopresti, B. J., et al. (2007). The high affinity peripheral benzodiazepine receptor ligand DAA1106 binds specifically to microglia in a rat model of traumatic brain injury: implications for PET imaging. Experimental Nerology , 207;(1):118–127.

Verleye, M., Akwa, Y., Liere, P., Ladurelle, N., Pianos, A., Eychenne, B., et al. (2005). The anxiolytic etifoxine activates the peripheral benzodiazepine receptor and increases the neurosteroid levels in rat brain. Pharmacology Biochemistry and Behavior , 82;(4):712–720.

Verma, A., Nye, J. S., & Snyder, S. H. (1987). Porphyrins are endogenous ligands for the mitochondrial (peripheral-type) benzodiazepine receptor. Proceedings of the National Academy of Sciences of the United States of America , 84;(8):2256-60.

Vivash, L., & O'Brien, T. J. (2016). Imaging Microglial Activation with TSPO PET: Lighting Up Neurologic Diseases. Journal of Nuclear Medicine , 57(2):165-8.

Weissmann, B. A., & Raveh, L. (2003). Peripheral benzodiazepine receptors: on mice and human brain imaging. Journal of Neurochemistry , 84(3):432-7.

Weissmann, B. A., Cott, J., Hommer, D., Quirion, R., Paul, S., & Skolnick, P. (1983). Pharmacological, electrophysiological, and neurochemical actions of the convulsant benzodiazepine Ro 5-4864 (4'-chlordiazepam). Advances in Biochemical Psychopharmacology , 38: 139–51.

Wolf, L., Bauer, A., Melchner, D., Hallof-Buestrich, H., Sarubin, N., Stoertebecker, P., et al. (2015). Enhancing neurosteroid synthesis-relationship to the pharmacology of translocator protein (18kDa) (TSPO). Pharmacopsychiatry , 72-77.

Yeliseev, A. A., & Kaplan, S. (1995). A sensory transducer homologous to the mammalian peripheral-type benzodiazepine receptor regulates pho-tosynthetic membrane complex formation in Rhodobacter sphaeroides. The Journal of biological chemistry , 270: 21167–21.

Yousefi, O. S., Wilhelm, T., Maschke-Neuß, K., Kuhny, M., Martin, C., Molderings, G. J., et al. (2013). The 1,4-benzodiazepine Ro5-4864 (4-chlorodiazepam) suppresses multiple pro-inflammatory mast cell effector functions. Cell Communication and Signaling. 2013 , 11-13.

Zamzami, N., Métivier, D., & Kroemer, G. (2000). Quantitation of Mitochondrial Transmembrane Potential in Cells and in Isolated Mitochondria. Methods in Enzymology , 322;():208–213.

Zhang, L. M., Qui, Z. K., Zhao, N., Chen, H. X., Liu, Y. Q., Xu, J. P., et al. (2014a). Anxiolytic-like effects of YL-IPA08, a potent ligand for the translocator protein (18kDa) in animal models of post-traumatic stress disorder. International Journal of Neuropsycopharmacology , 17;(10):1659–1669.

Zhang, L. M., Wang, Y. L., Liu, Y. Q., Xue, R., Zhang, Y. Z., Yang, R. F., et al. (2017). Antidepressant-like effects of YL-IPA08, a potent ligand for the translocator protein (18 kDa) in chronically stressed rats. Neuropharmacology , 113:567-575.

Zhang, L. M., Zhao, N., Guo, W. Z., Jin, Z. L., Qui, Z. K., Chen, H. X., et al. (2014b). Antidepressant-like and anxiolytic-like effects of YL-IPA08, a potent ligand for the translocator protein (18kDa). Neuropharmacology , 81:116–125.

Zhao, A. H., Tu, L. N., Mukai, C., Sirivelu, M. P., Pillai, V. V., Morohaku, K., et al. (2016). Mitochondrial Translocator Protein (TSPO) Function Is Not Essential for Heme Biosynthesis. Journal of Biological Chemistry , 291(4):1591-603.

Zürcher, N. R., Loggia, M. L., & Lawson, R. (2015). Increased in vivo glial activation in patients with amyotrophic lateral sclerosis: assessed with [(11)C]-PBR28. Neuroimage Clinical , 7:409-414.